CLASSIFICATION CHANGED
UNCLASSIFIEDTO: T.D. 71-617
By Authority of: Date 10/5/71

TECHNICAL MEMORANDUM

X - 400

Declassified by authority of NASA
Classification Change Notices No. 215
Dated **12/31/71

CONTROL FLUTTER STABILITY ANALYSIS

SATURN SA-1 (DUMMY UPPER STAGES)

By Robert S. Ryan

George C. Marshall Space Flight Center
Huntsville, Alabama

FACILITY FORM 602

N71-75276

(ACCESSION NUMBER)

(THRU)

(PAGES)

(CODE)

(NASA CR OR TMX OR AD NUMBER)

(CATEGORY)

NATIONAL AERONAUTICS AND SPACE ADMINISTRATION
WASHINGTON

January 1961

[REDACTED]

NATIONAL AERONAUTICS AND SPACE ADMINISTRATION

TECHNICAL MEMORANDUM X- 400

CONTROL FLUTTER STABILITY ANALYSIS

SATURN SA-1 (DUMMY UPPER STAGES) *

By Robert S. Ryan

SUMMARY

An investigation was carried out to determine the control feedback stability characteristics of the Saturn SA-1 vehicle, with a 220-inch dummy second stage and a 120-inch dummy third stage, including loadings due to sloshing propellants. Analyzed were the control frequency (pitch or yaw and roll) bending modes (4 lateral, 2 torsional) and propellant sloshing roots.

The results are accomplished by the determination of (1) free-free uncoupled bending mode deflection curves and frequencies, and uncoupled natural sloshing frequencies without the interaction of the control system (2) the gain and phase of filters for each control loop that will give absolute stability and desired relative stability, and (3) the computation of the coupled frequencies of the system under flight conditions.

Rate gyros were compared with a lead network as means of obtaining control damping. The use of a local pressure sensing or an Edcliff vane α -meter for α -control was studied with no apparent difference in effect upon vehicle stability.

The effect of aerodynamic forces upon vehicle bending stability was determined as well as the effect of propellant sloshing and structural damping. Artificial phase was introduced into the control loop as a way of determining the relative stability.

Stability exists for all cases investigated with very little or no instabilizing influences coming from the sloshing propellants. A statement can be made that baffles will not be needed in the lower parts of the booster tanks to achieve propellant sloshing stability. Enough damping will be provided by the Z-rings of the 70-inch diameter outer ring tanks. Aerodynamic forces had very little effect upon vehicle bending stability.

Bending mode stability was achieved by two methods: phase stabilization and attenuation stabilization. Attenuation stabilization is the most favorable when the magnitude of the bending mode frequency is well above the control frequency.

[REDACTED]

I. (C) INTRODUCTION

The purpose of this paper is to present the results of a control feedback stability analysis of Saturn SA-1 (dummy second and third stages).

For this analysis the vibrational results of the bending analysis were used considering the five booster lox tanks as contributing to the stiffness. It is believed, however, that due to the redundancy of the system the applied bending method leads to higher values than in the actual case. The first bending mode would be decreased by approximately 20%. This, however, will not drastically change the results of this analysis. An investigation treating this fact is in the process.

A comprehensive study was made for the coupled frequencies of the lateral and torsional bending modes, sloshing, pitch control, roll control, and of the swivel engine.

Different control systems were considered:

1. Edcliff angle-of-attack meter (alpha control).
Rate gyro for pitch control damping φ -channel
Lead network for roll control damping ψ -channel
2. Local angle-of-attack meters (alpha control).
Rate gyro for pitch control damping φ -channel
Lead network for roll control damping ψ -channel
3. Local angle-of-attack meters (alpha control).
Lead network for pitch control damping φ -channel
Lead network for roll control damping ψ -channel

As a preliminary study, phase and gain requirements necessary to give each control loop maximum control feedback stability were determined. Utilizing this data, Guidance and Control Division designed appropriate filters, and a further stability analysis was performed using the appropriately designed filters.

Sloshing stability was achieved independent of the control loops by the use of anti-sloshing devices. To further ascertain the effect of the propellant sloshing, an analysis was performed by considering the propellant solidified.

II. NOTATION

a_f	Radius of propellant tank
a_{op}	Gain factor φ -channel
a_{or}	Gain factor ϑ -channel
a_l	Gain factor φ -channel
a_{lr}	Gain factor ϑ -channel
b_o	Gain factor α -channel
A_i	Indicated acceleration in/sec ²
$A(s)$	Transfer function of amplifier plus actuator
β_{E_1}	Thrust vector angle engines 1 and 2
β_{E_2}	Thrust vector angle engines 3 and 4
β_{c_1}	Command signal to engines 1 and 2
β_{c_2}	Command signal to engines 3 and 4
ζ_p	Damping factor pitch rate gyro
$D_p(s)$	Transfer function demodulator φ -channel
$\bar{D}(s)$	Transfer function demodulator α -channel
$D_r(s)$	Transfer function demodulator ϑ -channel
$F_p(s)$	Transfer function filter φ -channel
$F_r(s)$	Transfer function filter ϑ -channel
$\bar{F}(s)$	Transfer function filter α -channel
T_i	Thrust of individual swivel engine
\bar{g}	Longitudinal vehicle acceleration
g_{mf}	Damping factor for sloshing propellant
g_2	Gain factor accelerometer channel

h_f	Propellant height
$L_p(s)$	Transfer function lead network φ -channel
$L_r(s)$	Transfer function lead network ψ -channel
Q	Dynamic pressure
Σ_E	First moment swivel engine about swivel point
X_a	Accelerometer X-station
X_v	Angle-of-attack meter X-station
X_T	Thrust application X-station
$X_{\varphi R}$	Location of roll gyros
$X_{\varphi P}$	Location of pitch gyros
Y'_μ	Slope of bending mode deflection curve
Y_μ	Bending mode deflection curves (normalized to 1 inch at the vehicle nose)
y	Complex amplitude of translation of vehicle
$S = \sigma + i\omega$	Coupled root of system
\mathcal{Z}	Complex amplitude factor of vehicle roll angle
\mathcal{Z}_μ	Complex amplitude factor in lateral vehicle bending
\mathcal{Z}_v	Aerodynamic damping factor angle-of-attack meter
\mathcal{Z}_m	Mechanical damping factor angle-of-attack meter
\mathcal{Z}_A	Damping factor accelerometer
\mathcal{Z}_E	Damping factor swivel engine
\mathcal{T}_μ	Complex amplitude factor of torsional bending
φ_P	Complex vehicle pitching angle
ω_v	Natural angular frequency of the angle-of-attack meter



ω_E	Natural angular frequency of the swivel engine
ω_a	Natural angular frequency of the accelerometers
ω_p	Natural angular frequency of the pitch rate gyro
ω_r	Natural angular frequency of the roll rate gyro
ψ	Rotation of swivel engine relative to space
ε	Compliance of swivel engine



III. (C) DISCUSSION

A. (C) Assumptions

We assume that

1. The response curves of the Saturn ψ -channel demodulator, amplifier, and actuator will be the same as those for the Jupiter.
2. The instationary aerodynamic forces computed by using slender body theory are valid for the Saturn vehicle configurations. This is appropriate since the maximum stagnation pressure is in the transonic speed range.
3. The effect of the flowing propellant upon stability can be neglected, since the flowing propellants cause a slight increase in damping of the system.
4. The effect of guidance terms upon stability is small and is not considered.
5. Four swivel engines will be used for both roll and pitch control.
6. The propellant sloshing of the second and third stage tanks will be suppressed by completely filling the tanks with water.

B. (U) Procedure

The basic procedure for analyzing the control stability of the Saturn SA-1 vehicle consists of three parts. These are the determination of:

- 1) The uncoupled free-free torsional and lateral bending mode frequencies and deflection curves, and the natural propellant frequencies (without the inclusion of the exterior forces and the control system)
- 2) The location of the sensors (gyros and accelerometers) with the phase and gain requirements of the control loop for this location; and
- 3) The coupled frequencies for the vehicle during flight. The results of part (1) are published in DA-TM-34-60. (Reference 3

To accomplish parts (2) and (3), the equations of motion of the system are determined by the use of Lagrange's equations in modified form.

The generalized coordinates, q_i 's, are independent of each other and specify the configuration of the system. The number of generalized coordinates is the same as that of the degrees of freedom for holonomic conditions. According to Figure 1 and Figure 2, the system under consideration has the following degrees of freedom:

1. The lateral translation y of the undeformed vehicle center line.
2. The rotation φ of the vehicle relative to an inertial system. (pitch).
3. The rotation \mathcal{V} of the vehicle relative to an inertial system (roll).
4. The displacement ξ_s of the sloshing propellant mass relative to the tank wall.
5. The rotation \mathcal{V} of the swivel engine relative to an inertial system.
6. The elastic deformation of the vehicle in lateral bending represented by the amplitude η_μ of the μ -th bending mode at the nose of the vehicle.
7. The elastic deformation of the vehicle in torsional bending represented by the amplitude τ_σ of the σ -th bending mode at the nose of the vehicle.
8. The compliance \mathcal{E} of the swivel engine which is the difference between the actual deflection angle of the swivel engine and the control signal ($\mathcal{E}_1 = \beta_{E_1} - \beta_{C_1}$; $\mathcal{E}_2 = \beta_{E_2} - \beta_{C_2}$).

The degree of freedom of the longitudinal translation was eliminated by the special choice of the coordinate system as mentioned above. For this investigation, 4 lateral bending modes ($\sigma = 2$) were used.

The derivation of the equations (without roll and torsion) is given in Reference 2. The additional equations needed to include the roll and torsional degrees of freedom were taken from an unpublished addendum to Reference 2. The resulting set of equations are linear, homogeneous, second order differential equations. A set of solutions is assumed in the form

$$q_i(t) = \bar{q}_i e^{st} \quad (1)$$

where $s = \sigma + i\omega$. This removes the time dependence and transforms the equations into algebraic, linear, homogeneous equations in \bar{q}_i . For non-trivial solutions to exist, the determinant of the coefficients must vanish. This is done by an iterative procedure (Reference 2). The values of s , thus obtained, is used to compute the values of the unknowns \bar{q}_i . The homogeneous set of equations gives only the ratios of the unknowns; therefore, one variable can be chosen arbitrarily. Since we know the minimum and maximum response amplitudes, neglecting second order effects, which are functions of the angular frequency ω , the logical choice is the engine deflection angle $\bar{\beta}_{E_2}$. The frequency dependent can be written as

$$\bar{\beta}_{E_2} \min(\omega) = 0.01 \text{ degrees or } 0.0001745 \text{ radians}$$

$$\bar{\beta}_{E_2} \max(\omega) = \frac{0.603142}{|\omega|} \quad \text{for } |\omega| > 4.94$$

$$\bar{\beta}_{E_2} \max(\omega) = 0.122173 \quad \text{for } |\omega| \leq 4.94$$

All phase relations are given relative to the engine deflection angle $\bar{\beta}_{E_2}$. The positive direction of $\bar{\beta}_{E_2}$ is in the negative y-direction (Figure 2). Two sets of solutions are now obtained which can be written in general form by using (1) as

$$q_i(t)_{\min} = \bar{q}_i \min e^{\sigma t} [\cos \omega t + i \sin \omega t] \quad (2)$$

$$q_i(t)_{\min} = \bar{q}_i \min e^{\sigma t} [\cos \omega t + i \sin \omega t] \quad (3)$$

The solutions are then damped if σ is negative, undamped if σ is equal to 0, and diverging if σ is positive in sign. If ω is equal to zero, we have static stability conditions. Other mathematical procedures are discussed under the section to which they are most applicable.

C. (U) Tank Arrangement

Figure 3 presents a cross section of the SA-1 vehicle showing the propellant tanks and their locations. The booster consists of a cluster of eight 70-inch diameter tanks surrounding one 105-inch diameter tank. The 105-inch diameter tank and four 70-inch diameter tanks contain LOX. The other four 70-inch diameter tanks contain fuel. The LOX or fuel tanks are connected by separate inner-connecting pipe lines leading into one feed line so that the propellant level in all LOX fuel tanks will be approximately the same.

Since the sloshing characteristics are the same for each of four 70-inch diameter fuel or LOX tanks, we denote the four 70-inch diameter fuel tanks as Tank 1 and the four 70-inch diameter LOX tanks as Tank 3; the 105-inch diameter LOX tank is denoted as Tank 2.

The theory for liquid oscillations used in this investigation was derived for flat bottom cylindrical tanks. To adapt the propellant tanks of the Saturn vehicle to this theory, the conical portions of the tanks were mathematically replaced by cylinders of equal volume.

D. (U) Control System

The control system used in this investigation consists of the Jupiter γ -channel demodulator and amplifier-actuator. The compliance of the swivel engine was taken into account by using an engine natural frequency of 14 cps and a damping value $\zeta_E = 0.07$.

For low frequency oscillations, the control equations can be written as:

$$\beta_{C_1} = a_{0p} \varphi_p + a_{1p} \dot{\varphi}_p - a_{0R} \vartheta_R - a_{1R} \dot{\vartheta}_R + b_0 \alpha_v \quad (4)$$

$$\beta_{C_2} = a_{0p} \varphi_p + a_{1p} \dot{\varphi}_p + a_{0R} \vartheta_R - a_{1R} \dot{\vartheta}_R + b_0 \alpha_v \quad (5)$$

Two equations are necessary since the same engines are used for roll and pitch (or yaw). If the signal is pure pitch or yaw, the equations become identical.

Eight actuators are used for roll control. The relation of the angle of the four swivel engines as used in this investigation is given on Figure 2.

Rewriting equations (4) and (5) in transfer function form and including both rate gyros and lead network for control damping, the control equations become:

$$\begin{aligned} \beta_{C_1} = & \left\{ \varphi_p \left[D_p(s) L_p(s) + \frac{3a_{1p}}{\left(\frac{s}{\omega_p}\right)^2 + \frac{2s\zeta_p}{\omega_p} + 1} \right] F_p(s) - \vartheta_R \left[D_R(s) L_R(s) + \right. \right. \\ & \left. \left. + \frac{3a_{1R}}{\left(\frac{s}{\omega_R}\right)^2 + \frac{2s\zeta_R}{\omega_R} + 1} \right] F_R(s) + \alpha_v b_0 \bar{D}(s) \bar{F}(s) \right\} A(s) \end{aligned} \quad (6)$$

$$\beta_{c_2} = \left\{ \varphi_p \left[D_p(s) L_p(s) + \frac{3a_{1p}}{\left(\frac{s}{\omega_p}\right)^2 + \frac{2s\zeta_p}{\omega_p} + 1} \right] F_p(s) - \vartheta_R \left[D_R(s) L_R(s) + \frac{3a_{1R}}{\left(\frac{s}{\omega_R}\right)^2 + \frac{2s\zeta_R}{\omega_R} + 1} \right] F_R(s) + \alpha_v b_o \bar{D}(s) \bar{F}(s) \right\} A(s) \quad (7)$$

where φ_p is the total pitch angle sensed by the gyros and is written as

$$\varphi_p = \varphi - \sum_{\mu=1}^{\infty} \gamma_{\mu} \gamma'_{\mu} (X_{\varphi}) \quad (8)$$

α_v is the total indicated angle-of-attack and is written as

$$\alpha_v = \frac{\sum_{v=1}^4 \left\{ -Y'_v(X_v) \left[1 + \frac{s^2}{\omega_v^2} + \frac{2s\zeta_v}{\omega_v} \right] + \frac{s}{V} Y_v(X_v) \right\} \gamma_v + \left\{ \left[1 + \frac{s^2}{\omega_v^2} + \frac{2s\zeta_v}{\omega_v} \right] + \frac{s}{V} \bar{X}_v \right\} \varphi - \frac{sY}{V}}{1 + \frac{s^2}{\omega_v^2} + \frac{2s\zeta_v}{\omega_v} (\zeta_v + \zeta_M)} \quad (9)$$

ϑ_R is the total roll angle and is written as

$$\vartheta_R = \vartheta + \sum_{\mu=1}^{\infty} \gamma_{\mu} \theta_{\mu} (X_{\varphi})$$

A block diagram of a control system that includes all possible control configurations is given on Figure 4. For example: If the lead network is used for control damping in lieu of rate gyros, the rate gyro transfer function is set equal to zero and the lead network transfer function is inserted in the appropriate block. Other components can be changed by the same procedure.

The transfer functions of the filters, lead network, and the rate gyros were calculated from the electrical or physical components of the system and are valid for complex frequencies. The transfer function of the actuators was found experimentally.

E. (C) Data

Electrical gain values, a_0 , a_1 , and b_0 for .3 cps control frequency is plotted on Figure 5 (versus flight time).

The uncoupled free-free lateral bending mode frequencies and deflection curves (normalized to 1 at the vehicle nose) are taken from DA-TM-34-60 (Reference 1). Trajectory data are presented on Table 1.

Figure 6 is a graph of the undisturbed propellant heights in inches vs flight time in seconds for the different propellant tanks. A plot of the natural free-free sloshing mode frequencies is given on Figure 7. Values for three sloshing modes are graphed.

The swivel engine natural frequency was assumed to be 14 cps with 7% of critical damping. The damping is due to the fluid in the actuators.

The structural damping factor in lateral and torsional bending was assumed to be a conservative 0.0020 and .0065, respectively.

The rate gyro used was assumed to be 70% critically damped with a natural frequency of 16 cps.

The phase and gain characteristics of the local angle-of-attack meter are taken from DA-M-211, 30 January 1958. (Reference 6)

The frequency of the Edcliff angle-of-attack meter is plotted on Figure 8. Its aerodynamic and mechanical damping was assumed to be 0.005 and 0.015, respectively.


F. (C) Cases Investigated

To assist in the determination of an appropriate control system for the Saturn vehicle, SA-1 dummy upper stages, several types of system were investigated and are as follows:



- | | | |
|----|--------------------|--|
| 1. | α -channel | Edcliff angle-of-attack meter |
| | φ -channel | Rate gyro for pitch control damping |
| | ψ -channel | Lead network for roll control damping |
| 2. | α -channel | Local angle-of-attack meters |
| | φ -channel | Rate gyro for pitch control damping |
| | ψ -channel | Lead network for roll control damping |
| 3. | α -channel | Local angle-of-attack meters |
| | φ -channel | Lead network for pitch control damping |
| | ψ -channel | lead network for roll control damping |

The effects of various parameters upon the systems are studied and include:

1. The effect of propellant sloshing by considering the liquid solidified and free to oscillate.

- 
2. Different propellant damping devices
 3. Rate gyro located at different positions

Coupled roots are obtained for:

1. Lateral bending modes
 2. Torsional bending modes
 3. Swivel engine mode
 4. Pitch control mode
 5. Roll control mode
 6. Sloshing propellant
- 
- 

IV. (C) RESULTS

A. (C) Basic Concepts Used for Interpretation and Direction

The guided vehicle may be thought of as an electromechanical system. The servo system contains electrical, mechanical and hydraulic devices. By the time the refined control stability analysis is to be made, the vehicle system is determined by performance requirements detailed by the mission of the vehicle. This leaves only the addition of a filter or shaping element to the control loop as a means to gain required stability characteristics. The characteristics for the filtering devices can be given in transfer function form as gain (K) and phase (ϕ). The role of the unit becomes evident in expressions for overall system performance. The purpose of this phase of the investigation is to determine the transfer function of the filter unit in terms of overall system performance. The system performance is by necessity frequency dependent; therefore, the transfer function of the unit must be specified as

$$K(f)e^{i\phi(f)} = \text{filter transfer function} \quad (10)$$

By simplifying the equations of motion (considering only one oscillation at a time and each control loop separately), the frequency dependent transfer function can be specified in terms of desired performance. This, then, uniquely determines the transfer function. The two performance questions that arise are: (1) absolute stability defined as any free oscillation in the system which does not continue indefinitely (2) relative stability defined as the magnitude of the damping, the time rate of decay for the oscillation, and the magnitude of frequency shift due to the control system coupling. The absolute stability is uniquely determined by the phase of the total control loop. This has been given in detailed form in previous reports (DA-TM-65-59, Reference 3 and DA-TM-110-59, Reference 4). The relative stability is basically determined by the total gain and structural damping of the system. Two methods of achieving absolute stability from bending modes can be used:

- (1) Phase stabilization: The filter is designed by lead and lag units to produce the maximum absolute stability for a prescribed gain level. The following figure is a root locus plot with phase lag σ as parameter showing maximum absolute stability.

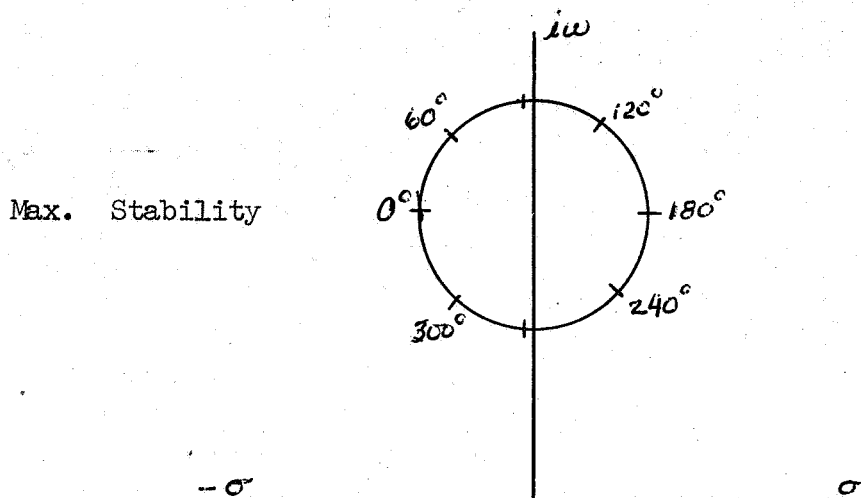


DIAGRAM 1

- (2) Attenuation stabilization: The signal sensed by the control sensor is attenuated in the control loop. Strong attenuation results in the domination of the mechanical damping, regardless of the phase of the control loop.

The second method lends itself to fewer uncertainties and is probably the superior method. It, however, cannot be accomplished when a mode frequency is near the control frequency (which is fixed). This is due to the attenuation of the filter interfering with the nominal a_0 , and a_1 gain values. The Saturn SA-1 has the first mode bending frequency close to the control frequency and, therefore, must be phase stabilized. The other modes can be attenuation stabilized.

The attenuation stabilization method can be justified since the time for total decay of the oscillation ($e^{\sigma t}$) takes precedence over the percentage of critical damping (ζ). At the bending mode frequencies, even low ζ will give a strong decay rate.

For the determination of the filter, transfer function $Ke^{-i s}$ is mathematically introduced in the control equation where $T(s)$ is the total transfer function of a lead network or rate gyro and demodulators and $\bar{T}(s)$ is the transfer function of the sensor and the demodulator filter for the α -channel.

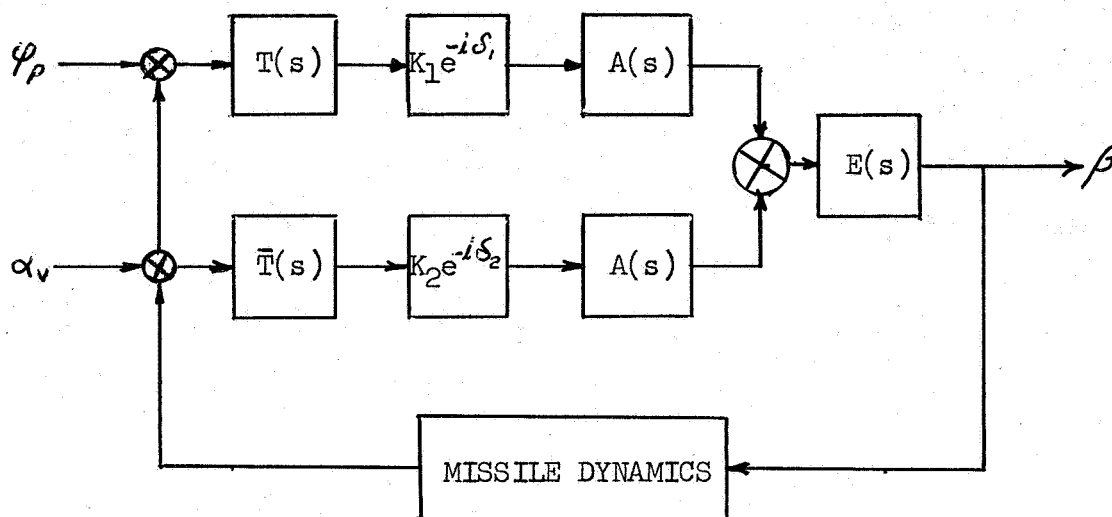


DIAGRAM 2

The procedure considers only one loop of the control system at a time by setting the appropriate gain (K_1 or K_2) equal to zero. The other $K(K_1$ or $K_2)$ value is set to unity. Artificial phase (δ) is introduced in 45° increments from $0-360^\circ$ and produces a root locus plot (diagram 1) for each bending mode at a given flight time. The phase producing maximum absolute stability is thus obtained. Using optimum phase, the appropriate gain factor for the control filter is computed. This gain value is determined for a ζ (percentage of critical damping) = .01. The value of ζ is kept at this low magnitude to restrict the root shift and to facilitate component design. The transfer function has been determined for all important frequencies by this procedure, and produces a filter transfer function

$$F(s) = K(s) e^{i\phi(s)} \quad (11)$$

By utilizing the transfer functions thus obtained, Guidance and Control Division designed filters which will produce the transfer function.

A. (C) Phase and Gain Study Results

1. ϕ -Channel

- a. Rate Gyro for Control Damping; Position Gyro for Angle Derivation.

Two locations were studied for the rate and position gyros, namely, station +36 and -474 inches. The actual rate gyro equation was used to compute the transfer function for the rate gyro which is 70% critically damped and has a natural frequency of 16 cps.

Gyros located at the top of the second stage ($X_y = -474$ inches)

The phase and gain requirements for this case are given on Figure 9. Stability is represented by the shaded area and instability by the unshaded area. Arbitrary phase lag introduced in the system is given on the ordinate axis. Frequency is plotted against the abscissa. The width of the block represents the change in frequency versus flight time. Initial and cutoff times are marked on the graph. The phase required to give maximum control feedback stability (maximum $-\sigma$) is represented by the solid line. At the top of each block the average gain value K is given which will result in a $\zeta = .01$. (a_0 and a_1 values used were for a control frequency of .3 cps, Figure 5).

For maximum absolute stability in the first bending mode, a 1 to 3 attenuation and a phase lag of 80° are needed. Attenuation, however, cannot be accomplished and from the response curve of the φ filter designed for this type control channel (Figure 10), it is noted that the gain is higher than that requested. This is acceptable since the phase is near that which is required for maximum absolute stability. The second and third bending modes are not dependent upon phase for stability for, as previously mentioned, stability is achieved by attenuation. Note, however, that the gain is much smaller than the .6 value specified but is a desirable quality as it assures further that the signal will be attenuated and the damping provided by structural damping and aerodynamic forces. A phase study is not made for the fourth mode. Filter will provide maximum attenuation for fourth and higher modes.

Shifting the position of the rate and position gyros to station $X_y = +36$ inches (Figure 11), it is found that the same filter can be utilized since the phase requirement for the first bending mode shows only slight changes for either gyro location. The phase requirement for absolute stability of the second bending mode is shifted 180° and the attenuation increased by a factor of 4. These are values which are within the tolerances that will insure stability. Desired attenuation for the third bending mode is fulfilled by the previous filter. Presentation of the location for the rate and position gyros with respect to the node and antinode points of the bending modes is given on Figures 12-15.

b. Lead Network

Utilizing a lead network and with the position gyro location at station $X_{\varphi} = +36$ inches the phase and gain requirements do not change to any great extent from those obtained when a rate gyro was used. (The top of the booster, station $X_{\varphi} = +36$ inches, was felt by Guidance and Control Division to be the most advantageous position for the gyros; hence, only one location will be investigated for the present and remaining cases). See Figure 16 for the gain and phase requirements and Figure 17 for the response curve and diagram of the φ -filter and lead network.

At the first bending mode frequencies, the filter is well adapted for desired phase and gain values. For the second and third bending modes which, as previously mentioned, are stabilized by attenuation and thus are independent of phase, the filter design is adequate. As a matter of fact, attenuation is greater than required.

2. Accelerometer Channel

With the accelerometer located at station $X_A = +36$ inches, the results indicate that, with the required gain, extremely large values of attenuation are required to achieve a $\zeta = 0.01$. (Figure 18.) As a result, only phase stabilization could be an acceptable method for control stability. At the present time, therefore, it is not deemed advantageous to attempt to utilize accelerometers for α -control on SA-1 vehicles. At a later date, further study will be made to investigate the feasibility of accelerometer control which will perhaps lead to an acceptable filter.

3. α -Channel

a. Edcliff angle-of-attack meter

From the phase and gain requirements shown on Figure 19, a filter was designed within the tolerances required for good stability. See Figure 20 for a graph of the response curve. For maximum stability in the first bending mode, the filter very closely gives the value of the phase required for optimum stability. A desirable quality is found in the gain since it is of such a value (low) to provide for an attenuation type damping. Second and higher bending mode signals are well attenuated.

b. Local angle-of-attack meter

Presented on Figure 21 are the values obtained for phase and gain necessary to give maximum feedback stability. The filter design utilized for the Edcliff meter contains characteristics which meet

the stability requirements in the present case; hence, it is used for our analysis.

4. Roll Channel

Figure 22 is the phase and gain requirements necessary for torsional bending mode stability. The control system designed to meet these requirements is given on Figure 23, and as shown the response of the system is adequate for use in the roll channel.

B. (C) Root Study for Final Control Systems

1. Bending Mode Roots

The basic philosophy used in achieving stability by phase or attenuation and the resulting design of an appropriate filter were discussed in Part III A. In this portion of the investigation, a study is made to determine the validity of the filter and to investigate further the effects caused by introducing various parameters.

a. Edcliff α -meter, Rate Gyro for Control Damping

Using an Edcliff angle-of-attack meter for α -control and a rate gyro for control damping in the ψ -channel, the control system is in an acceptable stability range for the first, third, and fourth bending modes; the second bending mode stability is of a marginal nature. As depicted on Figures 24-27, σ vs flight time, the difference in stability for either frozen or sloshing propellant (damped by Z-rings $g_{nf} = .065$) is of no consequence. To further indicate the stability of the control system, a second set of graphs is given (Figures 30-33) on which ζ (percent of critical damping) is plotted vs flight time.

Several stability characteristics of the third and fourth bending modes are worthy of mention. At 20 seconds of flight time, the third bending mode frequency reaches a resonance condition with the angle-of-attack meter frequency which results in an increase of stability. (See Figure 8 for a plot of the natural free-free frequencies.) At the fourth bending mode frequency, a resonance condition occurs with the angle-of-attack meter and swivel engine frequencies at 30 and 50 seconds flight time, respectively. The result is an increase in stability for the fourth bending mode.

(Note: Due to the resonance condition occurring between the bending mode and swivel engine frequencies, the swivel engine stability decreases at 70 seconds flight time. See Figure 32 for a plot of σ vs flight time for the swivel engine root associated with the lead network cases. Only one plot is given for the swivel engine root since the type of control system has little effect upon the stability of the swivel engine root.)

b. Local α -meter, Rate Gyro for Control Damping

Retaining the rate gyro for control damping in the φ -channel and changing from vane to a local type angle-of-attack meter for α -control, no basic change occurs in the stability of the system. (One advantage of the local angle-of-attack meter is that its natural frequency is not in the frequency band of the control system.) The stability of the system is further analyzed by, first, removing the aerodynamic forces ($Q = 0$) and, second, increasing the structural damping $g\mu$ from .002 to .005. Removing the aerodynamic forces (for this vehicle) has very little effect upon the stability of the oscillation; increasing the structural damping results in a stability increase. (Figures 32-36).

To determine the validity of the filter design and the attenuation of the signal, a phase study was made for the bending mode roots at 40 seconds flight time. A root locus plot (Figures 37-40) shows the phase of the first bending mode to be only 45° removed from optimum stability. The second bending mode, which has marginal stability for early flight times (Figure 25), is stable for all phase values (Figure 38). A larger structural damping would increase stability, and it is believed that the Saturn vehicle will have a larger value than the conservative $g\mu = .002$ used in this investigation. A practical value of $g\mu = .010$ is predicted by the Structures and Mechanics Division. The third and fourth bending modes are stable, independent of the phase (Figures 39-40). Again, a larger value for structural damping would increase the relative stability of the system.

c. Local Angle-of-Attack Meter, Lead Network for Control Damping

Replacing the rate gyro by a lead network, a local angle-of-attack meter is retained for α -control, and with the exception of third bending mode, which is unstable for the first 20 seconds of flight time, all bending modes are stable. The third bending mode instability is due to undesired gains in the φ -filter; however, the condition could be removed by increasing structural damping or by more attenuation in the filter.

To illustrate the effect of coupling between modes the percent and phase of the contributing part (β_{\min}) from each degree of freedom in relation to β_{E_2} (0° phase) is given on Tables 2-4. It is noted that very little, if any, coupling occurs between roll and pitch. Any oscillation is predominantly of one mode. For the third and fourth bending modes, feedback occurs through the α -channel. (Included on the table are the percent and phase values obtained when propellant is allowed to slosh. Only slight changes are noticed as a result of propellant sloshing.)

For the local α -meter and rate gyro control, the absolute value of the variables (β_{\min}) is given on Figure 41. Several factors are worthy of note. To excite the feedback loop, a vehicle nose deflection of approximately .006, .07, and .02 inch is required for the first, second, third, and fourth bending modes respectively. Note, also, that the fuel sloshing amplitude β_{nf} (Figure 42) is small.

The swivel engine compliance effect upon the control system is as follows. Near a resonance condition of the engine, gains and phase shifts are created in the system; however, no instability occurs as a result. Very little change is noted in the first bending mode stability.

d. Rate Gyro and Position Gyro at Different Locations

Of further interest in achieving optimum stability is the location of the rate and position gyros at separate stations. To analyze this effect, the rate and position gyro were placed respectively at the top ($X_{\varphi} = -474$ inches) and bottom ($X_{\varphi} = +36$ inches) of the second stage. The results (Figure 43) indicate that no detrimental effects will occur upon vehicle stability if the position and rate gyro are located as stated above.

2. Sloshing Roots

The criteria used for designing the filters neglected the effect of the sloshing propellant. This is permissible when correlated with the assumption that the forces resulting from fuel sloshing will not have an appreciable effect upon vehicle bending modes and control stability. The assumption is valid as long as the frequencies are well separated and no dependency is made upon the control system as a means of damping the sloshing propellant. Filters designed with this consideration proved to be effective for bending mode stability when the loading due to sloshing propellants were added to the investigation. Therefore, this portion of the analysis is concerned with the damping of the sloshing propellant and is performed using various control systems designed only for bending mode and control stability.

This leads to the fact that damping of the sloshing propellant must be achieved by the incorporation of anti-slosh devices introduced into the propellant tanks. Since weight is a critical problem in vehicle design, the baffling must be one which will provide an acceptable relative stability with minimum weight. This part of the analysis is thus concerned with the determination of the relative stability.

The loadings due to sloshing propellant can occur from four types of vehicle oscillations.

- (a) Translational oscillations
- (b) Pitching oscillations
- (c) Roll oscillations
- (d) Bending oscillations

(Only the propellant in the cluster of 70-inch diameter tanks is affected by the roll oscillations.)

To determine the effects of the preceding motions as interrelated with baffling and type of control system used, sloshing roots were obtained for

- (1) First and second sloshing modes - 70-inch diameter tanks.
- (2) First and second sloshing modes - 105-inch diameter tanks.
- (3) First roll sloshing mode - 70-inch diameter tanks.

The results indicate that the stability of the sloshing roots is affected very slightly by the type control system used. Figures 44-48 show σ vs flight time. These σ 's are basically the roots of the uncoupled sloshing equation and are changed very little with a change in control systems. Figures 49 and 50 give the damping factor ζ of the coupled root. This ζ is approximately the ζ of the damping device used in the propellant tank. For the rate gyro and Edcliff angle-of-attack meter case, the sloshing stability was investigated for two damping values, namely, $\zeta = .005$ (smooth wall) and $\zeta = .033$ (Z-rings) Figure 46. (The damping value $\zeta = .005$ is given only for the rate gyro and Edcliff angle-of-attack meter case since very little change is detected when another control system is used.)

To further substantiate the sloshing stability as presented by the above results, an artificial phase lag δ was introduced into the control system in increments from 0° to 360° . The effect of the artificial phase lag introduction was found to be negligible; therefore, Figures 44-48 are valid for any artificially introduced phase lag.

Stability can be achieved already with damping. Without anti-slosh devices the result is one of low relative stability, in the order of $e^{-.03t}$, and for the Z-rings, this factor becomes $e^{-.15t}$. Hence, damping in the 70-inch diameter tanks should be provided by using Z-rings; damping provided by the smooth walls ($\zeta \approx .005$) of the 105-inch diameter tank is sufficient.

It was observed that the first sloshing mode of any tank is coupled very little with bending modes. Tables 2-4 present the percent and phase of the contributing part (β_{\min}) in relation to the total β_{\min} . The major portion of β is contributed by the rigid φ -oscillation.

Figures 52-53 present the absolute values of unknowns for the rate gyro and local angle-of-attack meter as a function of flight time for the sloshing roots. Several factors worthy of note are:

- (1) bending mode amplitudes are small
- (2) the surface amplitude of the propellant decreases as flight time increases, and
- (3) the φ angle increases with flight time.

An increase in the moment due to sloshing is observed (Figure 54) with a slight increase in the force due to translation and a decreasing force due to bending. The moment increase is a result of two factors:

- (1) There is a larger φ angle.
- (2) The sloshing mass μ is displaced further from the vehicle center of gravity as flight time increases.

The clustering of the booster tanks has a decided advantage for sloshing stability. This is due mainly to the small diameter (70-inch) tanks which result in an increased sloshing frequency and decreased sloshing mass. Figure 55 is a plot of the ratio of the propellant sloshing mass μ to the vehicle mass m . The percentage of sloshing mass is always below 3% of the total vehicle mass.

It can be concluded that the stability of the sloshing propellant depends primarily upon the type of anti-slosh device used, and the location of the sloshing mass. For the SA-1 vehicle (propellant in the booster), the tanks are well located in that the sloshing mass is behind the vehicle center of gravity. Report MNM-M-AERO-1-60 (Reference 5) shows this to be very advantageous from stability stand-points for a simplified system.

3. Torsion Roots

The same philosophy and definitions stated under the section on lateral bending modes are applicable to torsional bending; therefore, they are not restated.

The results indicate a stable oscillation for the two torsional modes investigated (Figure 56). Table 2, defined previously, reveals that there is practically no coupling between the torsional, pitching, and bending oscillations. This is a very desirable quality. The only coupling present originates through the gyroscopic reaction moment of the spinning turbines. (Since the torsion root is practically identical when the propellant is frozen or free to oscillate, only one set of values is given. It is further observed that irrespective of the control system used in pitch or yaw, the torsional roots are the same; therefore, only one case is presented. (See Table 2).

The effect of engine failure was not studied in this analysis. In the near future an investigation will be made and the results published in a subsequent report.

4. Swivel Engine Roots

Two roots associated with the natural frequency of the swivel engine were obtained. One, fed through the roll channel, is coupled with the second torsional bending mode; the other is coupled with the fourth lateral bending mode. In the torsional coupled root, engines 1 and 2 oscillate 180° out of phase with engines 3 and 4; the result is a lower frequency. (See Tables 3-4 for the coupling and Figure 32 for the stability plot.) The stability of the root coupled with the fourth bending mode decreases but does not become unstable when resonance occurs at 70 seconds flight time.

The different control systems had very little effect upon the stability of the engine roots. (Tables 2-4).

It can be stated that the swivel engine oscillations have good absolute and relative stability.

5. Control Frequencies

For the present vehicle, two control frequencies exist; one in pitch or yaw and one in roll. For this investigation both frequencies were chosen as .3 cps; however, it is now believed that the roll frequency should be increased to .5 cps. This will be investigated at a later time.



Since the different control systems (pitch or yaw and roll) were designed for a .3 cps undamped frequency and used the same a_0 , a_1 and b_0 gain values, only one set of roots is presented. Figure 57 gives the value of σ and ω for the pitch or yaw and roll root.

Torsional or lateral bending modes had little effect upon the control frequency (Tables 2-4); the feedback was through the rigid body rotational motion and the angle was sensed by both the gyros (position and rate) and angle-of-attack meter.

V. (C) CONCLUSIONS

1. The control system has no adverse effect upon the stability of the sloshing propellants; anti-slosh devices placed in the tanks provide the damping. The vehicle would fly safely without any anti-slosh devices in the 105-inch diameter tank and with Z-rings in the 70-inch diameter tanks.
2. The coupling between the roll and pitch is negligible.
3. Several different type control loops can be used to provide vehicle stability. The type control used is to be determined by factors other than stability achievements, since all perform equally well.
4. Loadings due to propellant sloshing had no noticeable effect upon bending and torsional mode stability.
5. There is little or no interaction among lateral bending modes.
6. Control frequencies are well defined for all cases.
7. The use of accelerometers for angle-of-attack control is not practical at the present time, due to high gains in the accelerometer loop at bending mode frequencies. These high gains make appropriate filter design impractical.

REFERENCES

1. D. Beasley, Vibration Analysis of Saturn SA-1, ABMA Report DA-TM-60, May 4, 1960
2. M. H. Rheinfurth, Control -Feedback Stability Analysis, ABMA Report DA-TR-2-60, January 11, 1960
3. R. S. Ryan, Control Feedback Flutter Analysis Saturn 3, 4, (Atlas Second Stage) Using Edcliff Angle-of-Attack Meter for Alpha Control (U), ABMA Report DA-TM-65-59, May 26, 1959
4. R. Ryan, J. Rees, Control Flutter Stability Analysis Saturn 3, 4 (120" Diameter Second Stage) for First Stage Flight, Using Accelerometers As Alpha Control (U), ABMA Report DA-TM-110-59, August 31, 1959
5. M. H. Rheinfurth, The Effect of Propellant Oscillations on the Stability of a Rigid Space Vehicle, MSFC Report MNN-M-AERO-1-60, August 1, 1960
6. J. Fikes, J. P. Baur, The Dynamic Characteristics of the Topp Industries, Probe Type, Local Angle of Attack Indicator, DA Memorandum No. 322, January 30, 1958, available at ABMA Technical Documents Library.

TABLE I

<u>Time</u>	<u>Q</u>	<u>F Total</u>	<u>V</u>
10	16,306	1,317,353	1679.58
20	72,575	1,331,746	3660.14
30	173,008	1,355,479	6002.40
40	305,702	1,386,321	8771.93
50	430,264	1,420,064	11,944.03
60	487,234	1,451,249	15,371.05
70	444,121	1,475,329	19,639.95
80	345,964	1,490,250	25,387.48
90	229,081	1,498,184	32,985.21
100	116,584	1,501,597	42,655.41
110	50,978	1,502,792	54,520.87

$$e_0 = 0$$

$$e_1 = 0$$

$$\sum e = 451.224$$

$$\theta_e = 27,648$$

EDCLIFF ANGLE-OF-ATTACK METER
RATE GYRO

60 sec's

AMOUNT OF β FROM EACH VARIABLE (β_{min})

SA-1

			BENDING MODES										TORSIONAL MODES								
ROOT	REAL	IMAG.	1st Mode		2nd Mode		3rd Mode		4th Mode		1st Mode		2nd Mode		PITCH		ROLL		ANGLE-OF-ATTACK		
			%	PHASE	%	PHASE	%	PHASE	%	PHASE	%	PHASE	%	PHASE	%	PHASE	%	PHASE	%		
BENDING MODE 1	* -0.6719 ** -.6345	21.39 21.45	91.4 91.4	180.83 180.94	1.14 1.19	222.22 216.00	1.09 1.09	223.08 218.58	0.7426 .7400	39.63 41.37	0.72-10 ⁻¹¹ 41.28	41.28	0.28-10 ⁻¹⁰	308.04	3.82 3.66	36.55 39.58	58.28	1.77 1.83	189.89 189.72		
BENDING MODE 2	* -.1441 ** -.2603	46.50 47.64	4.95 1.63	270.84 273.99	54.99 54.99	269.27 271.07	5.17 1.74	271.10 275.51	2.86 4.11	91.19 92.47	.62-10 ⁻¹² 296.37	296.37	.82-10 ⁻¹¹	27.05	1.21 2.50	84.03 88.81	173.64	30.79 34.99	326.49 330.67		
BENDING MODE 3	* -.2737 ** -.3168	64.90 65.49	1.65 1.29	244.74 241.23	1.92 1.06	63.96 57.29	24.42 24.47	249.02 247.56	2.84 3.59	64.84 64.38	.29-10 ⁻¹² 93.22	93.22	.41-10 ⁻¹⁰	188.57	.427 .676	61.82 63.08	281.67	68.65 68.82	140.18 138.80		
BENDING MODE 4	* -1.7800 ** -1.5230	90.31 90.76	.54 .54	325.32 327.47	.46 .50	144.95 148.28	1.84 1.80	142.24 144.84	18.46 17.99	186.23 186.54	.20-10 ⁻¹¹ 43.03	43.03	.10-10 ⁻⁹	305.98	.15 .098	147.93 143.18	223.59	78.45 78.93	295.7 295.6		
SLOSH 70" DIA. TANK	# -.2010 ## -.3420	6.18 10.52	2.94 31.00	181.83 202.69	.52 .55	203.74 120.12	.27 2.24	195.97 204.17	.70 2.84	207.46 47.26	.24-10 ⁻⁵ .18-10 ⁻⁶	286.74 23.68	.96-10 ⁻⁵ .52-10 ⁻⁶	194.17 302.28	74.79 50.96	195.37 174.56	202.41 184.26	20.67 12.31	87.1 25.6		
SLOSH 105" DIA. TANK	# -.1758 ## -.2790	5.05 8.58	2.97 53.24	291.43 27.66	.62 7.35	155.99 205.35	.33 3.80	105.79 208.09	.93 4.31	198.38 200.46	.32-10 ⁻⁵ .12-10 ⁻⁶	283.79 310.41	.14-10 ⁻⁴ .43-10 ⁻⁵	191.27 10.23	75.49 9.89	192.98 196.95	202.00 142.00	19.54 21.30	94.5 30.58		
CONTROL SWIVEL	-1.4300 -5.0400	2.34 94.55	3.43 .91	261.43 290.43	.36 .74	82.74 109.34	.42 2.76	81.27 104.06	.28 17.85	267.02 226.91	.14-10 ⁻⁷ .1087	184.81 269.12	.0264 .28-10 ⁻⁶	263.21 8.15	66.19 .26	202.54 110.22	156.01 141.84	29.20 77.47	104.06 353.69		
g _u = 0.002																					
g _{ir} = 0.065																					
* w/o Sloshing																					
** With Sloshing																					
# 1st Mode																					
## 2nd Mode																					

 $\xi_{\mu} = 0.002$ $\xi_{\mu f} = 0.065$

*W/O Sloshing

**With Sloshing

1st Mode

2nd Mode

TABLE 3

LOCAL ANGLE-OF-ATTACK METER
RATE GYRO
WITH SLOSHING

60 sec's

AMOUNT OF β FROM EACH VARIABLE (β_{min})

SA-1

		BENDING MODES										TORSIONAL MODES										ANGLE-OF-ATTACK	
		ROOT		1st Mode		2nd Mode		3rd Mode		4th Mode		1st Mode		2nd Mode		PITCH		ROLL					
				REAL	IMAG.	%	PHASE	%	PHASE	%	PHASE	%	PHASE	%	PHASE	%	PHASE	%	PHASE	%			
B. MODE 1	-0.5983	21.51	87.37	183.36	215.30	1.17	215.30	1.08	217.56	0.69	40.07	0.72-10 ⁻¹¹	41.28	0.28-10 ⁻¹⁰	308.04	3.52	38.72	0.36-10 ⁻¹¹	58.28	6.17	146.27		
B. MODE 2	-.0017	47.60	1.44	271.92	266.15	42.14	273.96	1.53	273.96	3.29	88.48	.62-10 ⁻¹²	296.37	.82-10 ⁻¹¹	27.05	1.98	84.42	.63-10 ⁻¹²	173.64	49.62	214.16		
B. MODE 3	-.2330	65.57	2.74	239.86	57.02	2.13	244.25	52.21	244.25	7.61	62.12	.29-10 ⁻¹²	93.22	.41-10 ⁻¹⁰	188.57	1.37	60.54	.24-10 ⁻¹³	281.67	33.94	32.50		
B. MODE 4	-1.8104	91.21	1.62	328.59	149.79	1.47	145.45	5.26	145.45	59.20	200.78	.20-10 ⁻¹¹	43.03	.10-10 ⁻⁹	305.98	.31	142.58	.18-10 ⁻¹³	223.59	32.14	310.90		
SLOSH 70"	*-.2012	6.18	4.09	136.16	210.63	.66	158.48	.29	158.48	1.07	225.43	.24-10 ⁻⁵	286.74	.96-10 ⁻⁵	194.17	81.75	189.82	.54-10 ⁻⁴	202.41	12.14	93.57		
DIA. TANK	**-.3420	10.52	29.80	209.53	126.37	.72	211.28	2.16	211.28	2.89	61.37	.18-10 ⁻⁶	23.68	.52-10 ⁻⁶	302.28	56.51	174.93	.34-10 ⁻⁵	184.26	7.92	100.98		
SLOSH 105"	*-.1797	5.04	4.76	287.04	140.30	.84	103.38	.52	103.38	.98	192.35	.32-10 ⁻⁵	283.79	.14-10 ⁻⁴	191.27	80.68	186.00	.33-10 ⁻⁵	202.00	12.22	94.31		
DIA. TANK	**-.2790	8.59	27.67	32.76	209.26	3.90	214.25	2.00	214.25	2.49	200.82	.12-10 ⁻⁶	310.41	.43-10 ⁻⁵	10.23	57.82	197.12	.45-10 ⁻⁴	142.00	6.11	78.88		
CONTROL P	-1.5740	1.89	2.90	273.01	94.72	.31	92.79	.35	92.79	.24	281.23	.14-10 ⁻⁷	184.81	.0264	263.21	69.85	199.95	.22-10 ⁻³	156.01	26.36	90.47		
SWIVEL P	-4.8370	94.06	3.20	295.74	114.80	2.73	109.41	9.69	109.41	56.08	227.49	.1087	269.12	.28-10 ⁻⁶	8.15	.71	115.14	.32-10 ⁻⁶	141.84	27.59	357.45		
SWIVEL R	-6.151	89.83	.2-10 ⁻⁷	212.00	.11-10 ⁻⁷	2.5	19.00	.8-10 ⁻⁷	19.00	.5-10 ⁻⁸	3.0	.23-10 ⁻²	222	99.8	121	.3-10 ⁻⁸	28.00	.15-10 ⁻¹²	43.60	.85-10 ⁻⁷	83.19		
CONTROL R	-8.38	2.310	.53-10 ⁻⁹	290.00	.73-10 ⁻⁹	121.9	302.1	.99-10 ⁻⁹	302.1	.105-10 ⁻¹⁰	119.5	.48-10 ⁻⁵	151.6	.36-10 ⁻⁴	60.72	.21-10 ⁻⁸	118.2	.99.6	180.0	.33-10 ⁻⁷	170.1		

$\xi_1 = 0.002$

$\xi_{dr} = 0.065$

* 1st Mode

** 2nd Mode

 $S_{11} = 0.002$ $S_{11f} = 0.065$

* 1st Mode

** 2nd Mode

TABLE 4

RATE GYRO
LOCAL α -METER

Q = 0

WITH SLOSHING

AMOUNT OF β FROM EACH VARIABLE (β_{min})

60 sec's

SA-1

ROOT			BENDING MODES												TORSIONAL MODES						ROLL		ANGLE-OF-ATTACK	
		IMAG.	1st Mode		2nd Mode		3rd Mode		4th Mode		1st Mode		2nd Mode		PITCH		PHASE		PHASE		ANGLE-OF-ATTACK			
REAL			%	PHASE	%	PHASE	%	PHASE	%	PHASE	%	PHASE	%	PHASE	%	PHASE	%	PHASE	%	PHASE	%			
B. MODE 1	-0.5910	21.58	87.57	183.16	1.17	214.77	1.10	216.12	0.64	41.84	$0.72 \cdot 10^{-11}$	41.28	$0.28 \cdot 10^{-10}$	308.04	3.26	35.96	$0.36 \cdot 10^{-11}$	58.28	6.26		147.13			
B. MODE 2	-.0067	46.54	1.47	270.46	41.11	265.00	1.52	272.26	3.07	87.37	$.62 \cdot 10^{-12}$	296.37	$.82 \cdot 10^{-11}$	27.05	1.88	86.32	$.63 \cdot 10^{-12}$	173.64	50.95		216.06			
B. MODE 3	-.2500	65.73	2.45	239.34	2.14	56.39	50.61	244.20	7.49	61.95	$.29 \cdot 10^{-12}$	93.22	$.41 \cdot 10^{-10}$	188.57	1.38	62.52	$.24 \cdot 10^{-13}$	281.67	35.93		39.19			
B. MODE 4	-1.8790	91.45	1.60	328.32	1.43	148.47	5.14	144.71	56.71	201.51	$.20 \cdot 10^{-11}$	43.03	$.10 \cdot 10^{-9}$	305.98	.29	138.68	$.18 \cdot 10^{-13}$	223.59	34.83		324.25			
SLOSH 70"	* -.2010	6.18	3.26	139.74	.66	206.75	.27	156.32	1.10	219.30	$.24 \cdot 10^{-5}$	286.74	$.96 \cdot 10^{-5}$	194.17	82.57	189.30	$.54 \cdot 10^{-4}$	202.41	12.14		93.60			
DIA. TANK	** -.3420	10.52	29.82	210.37	.72	123.75	2.13	211.10	2.88	62.47	$.18 \cdot 10^{-6}$	23.68	$.52 \cdot 10^{-6}$	302.28	56.56	174.58	$.54 \cdot 10^{-5}$	184.26	7.89		101.12			
SLOSH 105"	* -.1800	5.04	4.78	283.16	.78	138.11	.51	100.35	.98	191.63	$.32 \cdot 10^{-5}$	283.79	$.14 \cdot 10^{-4}$	191.27	80.68	185.95	$.33 \cdot 10^{-5}$	202.00	12.27		94.77			
DIA. TANK	** -.2790	8.59	27.26	33.74	3.87	210.67	1.98	215.88	2.49	200.85	$.12 \cdot 10^{-6}$	310.41	$.43 \cdot 10^{-5}$	10.23	58.20	197.18	$.45 \cdot 10^{-4}$	142.00	6.20		79.93			
TORSTION 1	* -.3876	28.10	$.73 \cdot 10^{-6}$	186.73	$.93 \cdot 10^{-7}$	195.58	$.62 \cdot 10^{-7}$	196.47	$.57 \cdot 10^{-7}$	15.91	97.79	184.81	.0284	263.21	.0015	14.92	2.098	15.82	$.12 \cdot 10^{-6}$		150.64			
TORSTION 2	** -1.4460	130.66	$.31 \cdot 10^{-6}$	298.49	$.44 \cdot 10^{-6}$	119.84	$.58 \cdot 10^{-5}$	302.10	$.63 \cdot 10^{-6}$	118.83	.1087	269.12	99.02	8.15	$.69 \cdot 10^{-7}$	118.83	.868	104.08	$.197 \cdot 10^{-4}$		168.66			

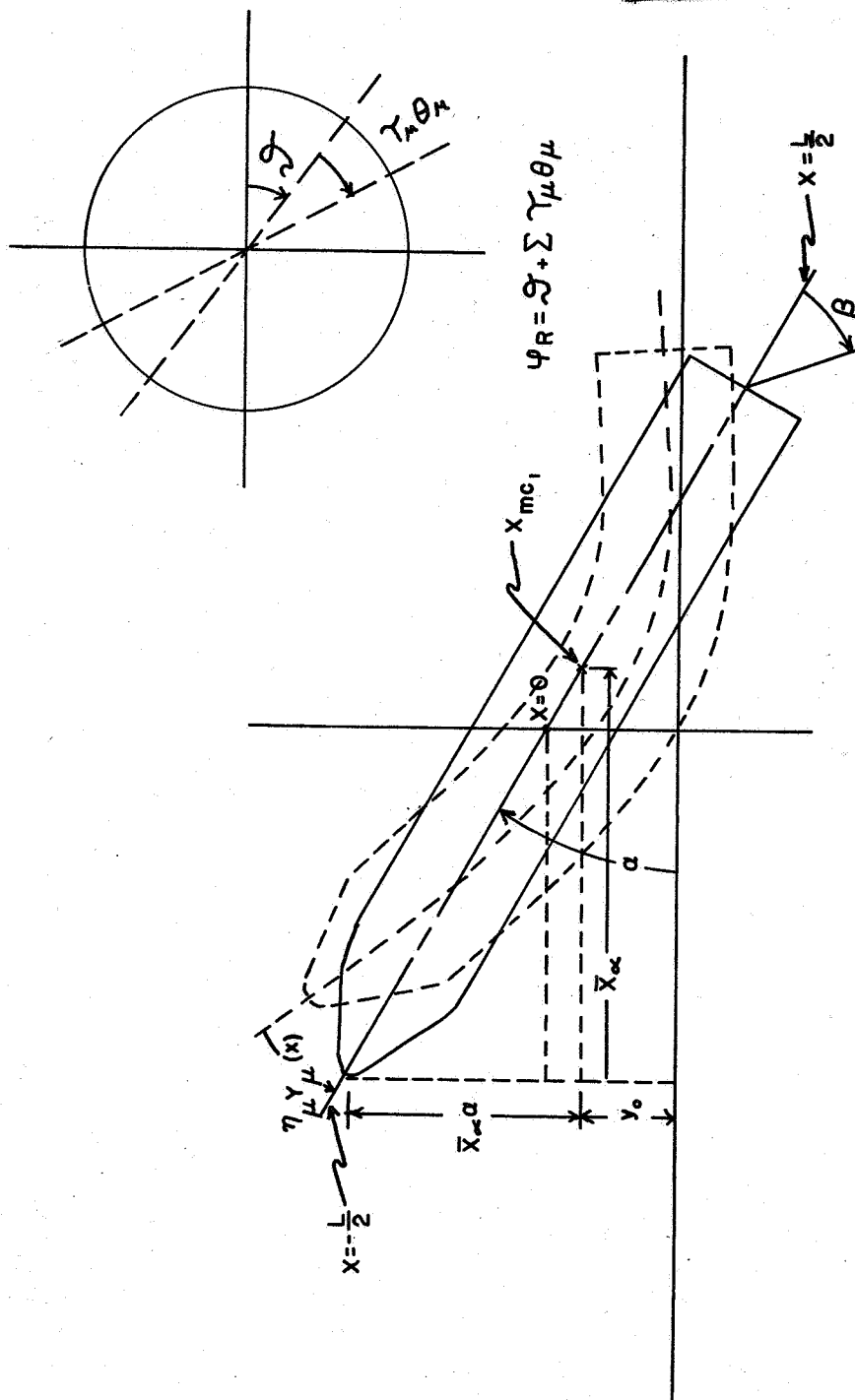
$\xi_1 = 0.002$

* 1st Mode
** 2nd Mode

$\xi_1 = 0.002$

* 1st Mode

** 2nd Mode



$$\begin{aligned}
 \eta_{\mu} \gamma_{\mu}(x) &= \text{BENDING DEFLECTION} \\
 y_0 - \bar{x}_{\alpha} a &= \text{RIGID MISSILE DEFLECTION} \\
 y = y_0 - \bar{x}_{\alpha} a + \sum_{\mu=1}^n \eta_{\mu} \gamma_{\mu}(x) &= \text{TOTAL DEFLECTION} \\
 - \sum_{\mu=1}^n \eta_{\mu} \gamma_{\mu}(x) &= \text{ANGULAR DEFLECTION DUE TO BENDING} \\
 a - \sum_{\mu=1}^n \eta_{\mu} \gamma_{\mu}(x) &= \text{TOTAL ANGULAR DEFLECTION} \\
 \beta &= \text{ENGINE DEFLECTION ANGLE}
 \end{aligned}$$

FIGURE 1

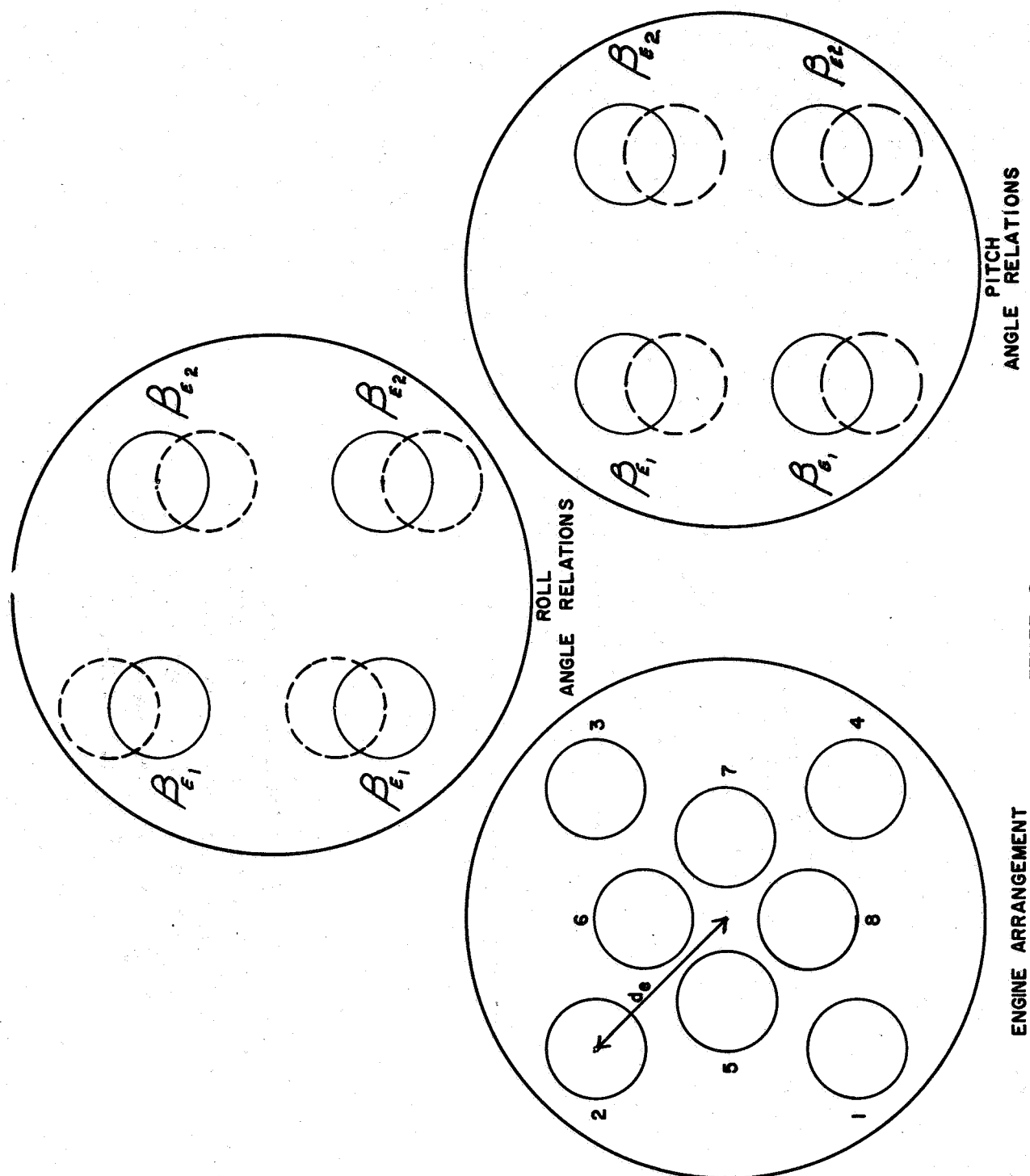
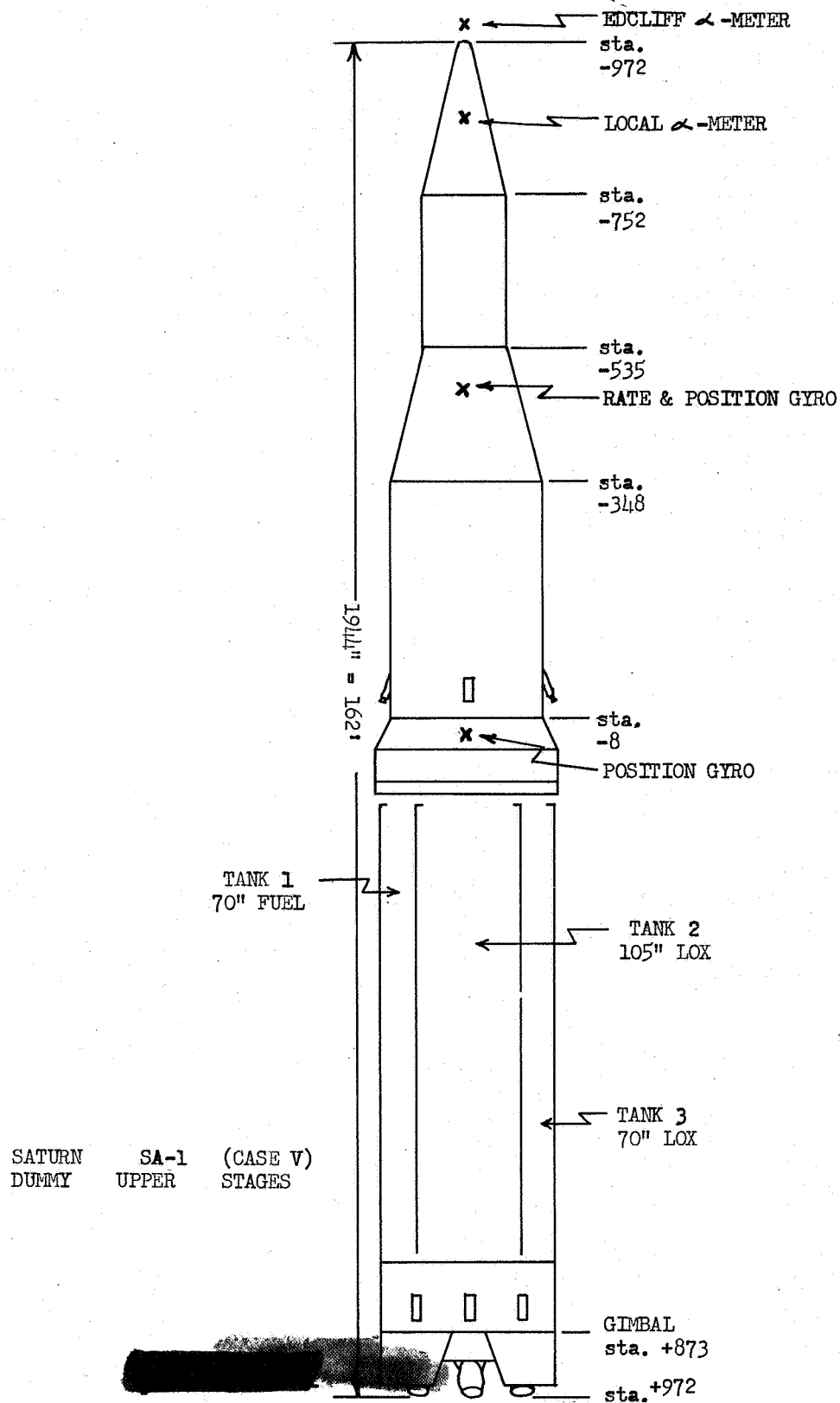


FIGURE 2

FIGURE 3



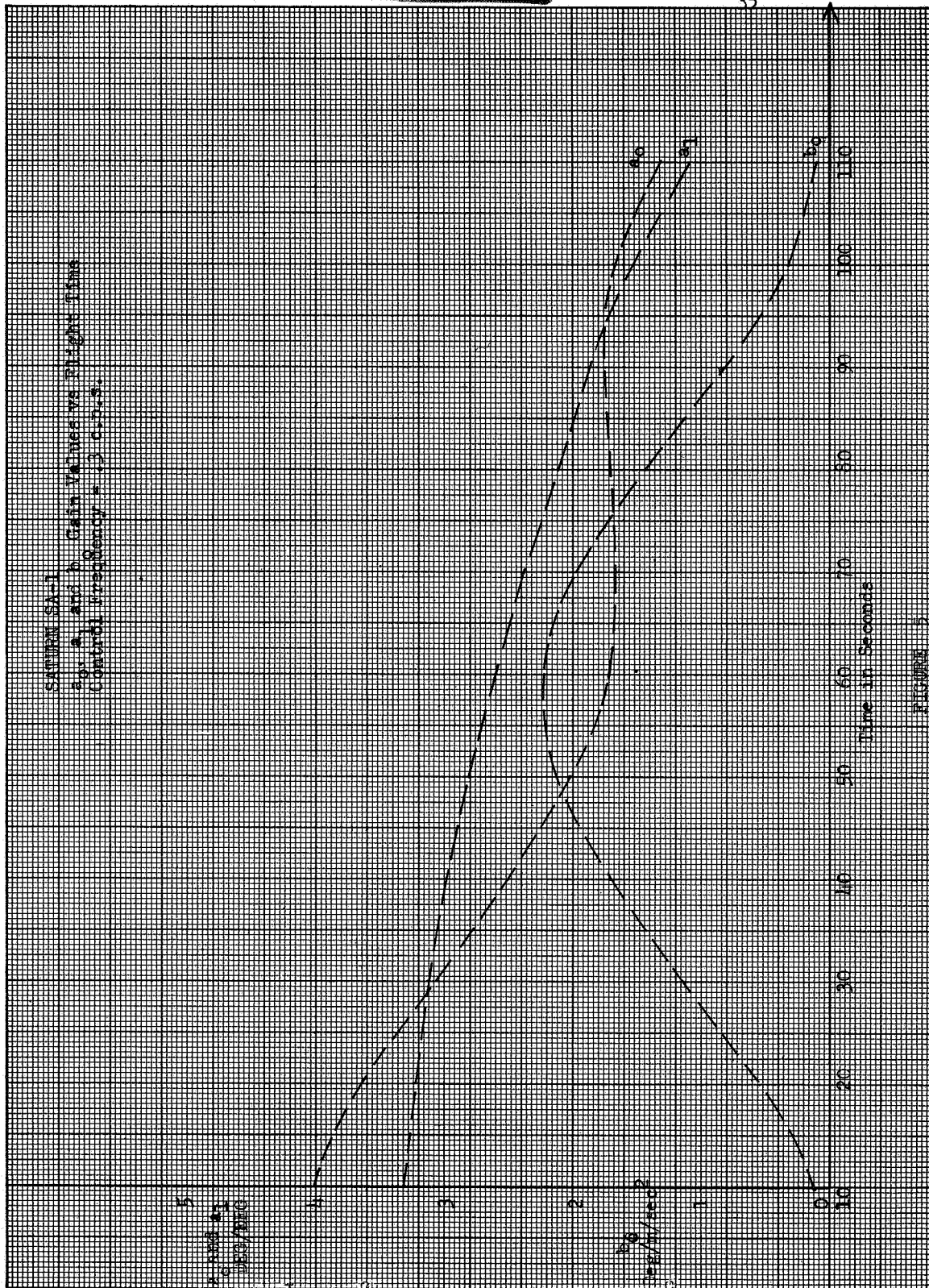


FIGURE 1

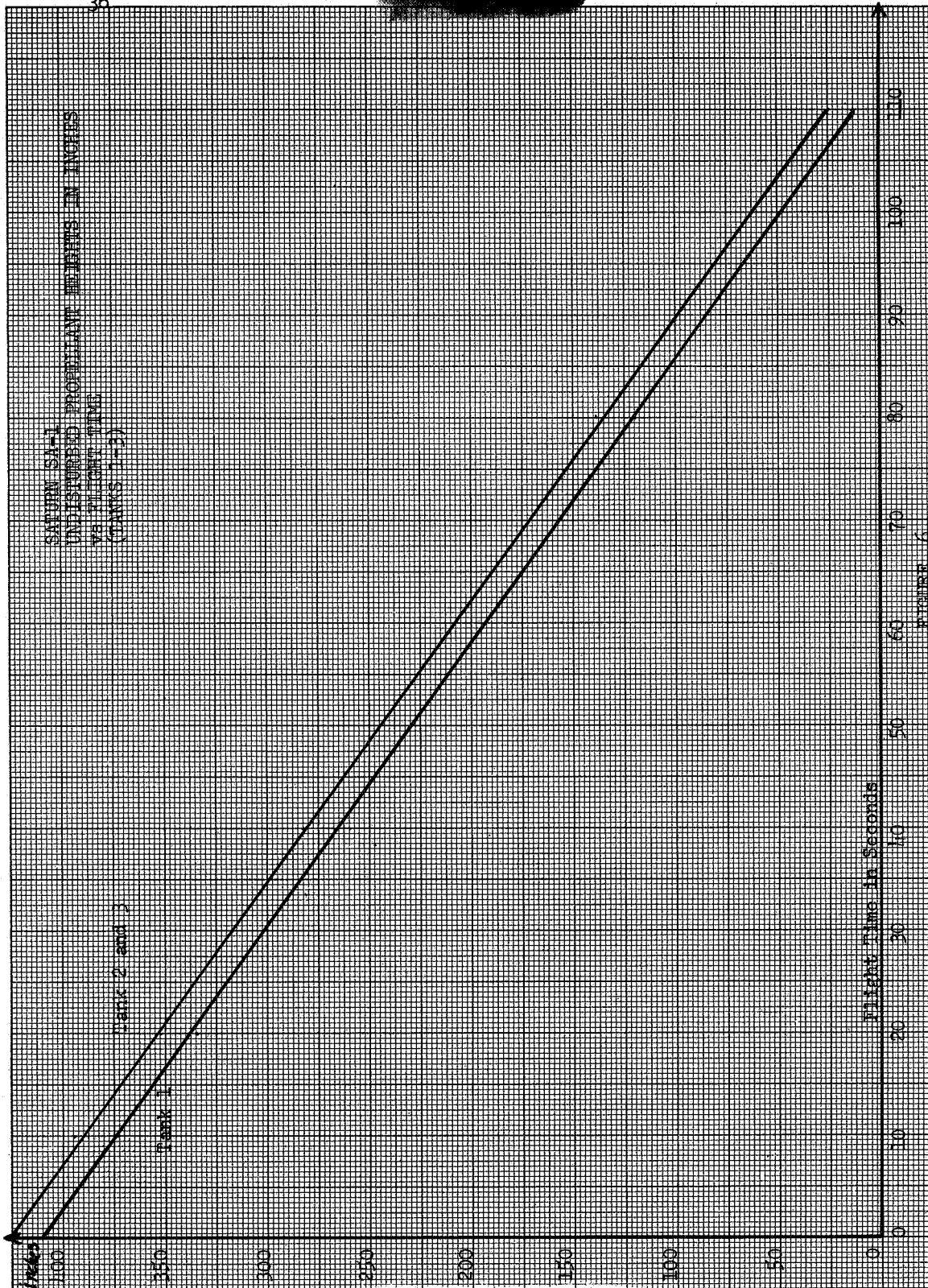


FIGURE 6

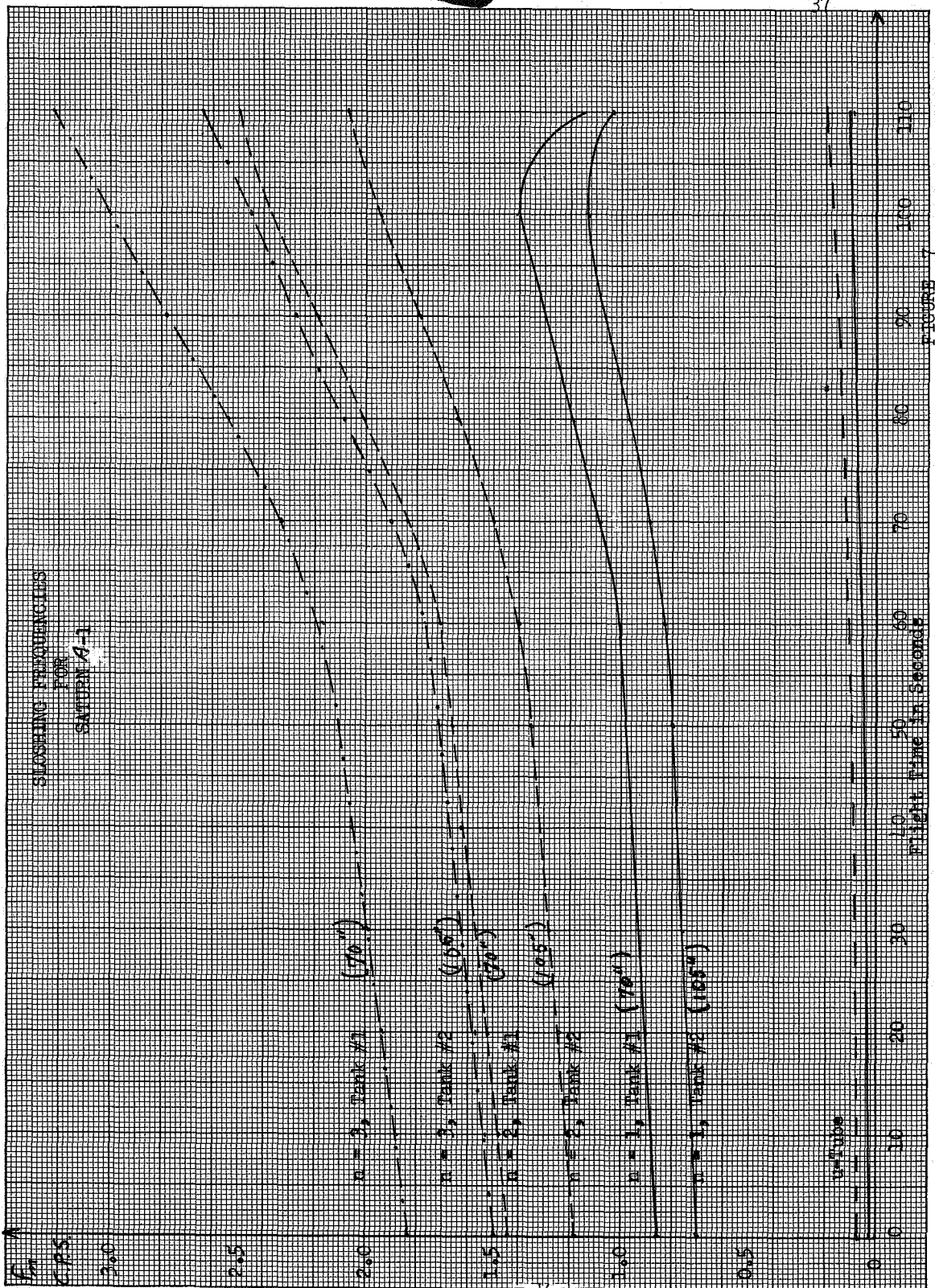
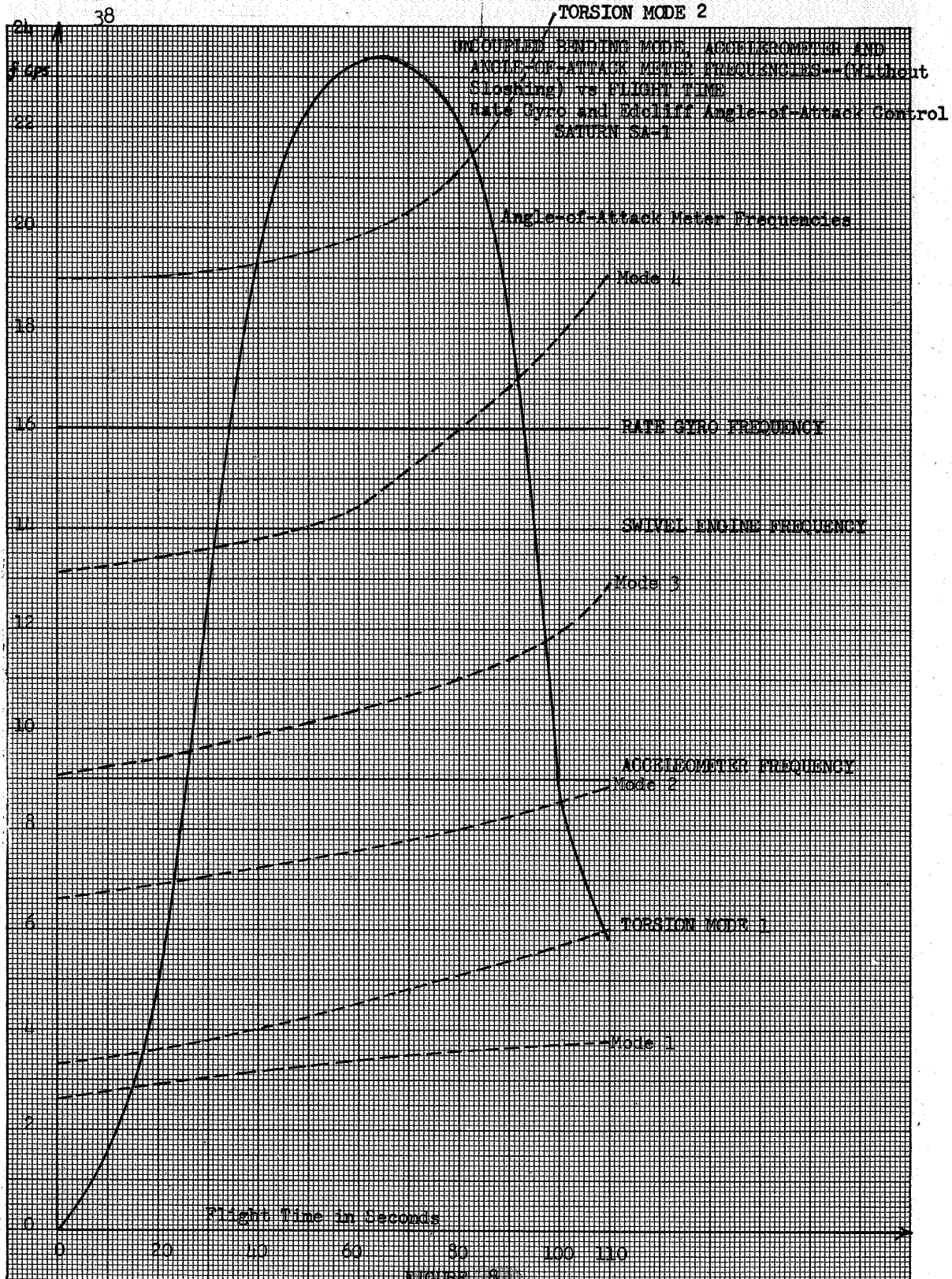


FIGURE 7

CONFIDENTIAL



CONFIDENTIAL

CONFIDENTIAL

39

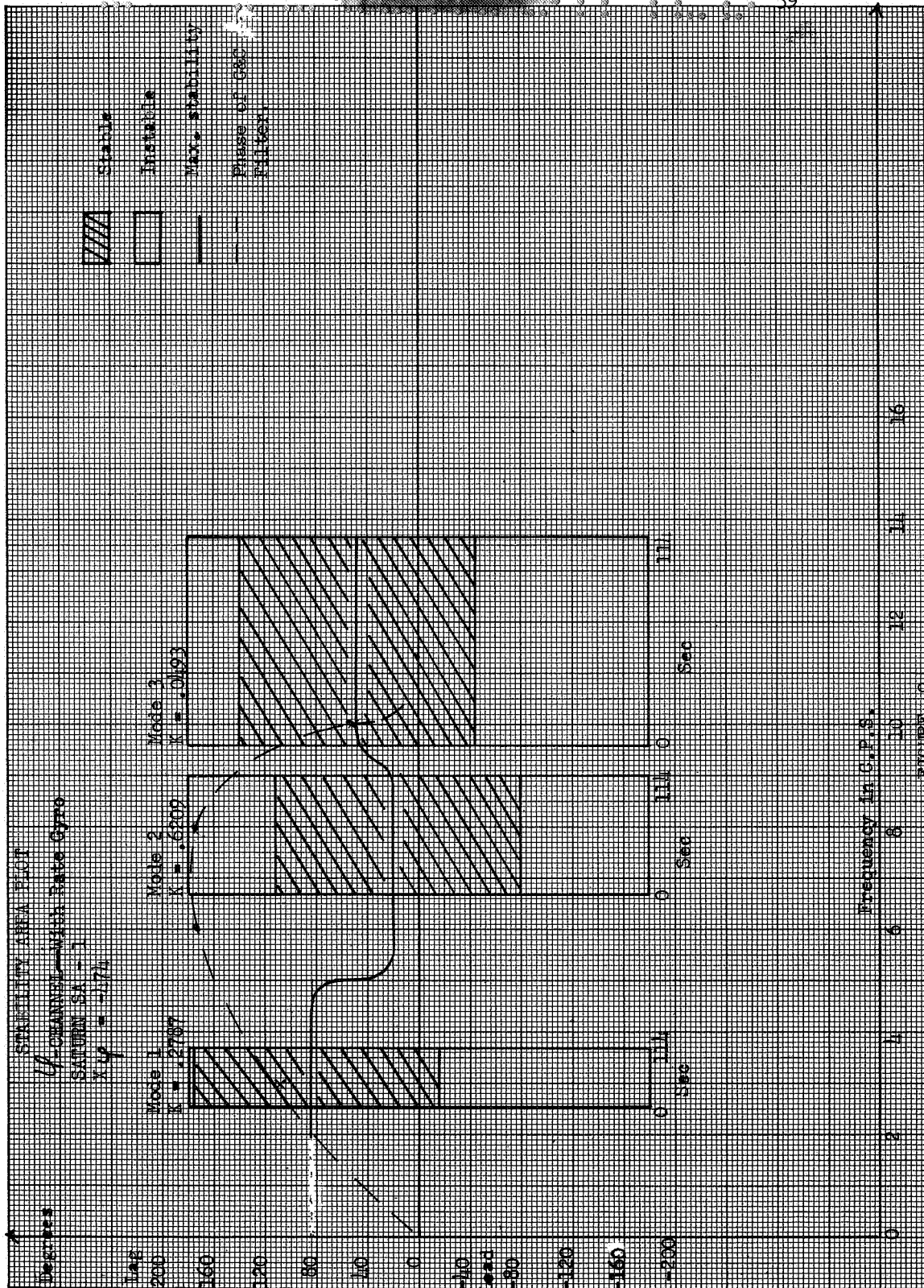
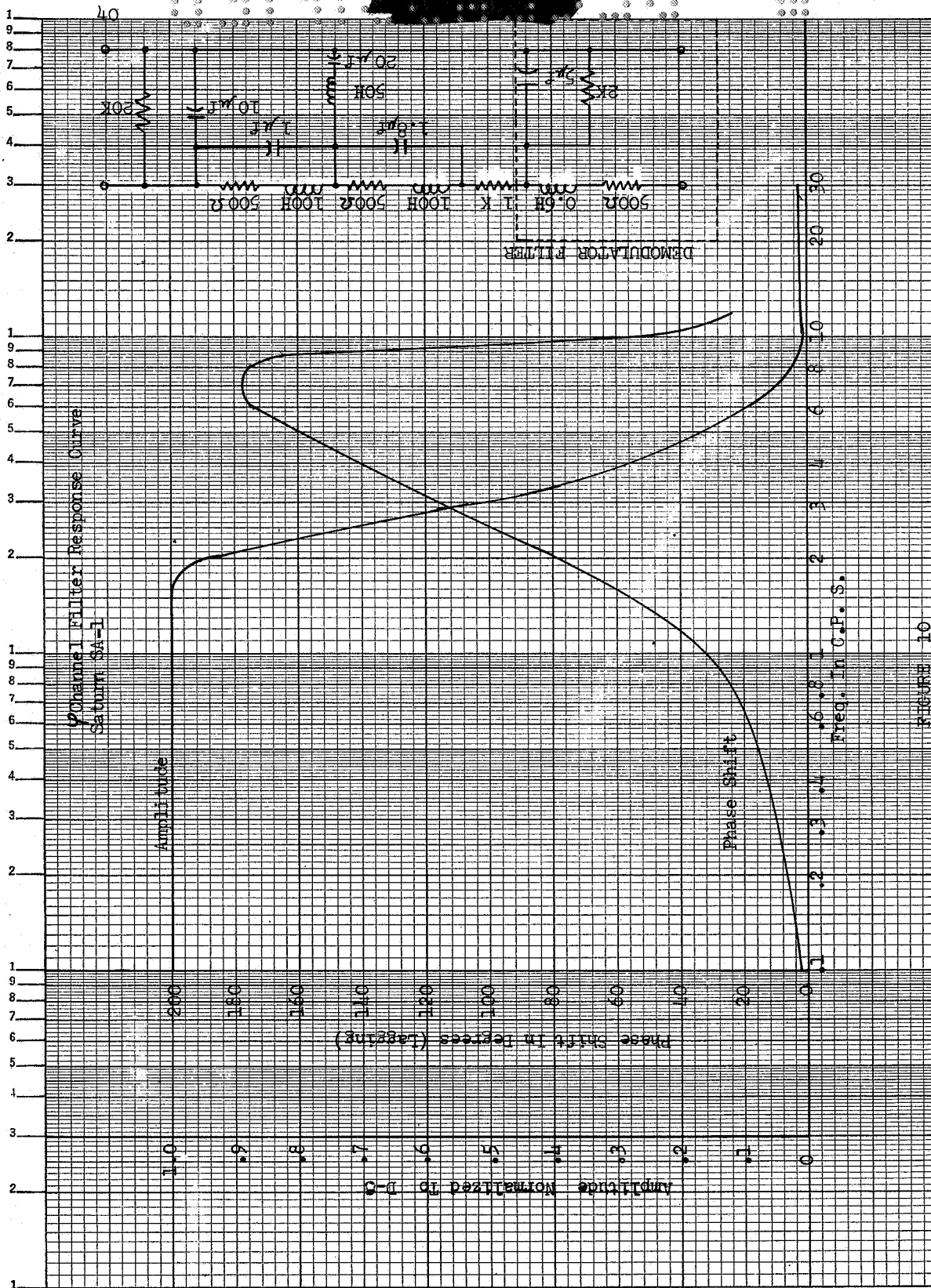
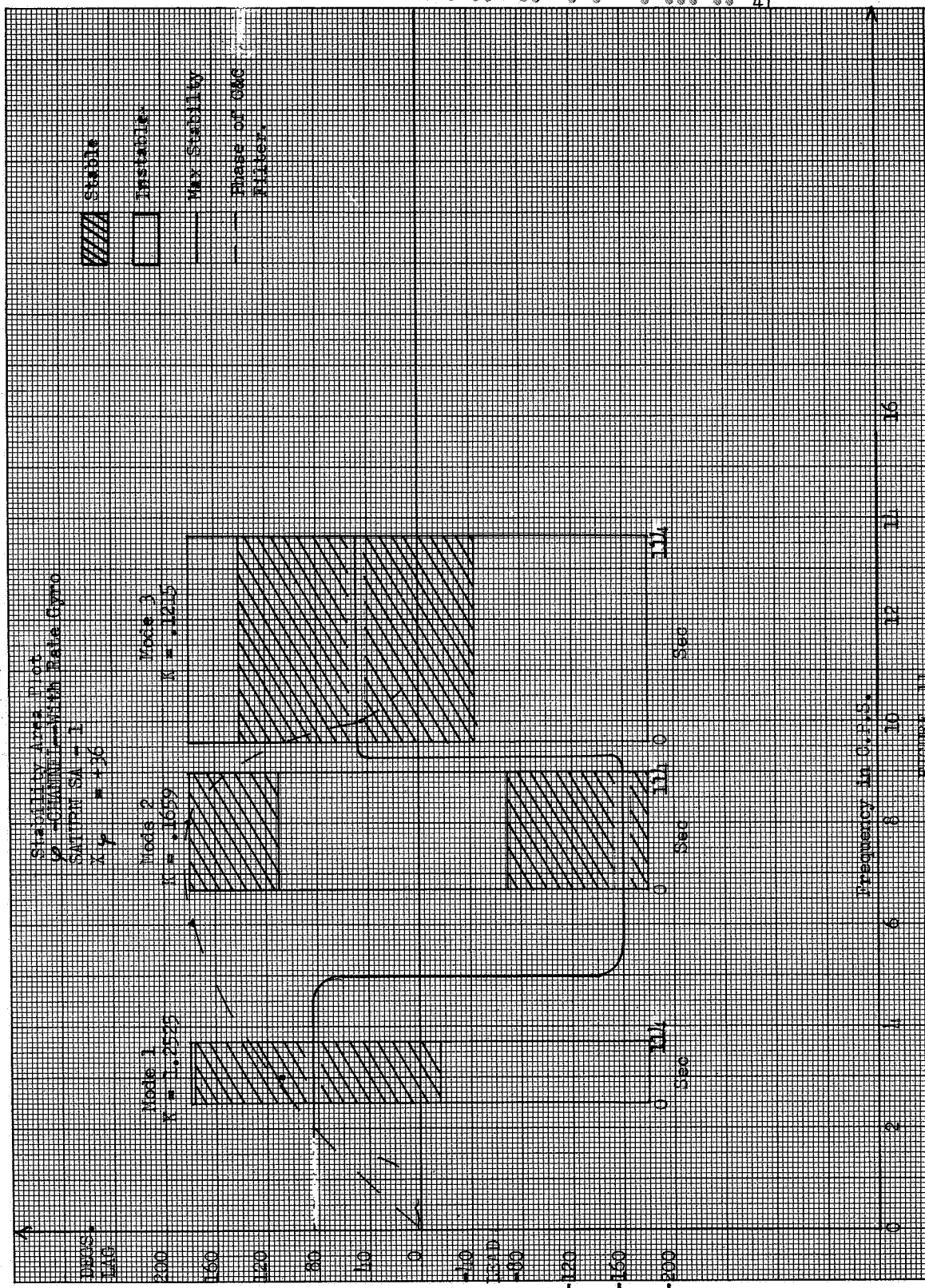
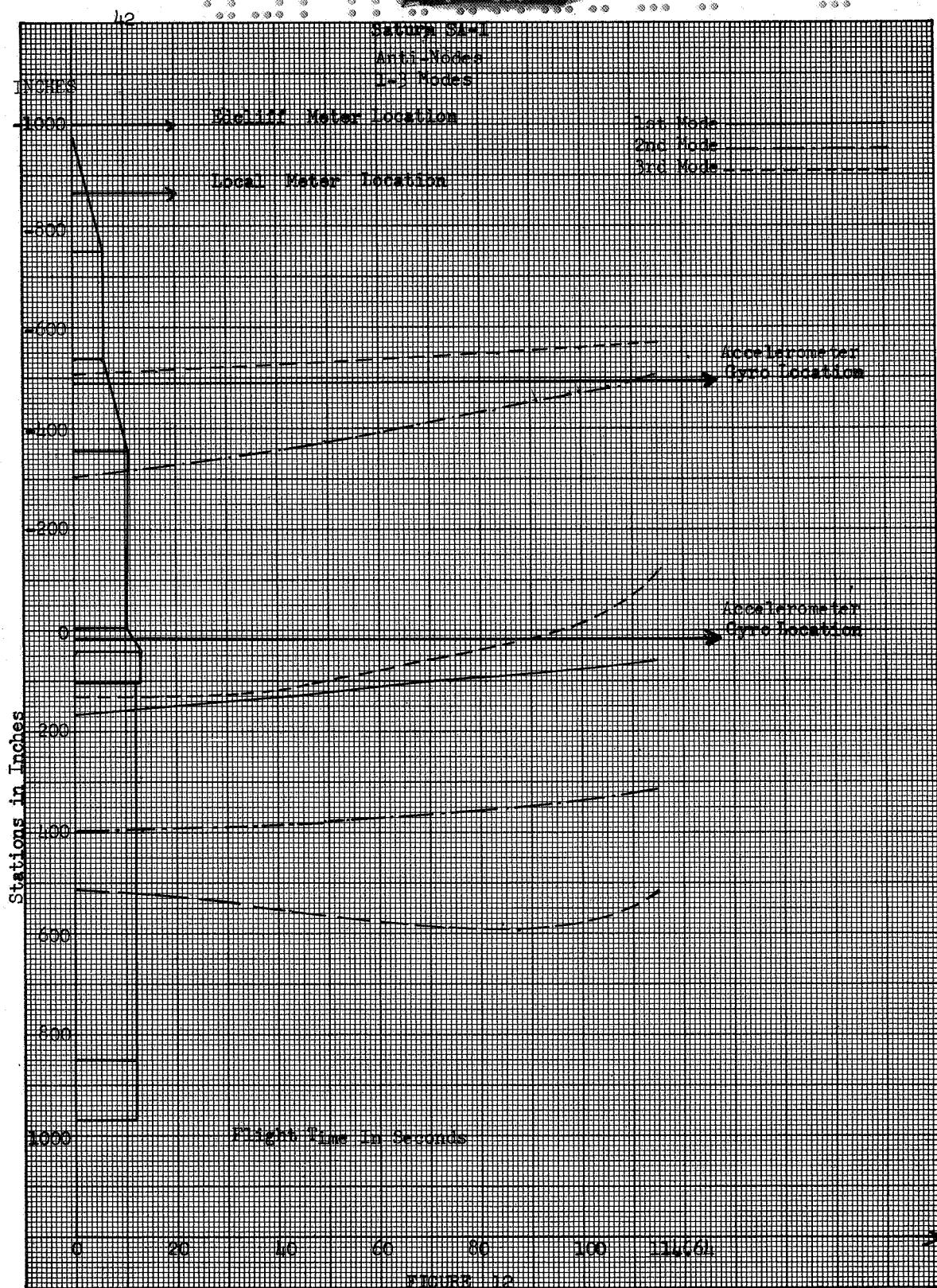


FIGURE 9

CONFIDENTIAL







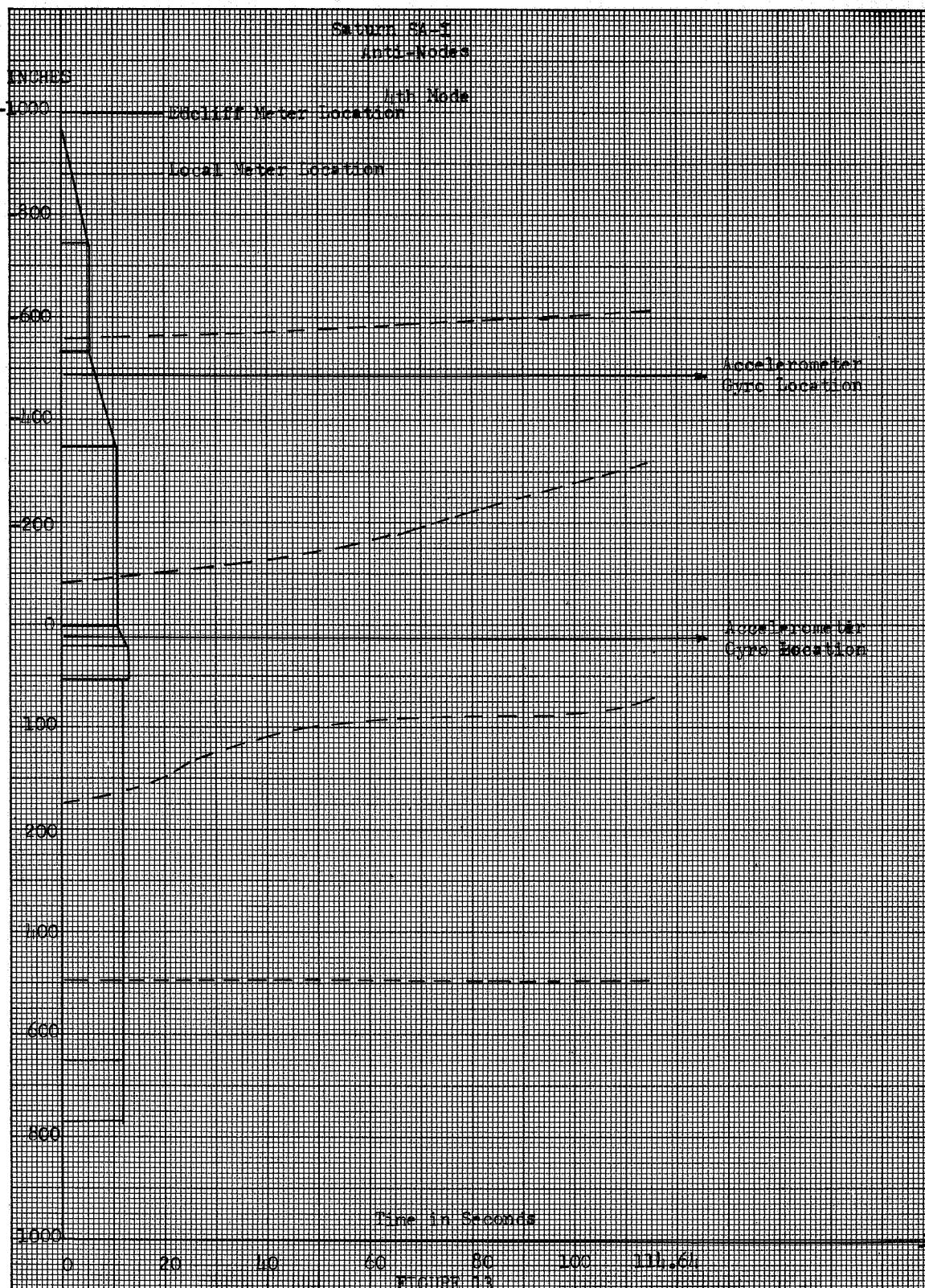
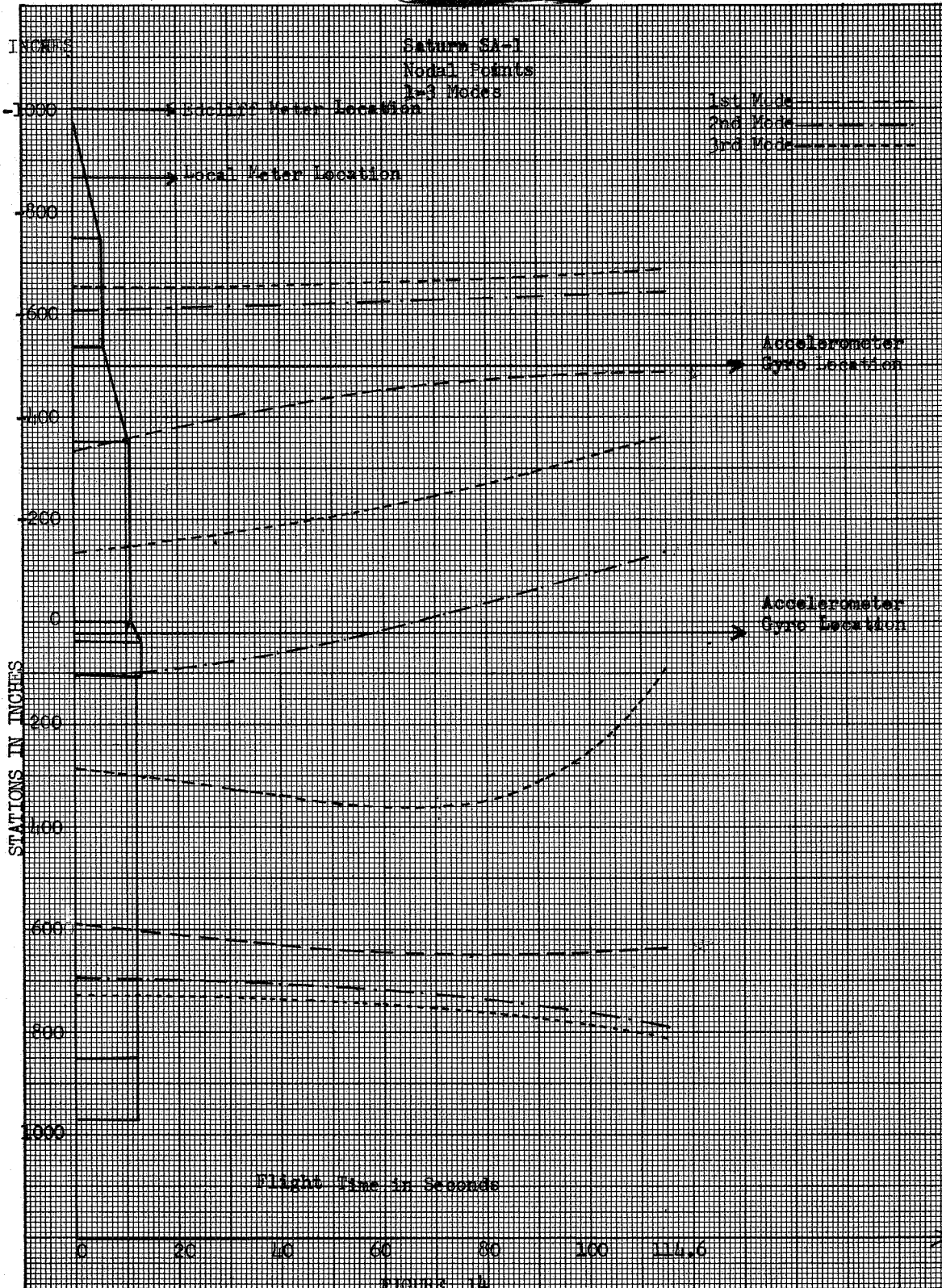
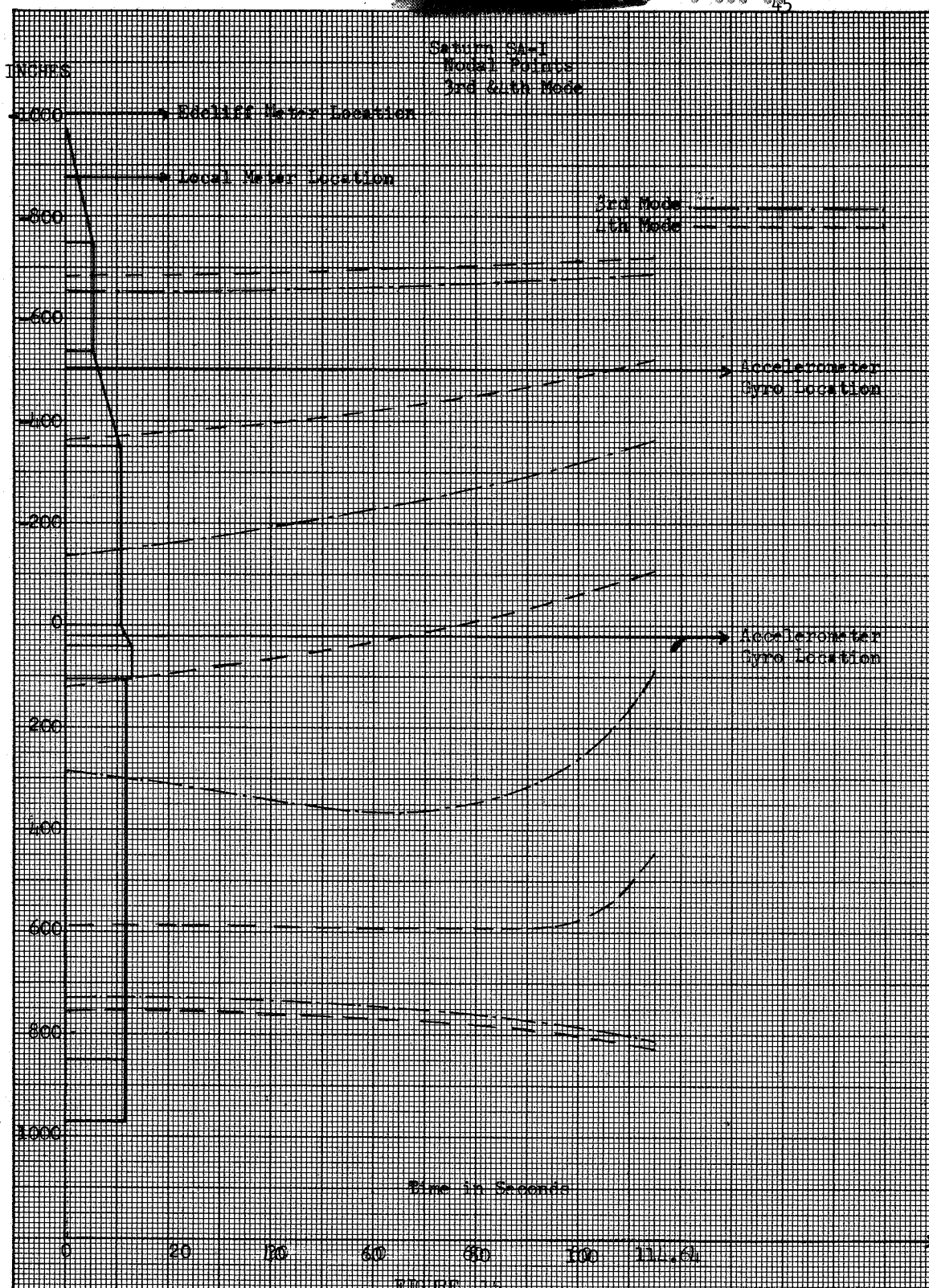
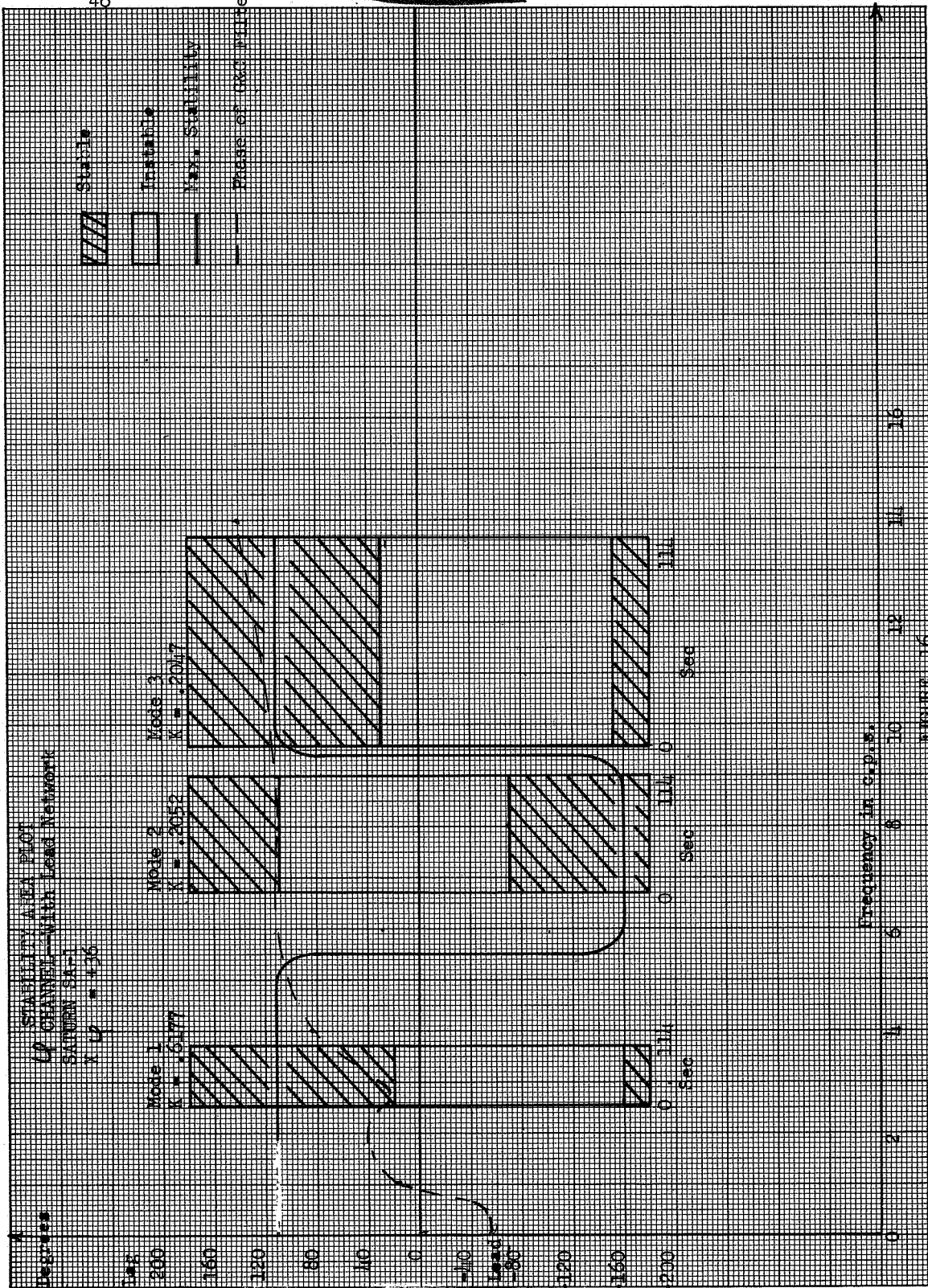
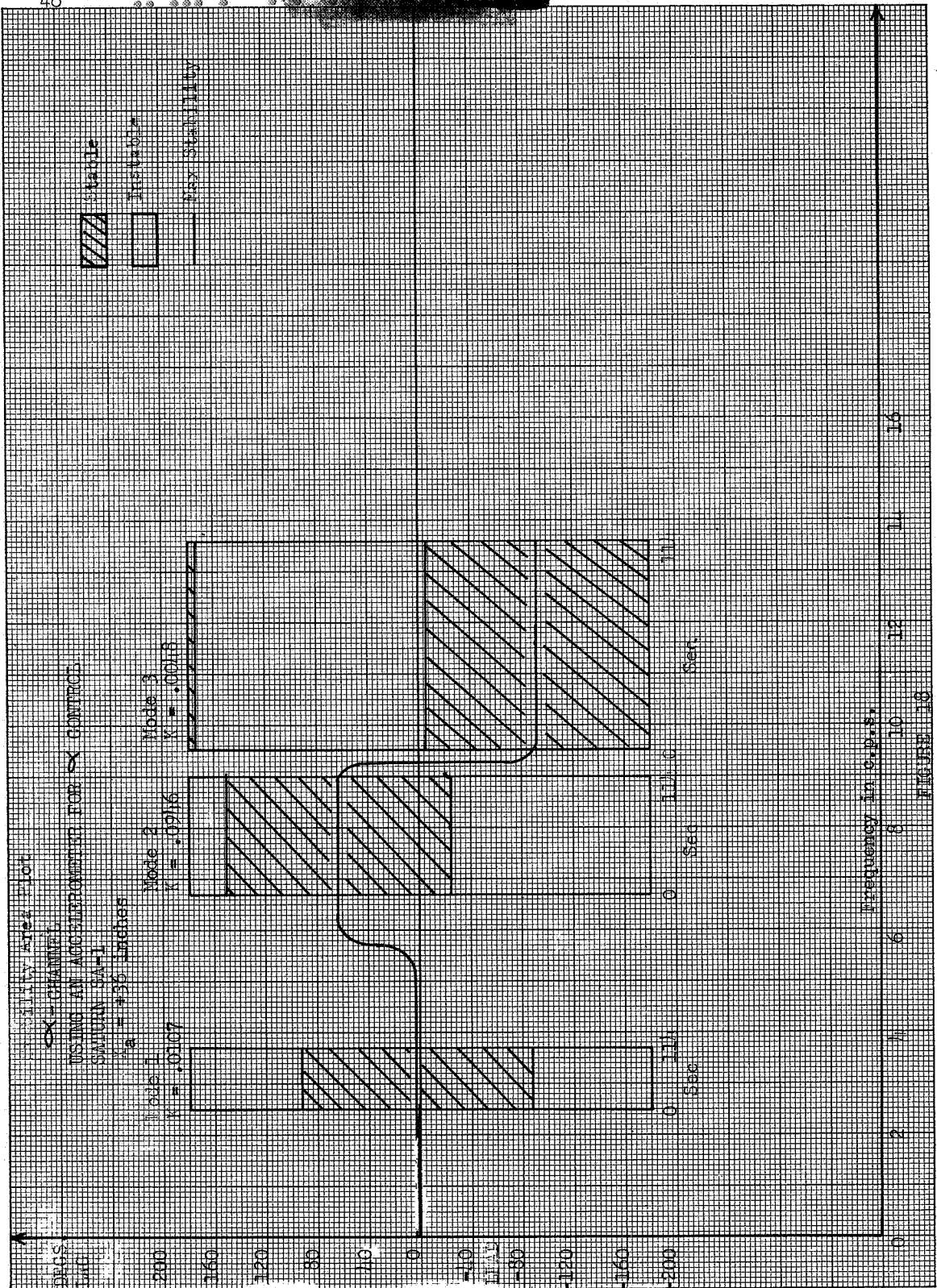


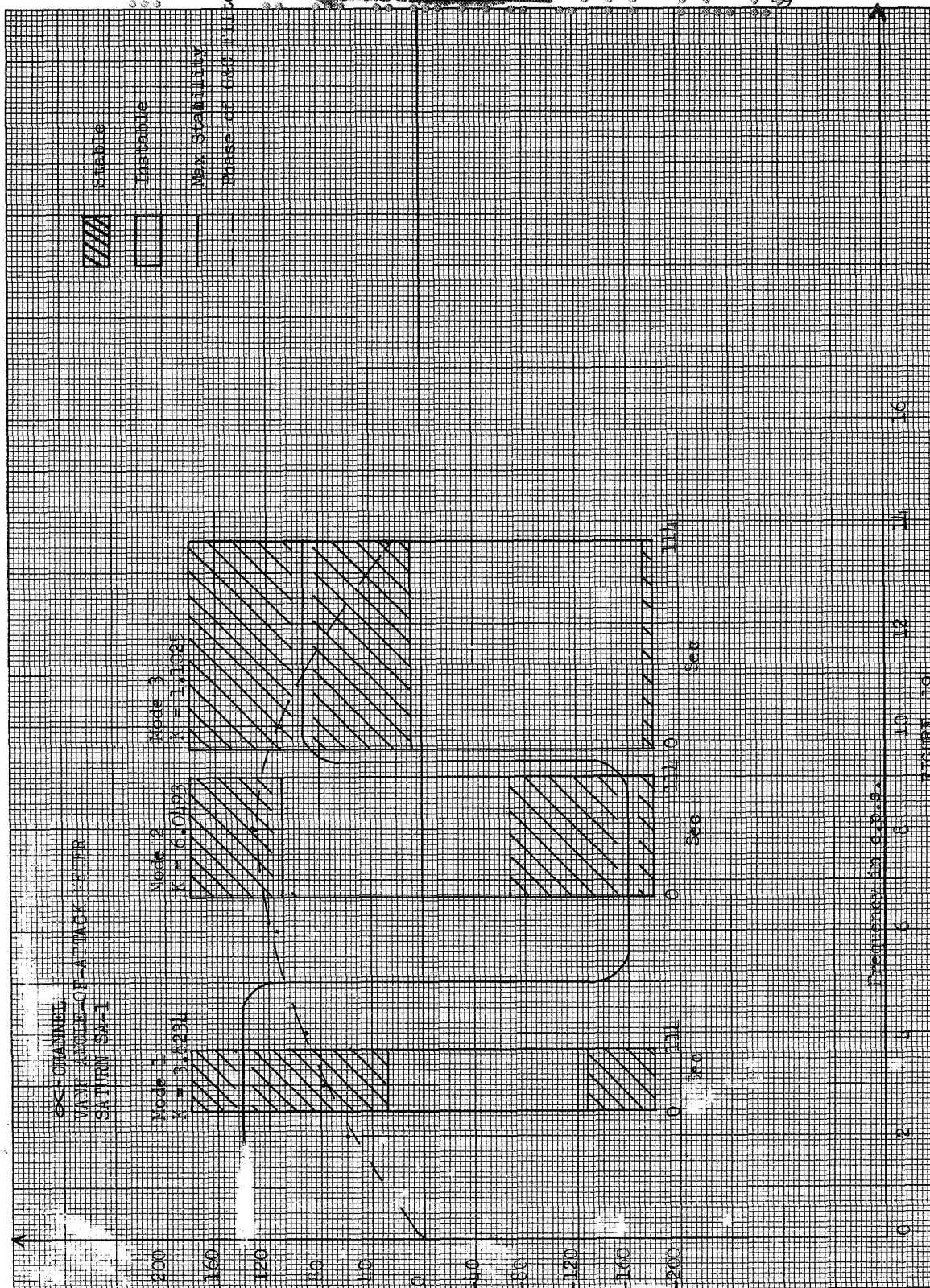
FIGURE 13

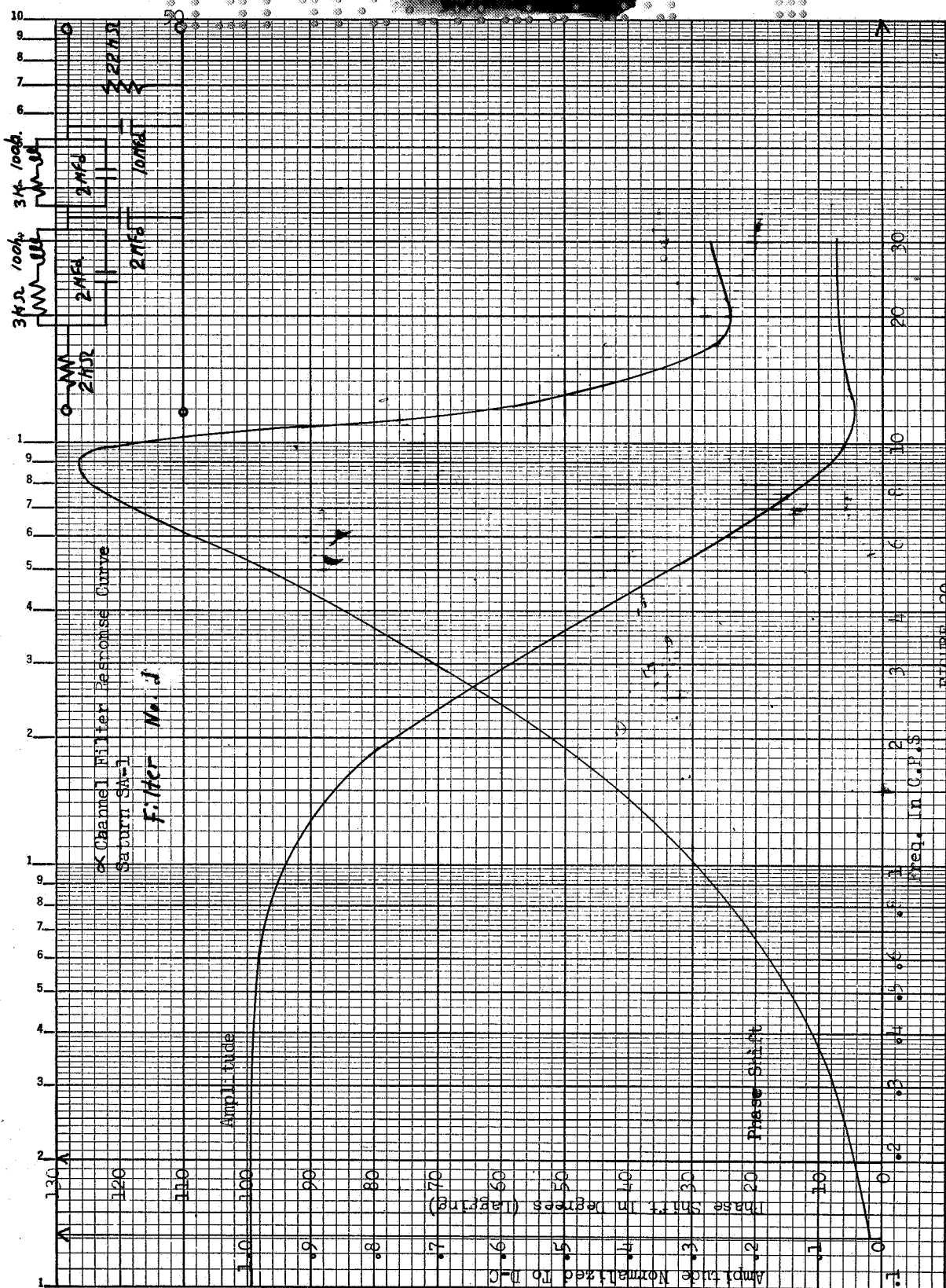












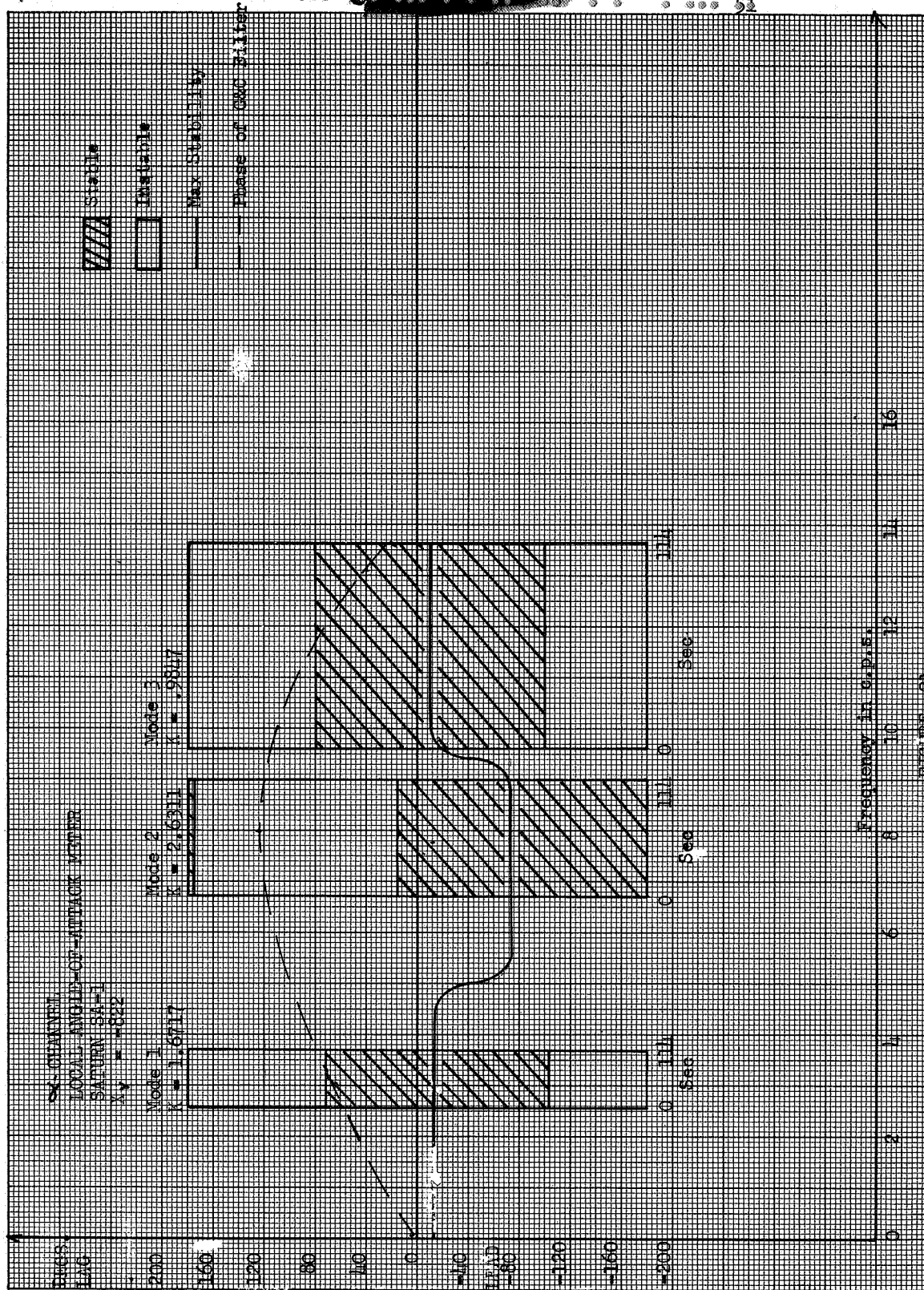
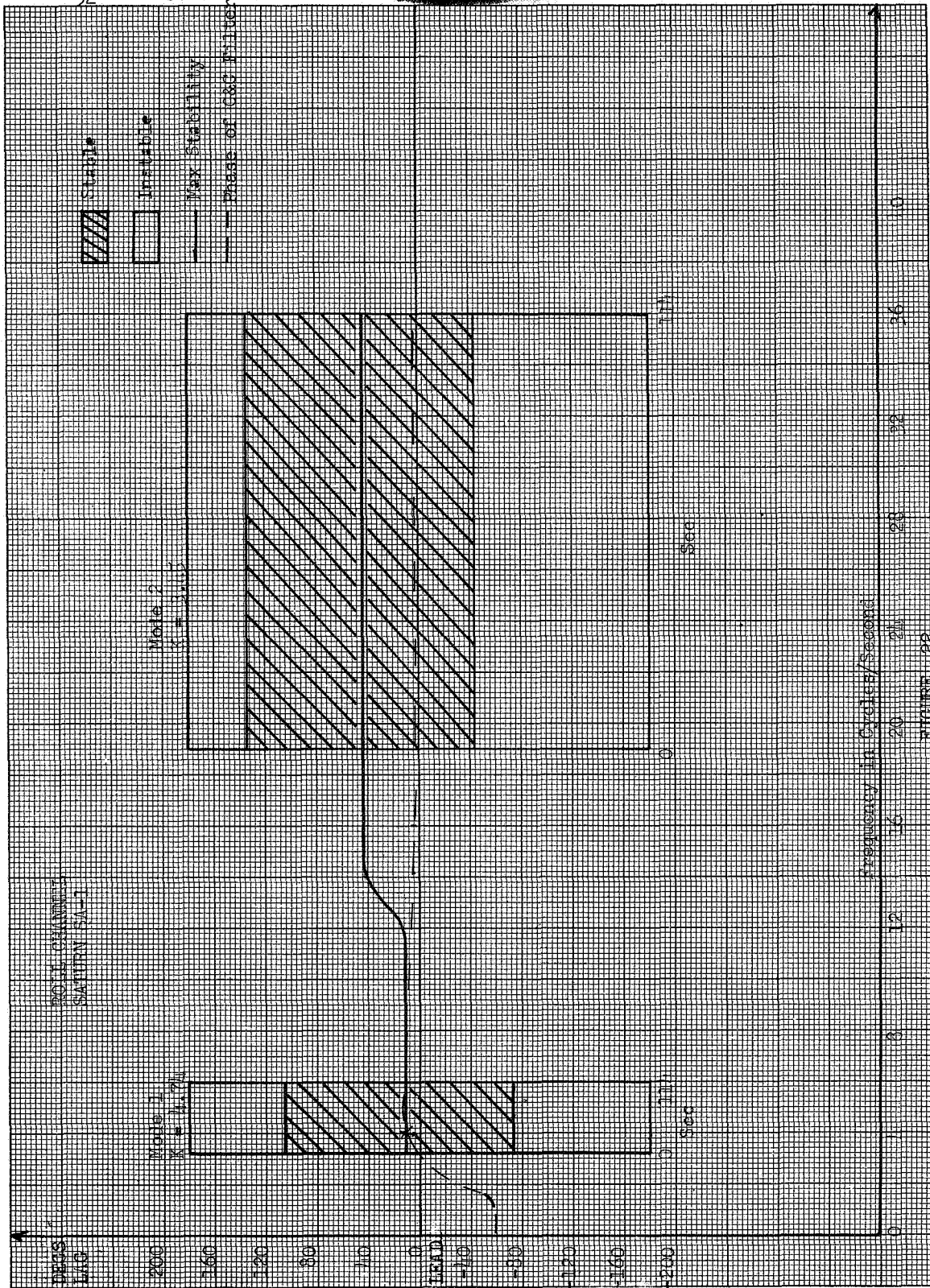


FIGURE 21



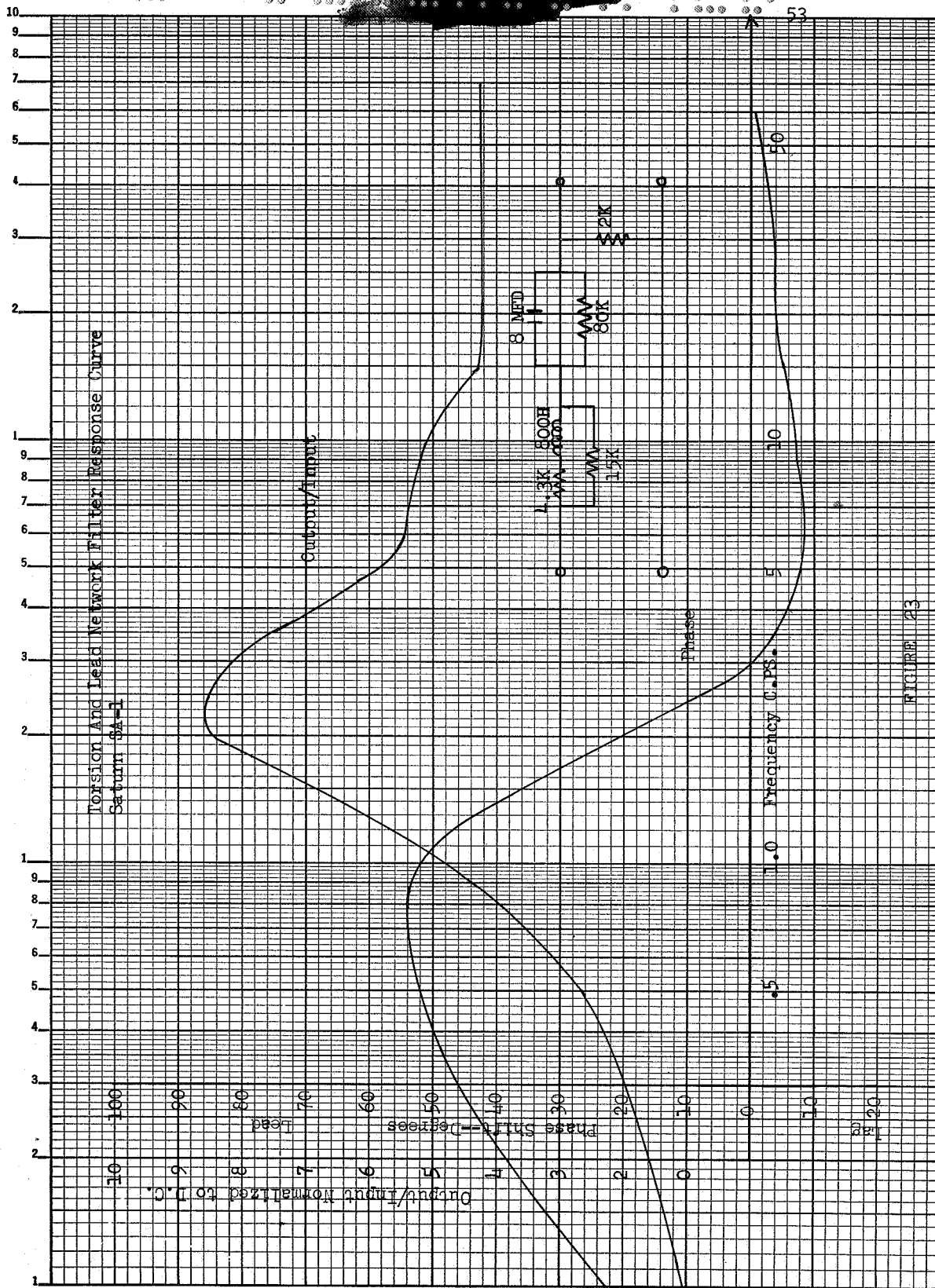


FIGURE 23

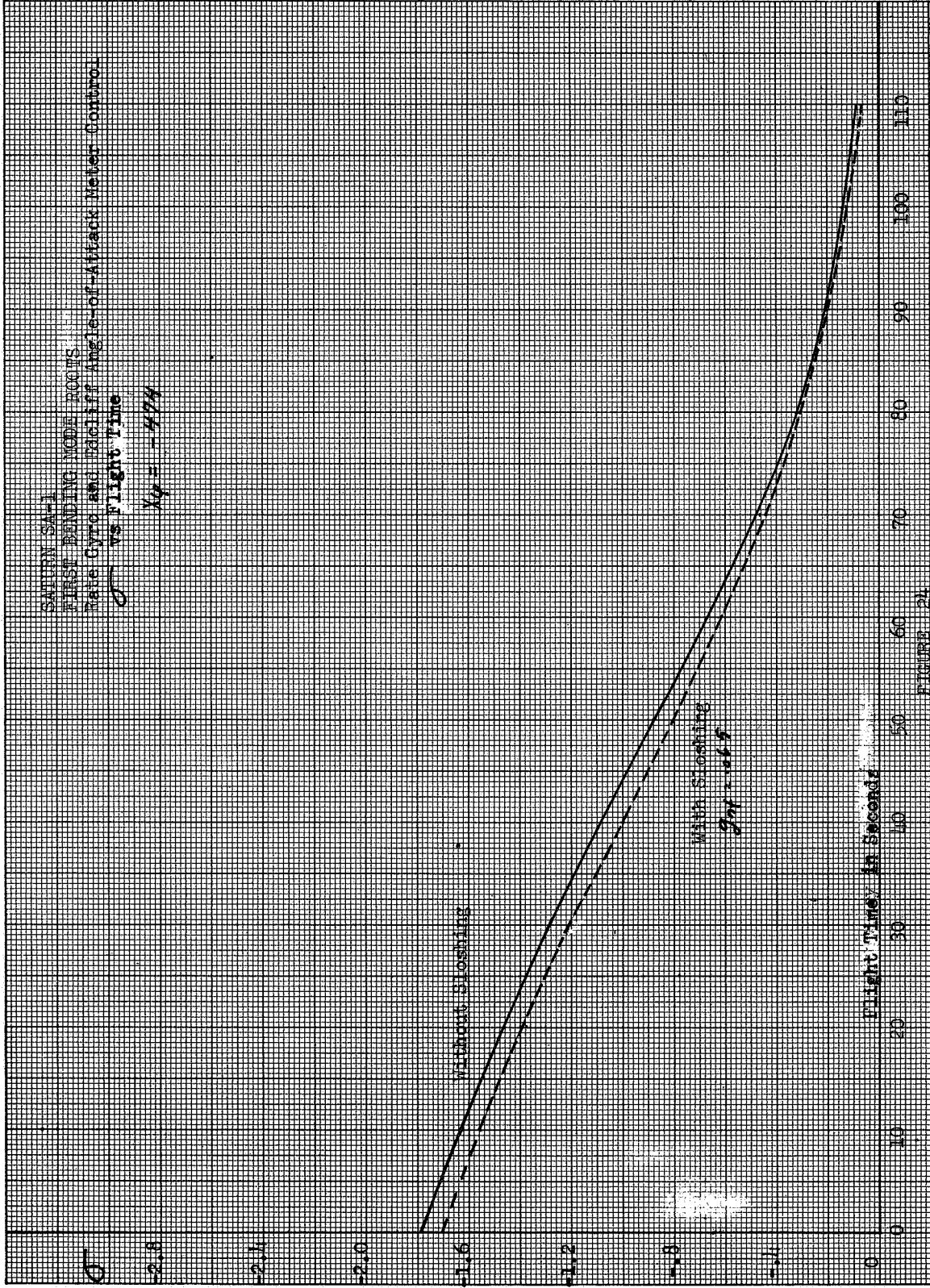


FIGURE 24

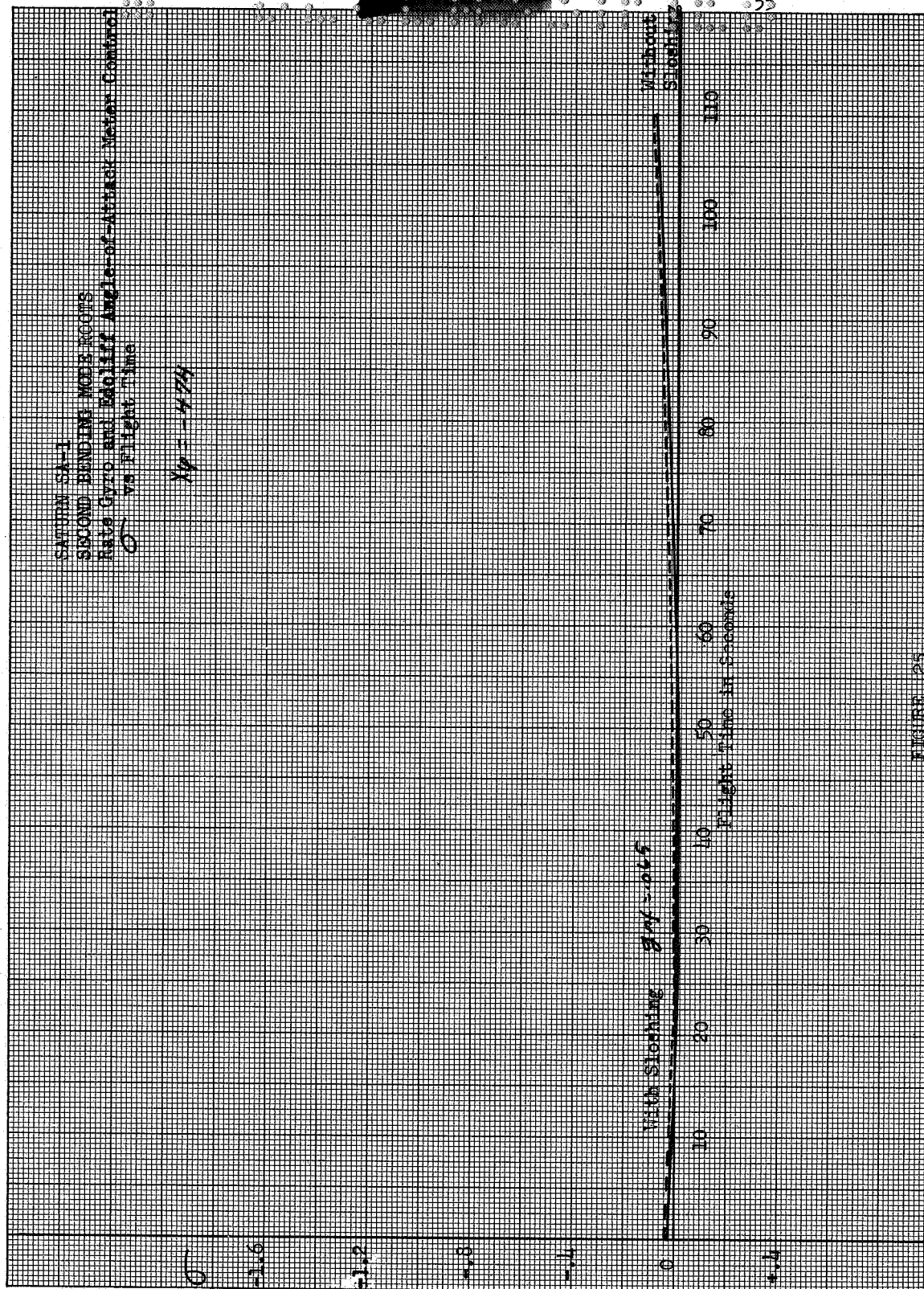


FIGURE 25

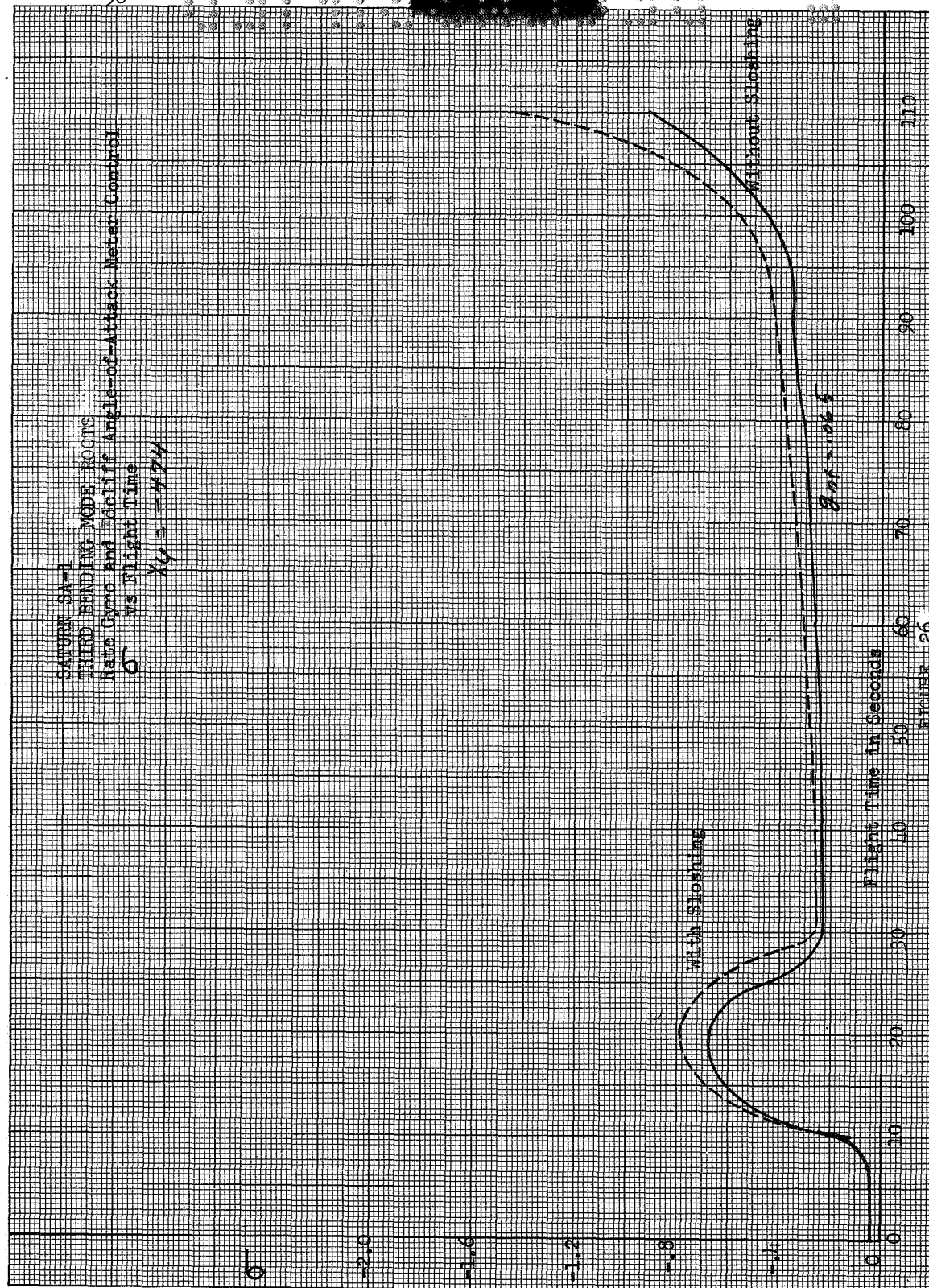
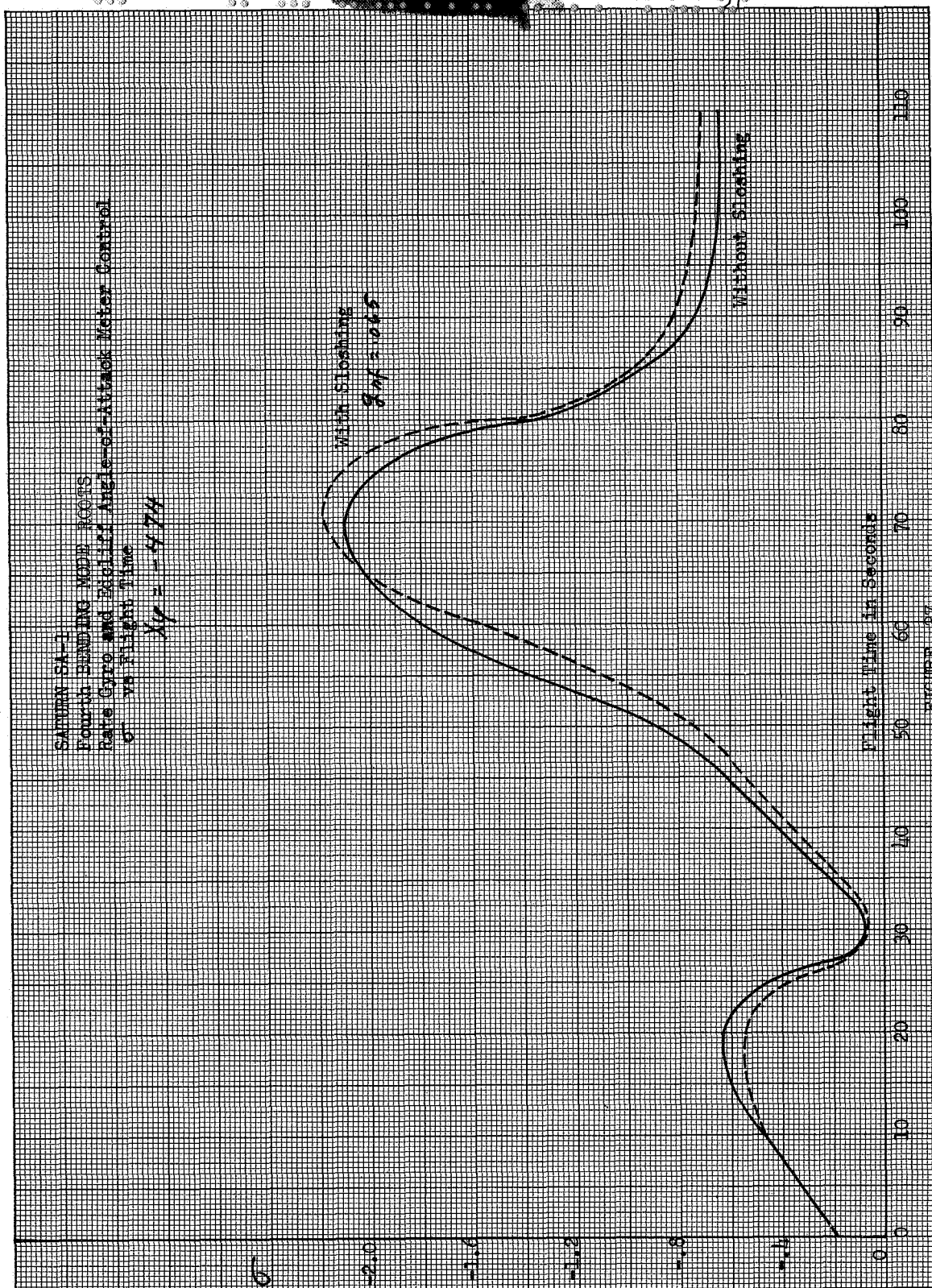


FIGURE 26

SATURN SA-3
Fourth BENDING MODE ROOTS
Rate Gyro and Roll/tilt Angle-of-Attack Meter Control
 σ vs Flight Time

$X_4 = -474$



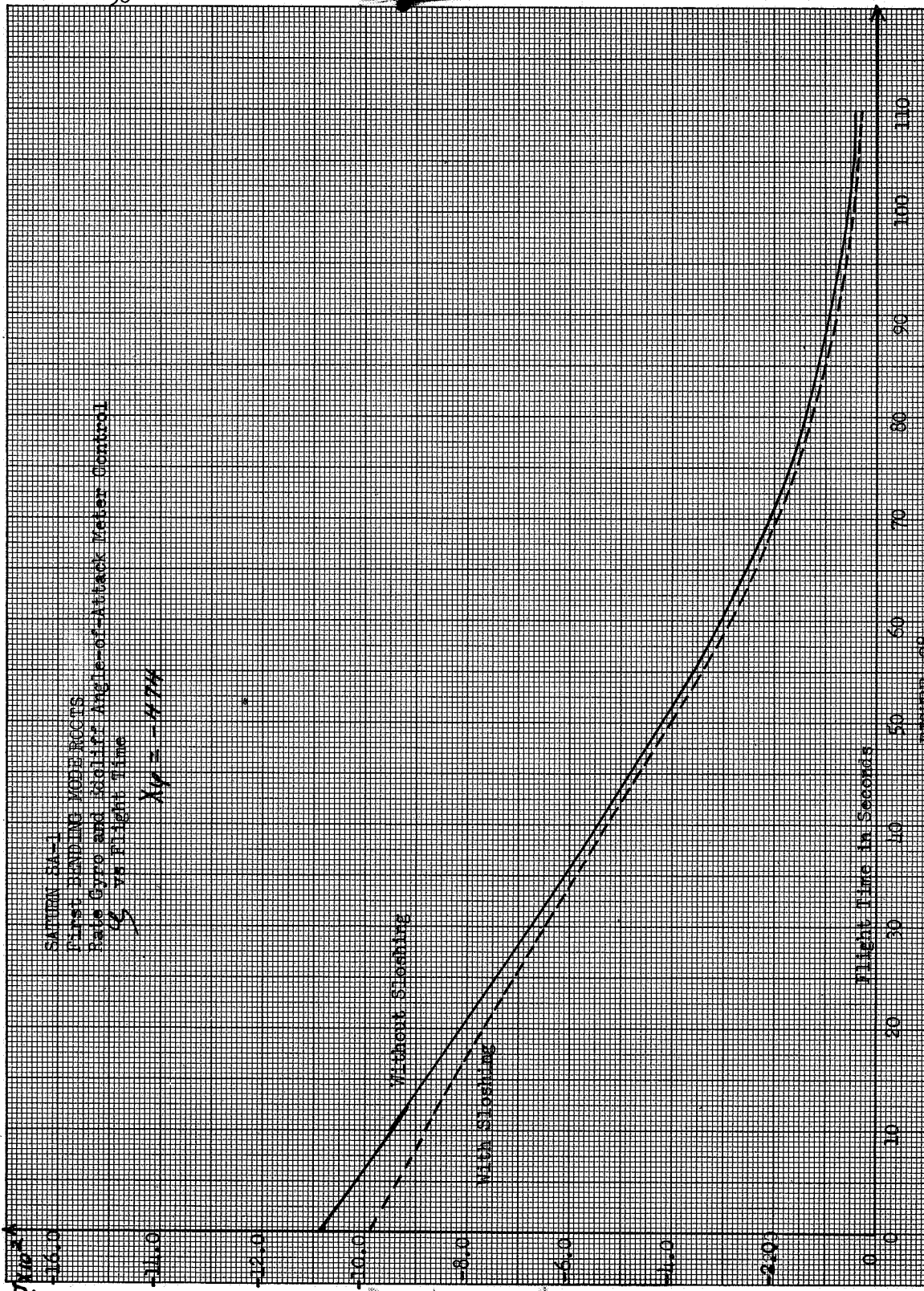
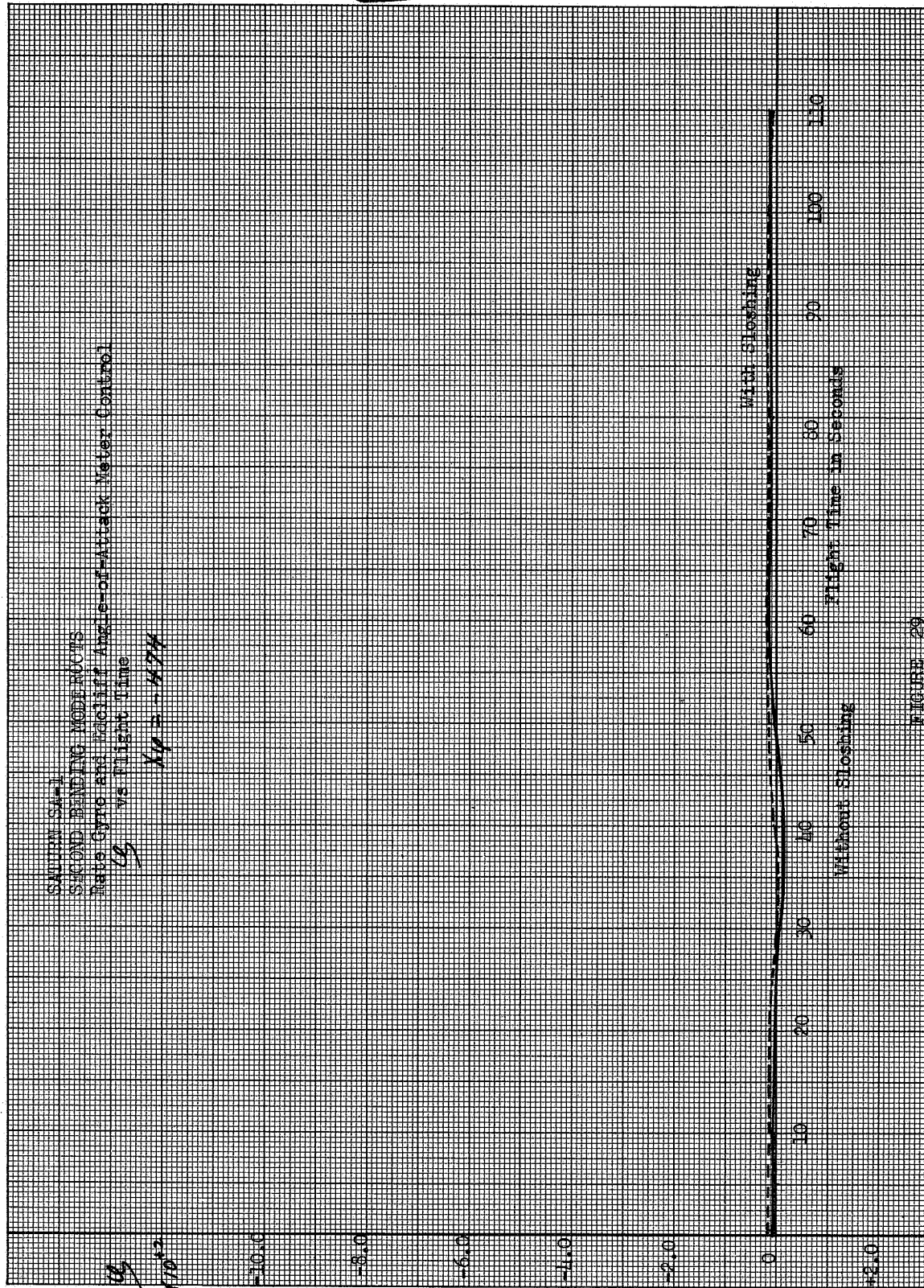


FIGURE 26



SATURN SA-1
 THIRD BENDING MODE ROOTS
 Rate Gyro and Side-Off Angle-of-Attack Meter Control
 vs Flight Time

$$\lambda_4 = -4.74$$

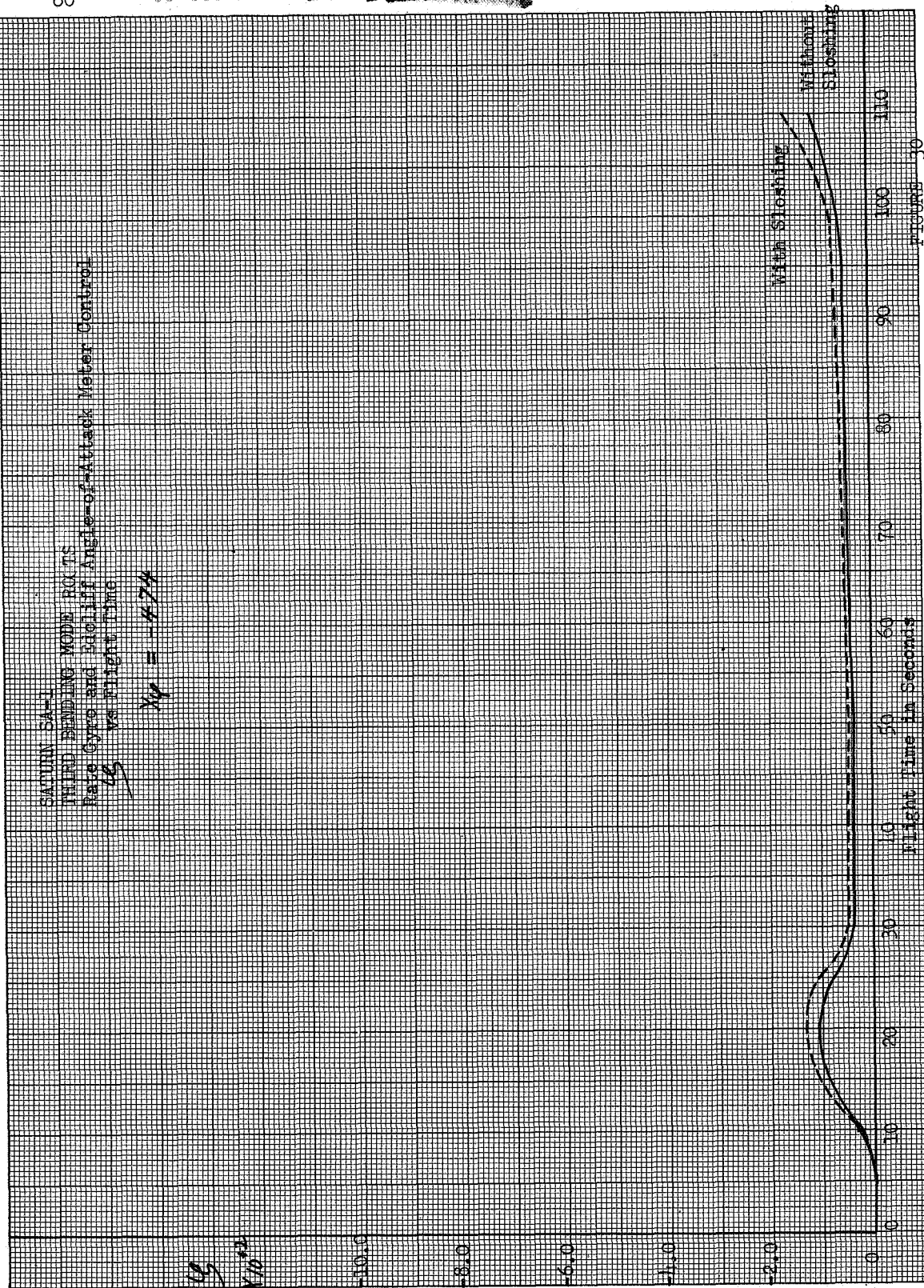


FIGURE 30

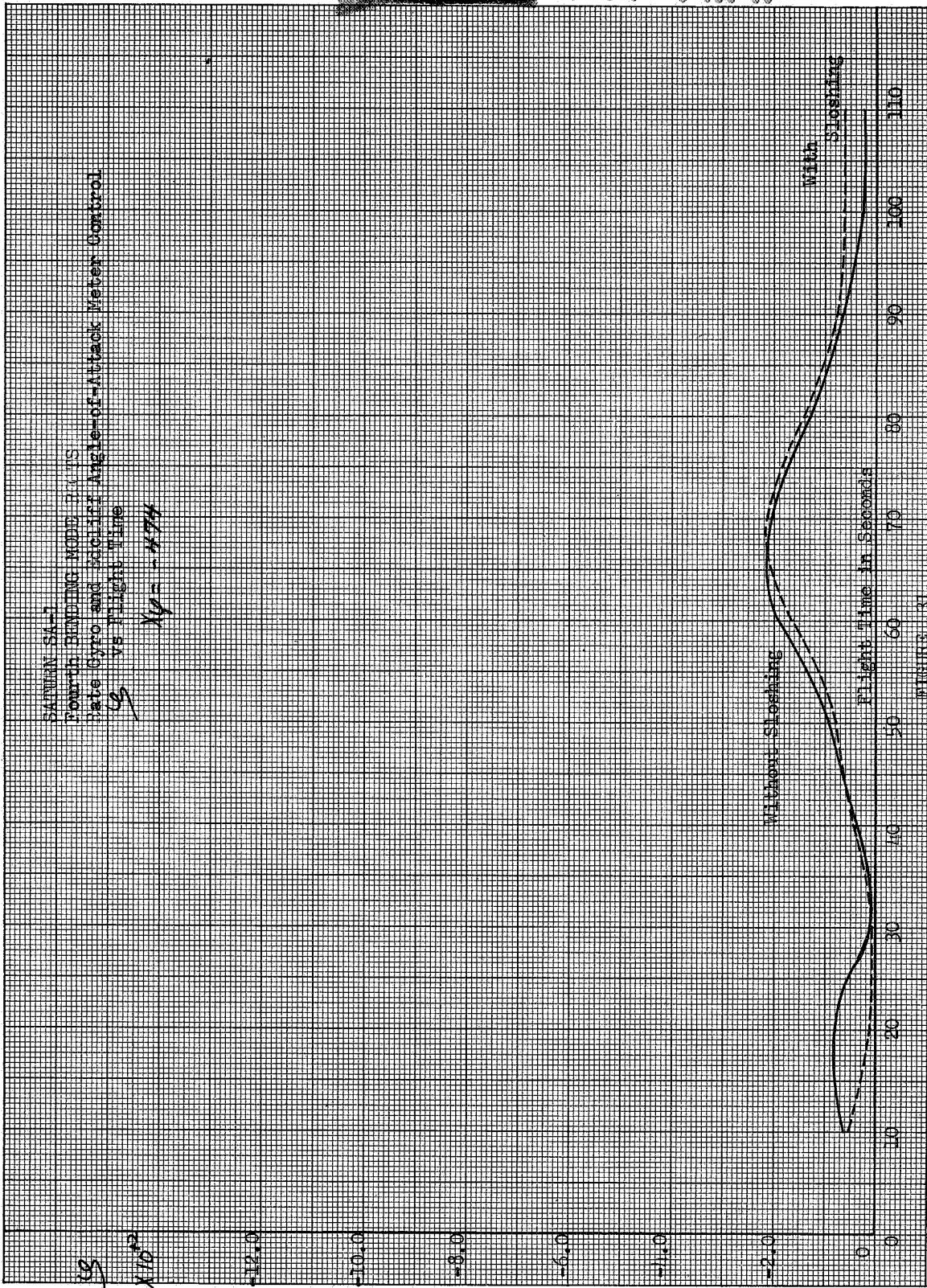
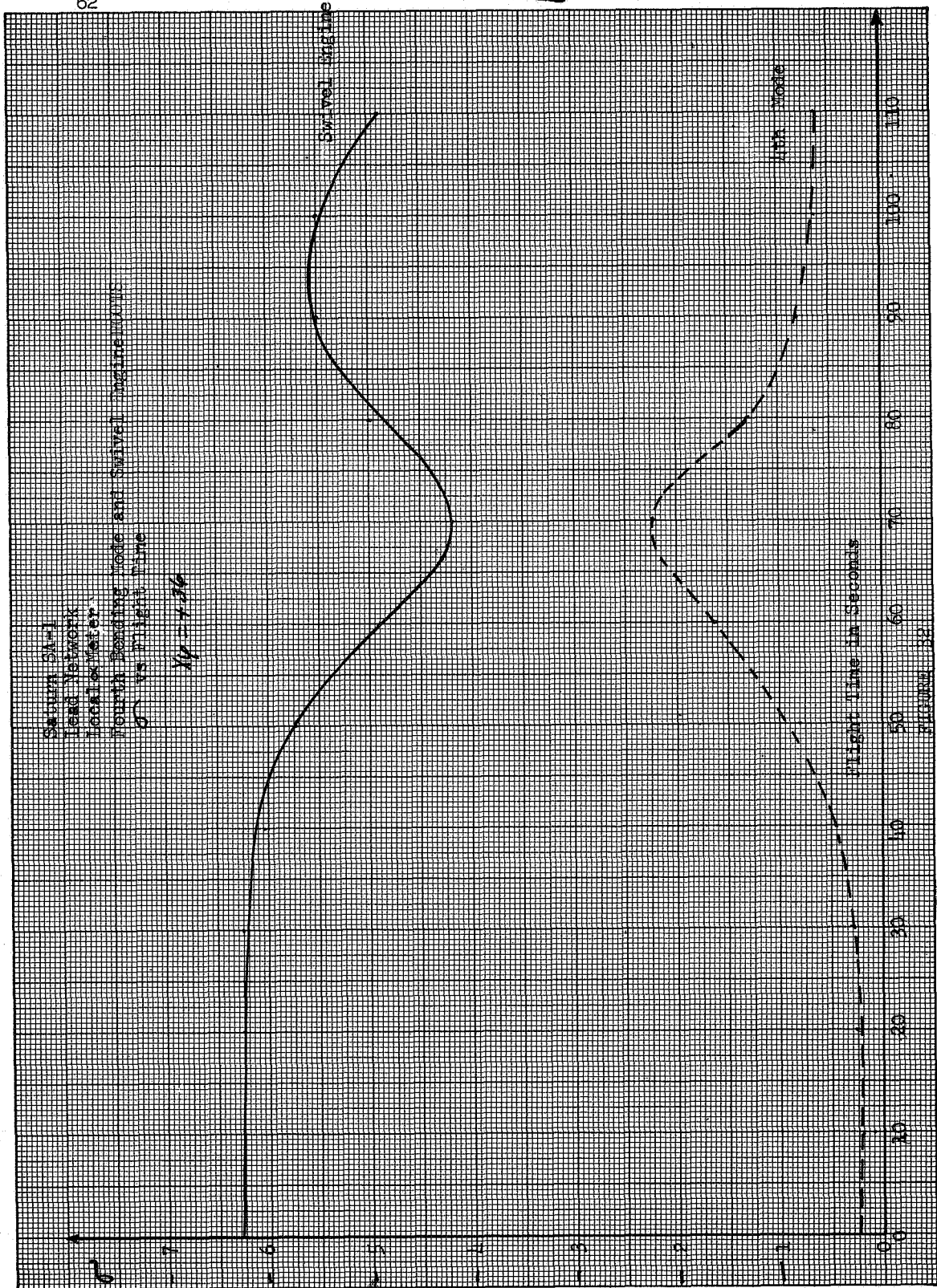
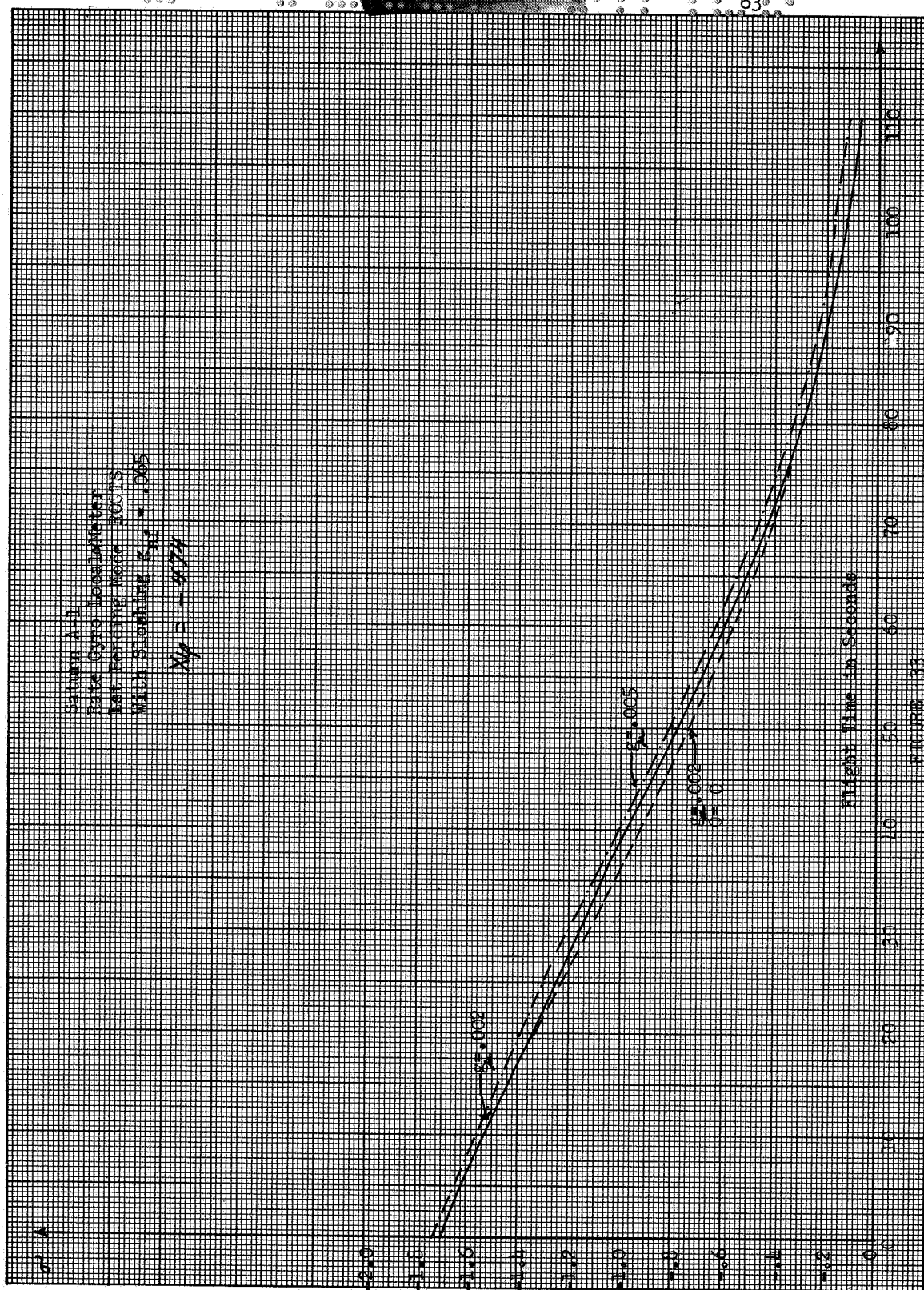
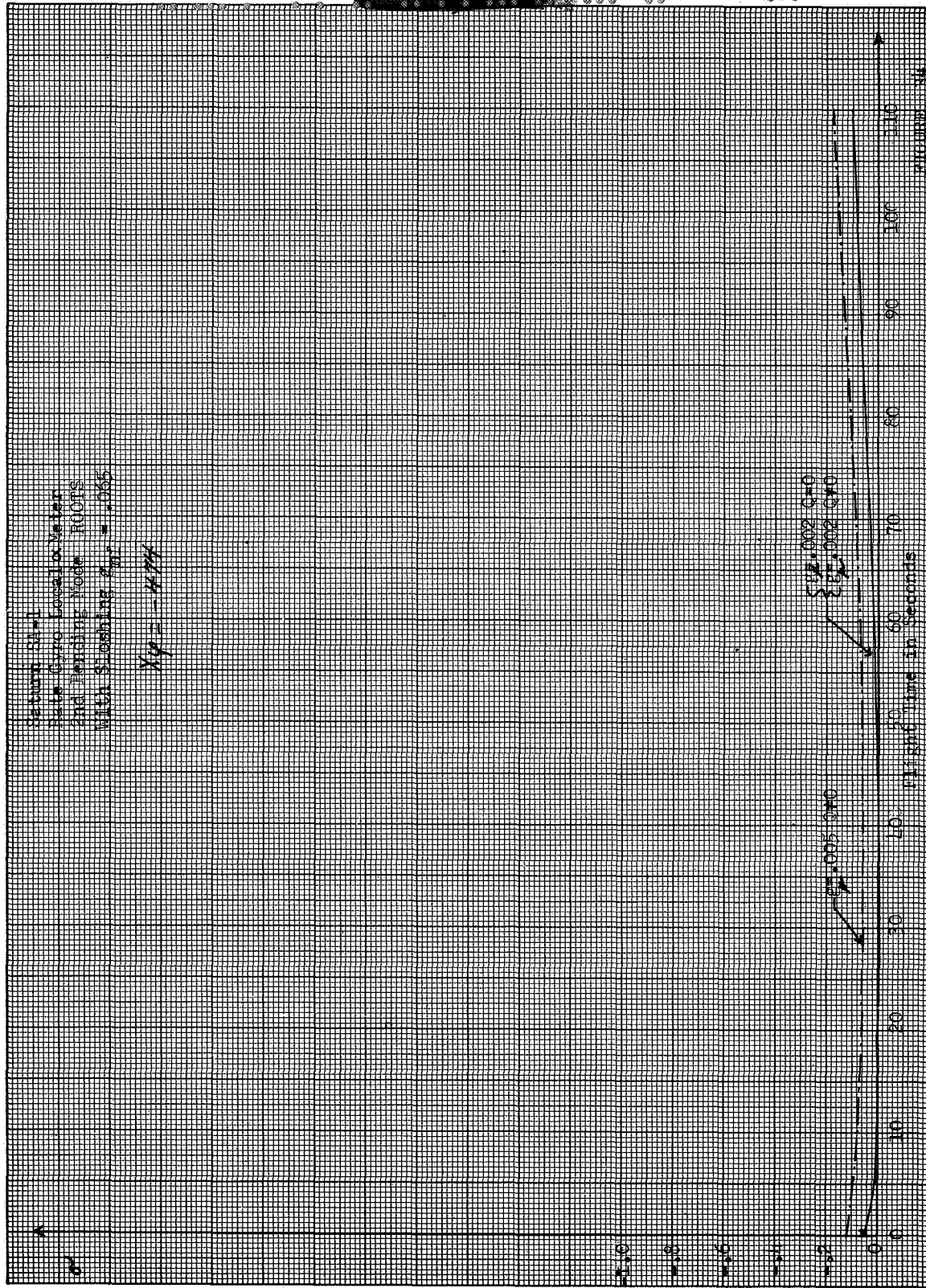


FIGURE 31





$$x_4 = -4.94$$


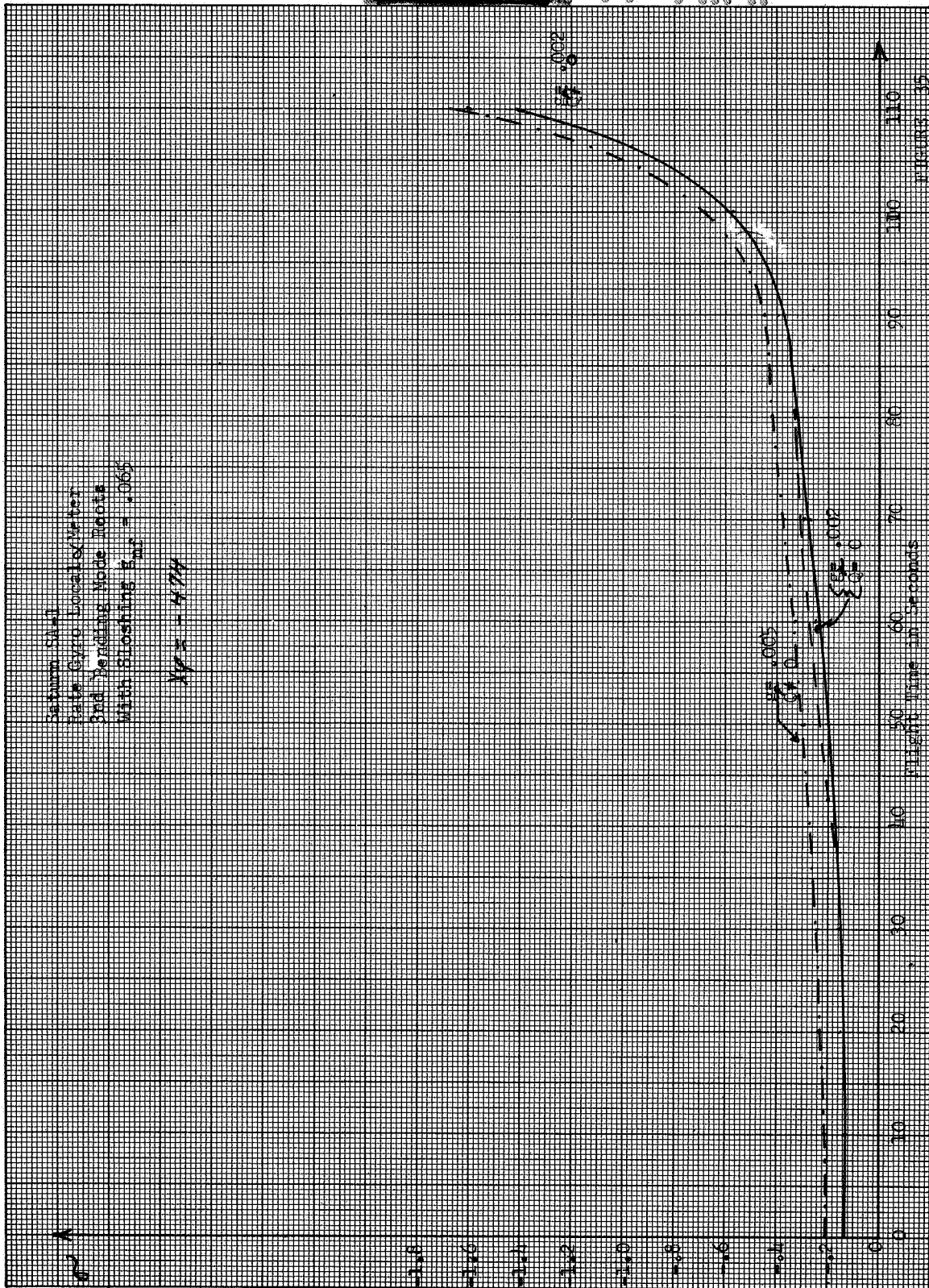
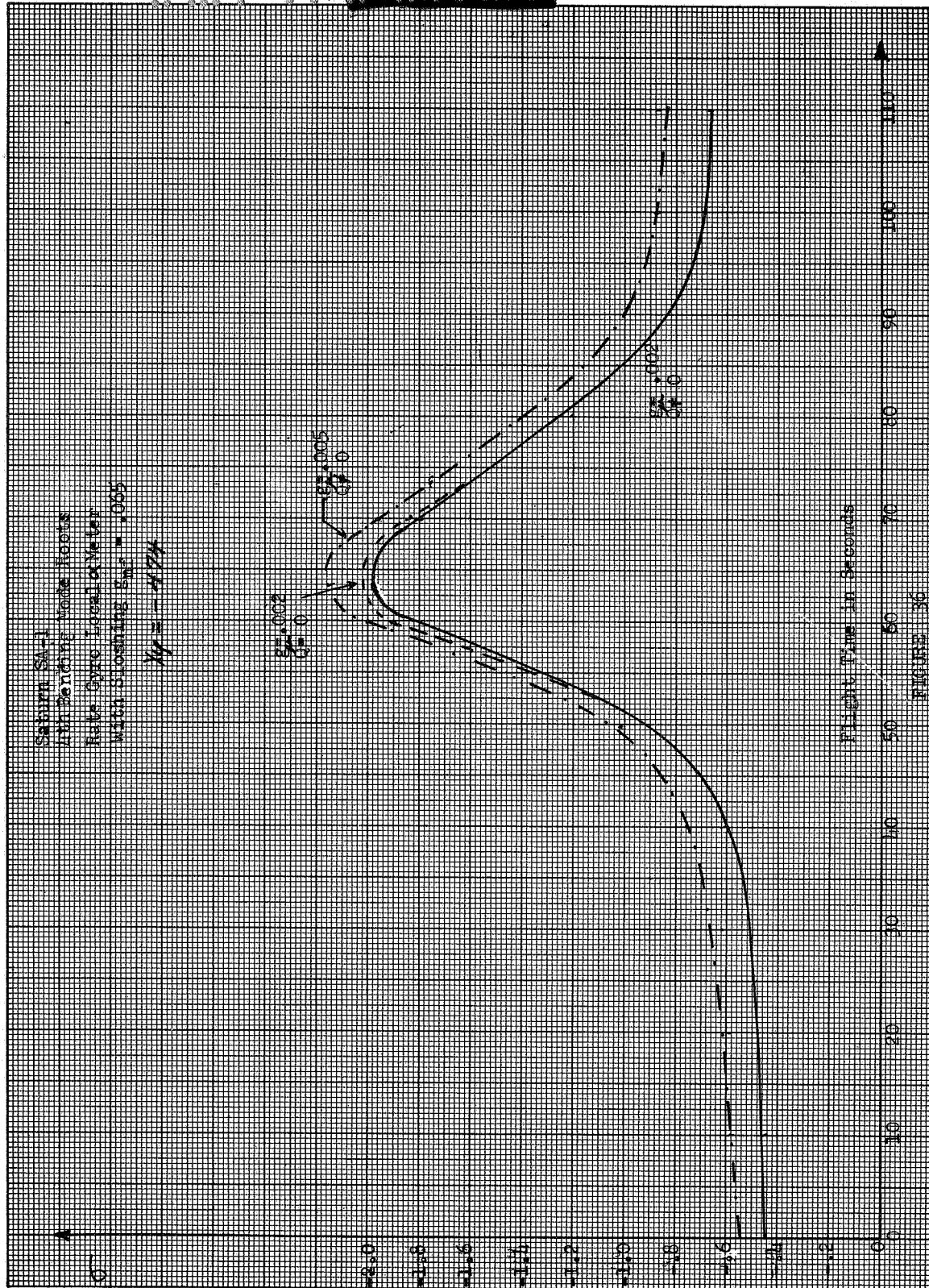


FIGURE 55





▲ 3. 集計方法

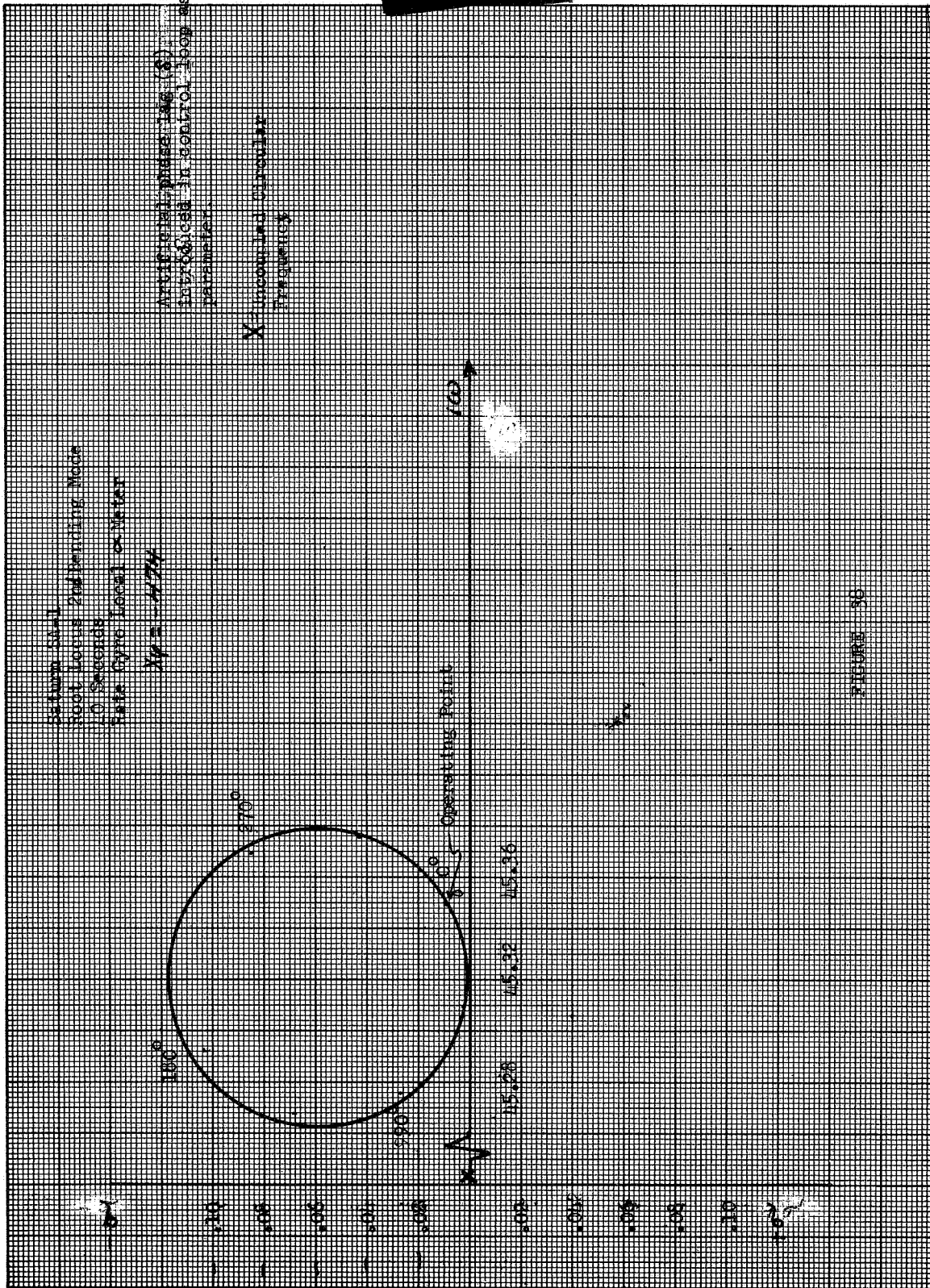


FIGURE 30

System 54-1
 Root Locus 3rd Pending Vote
 10 Seconds
 Base Cycle Indicator Meter

$$K_f = -4.74$$

Artificial phase lag (s)
 introduced in control
 loop as parameter.

X - Uncoupled Circular
 Frequency

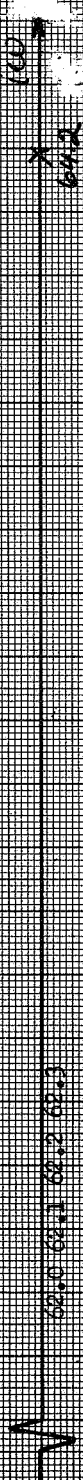
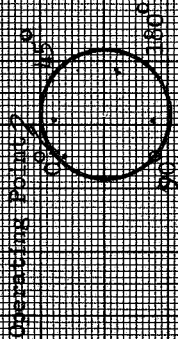


FIGURE 39

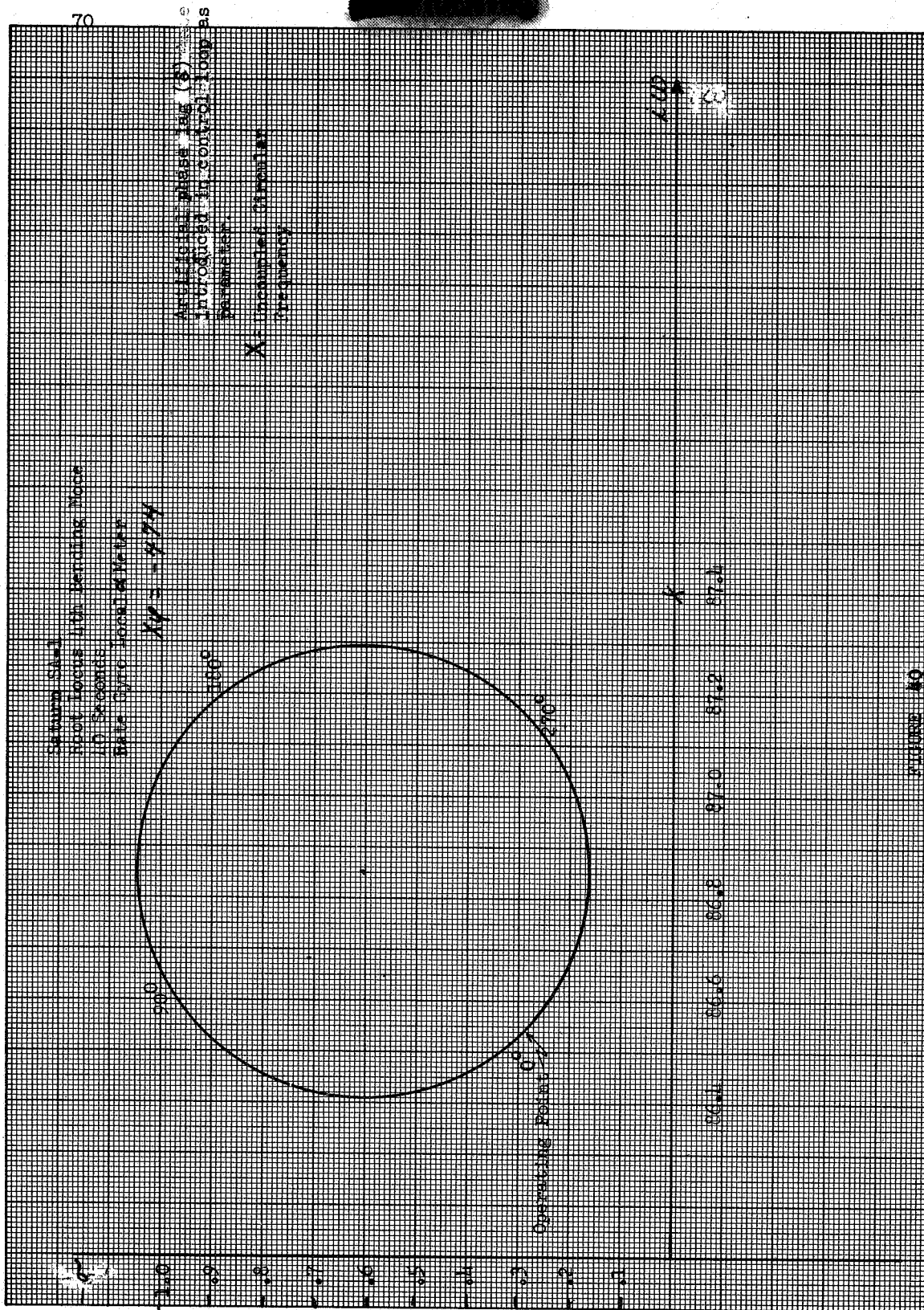


FIGURE 40

RATE GYRO AND LOCAL ϕ - METER
 1st BEADING MODE ROOT
 ABSOLUTE VALUE OF VARIABLES

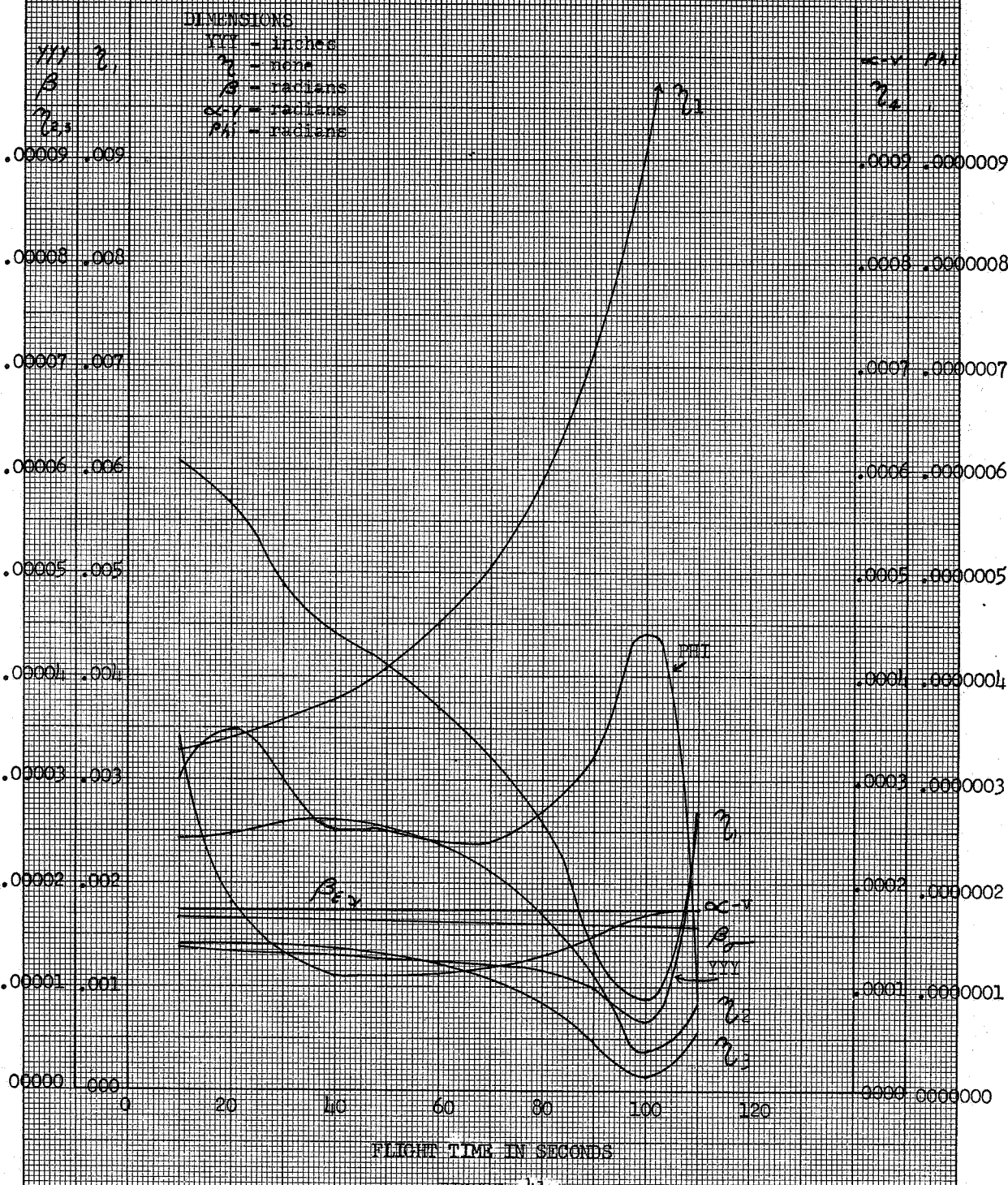


FIGURE 41

FUEL SURFACE AMPLITUDES

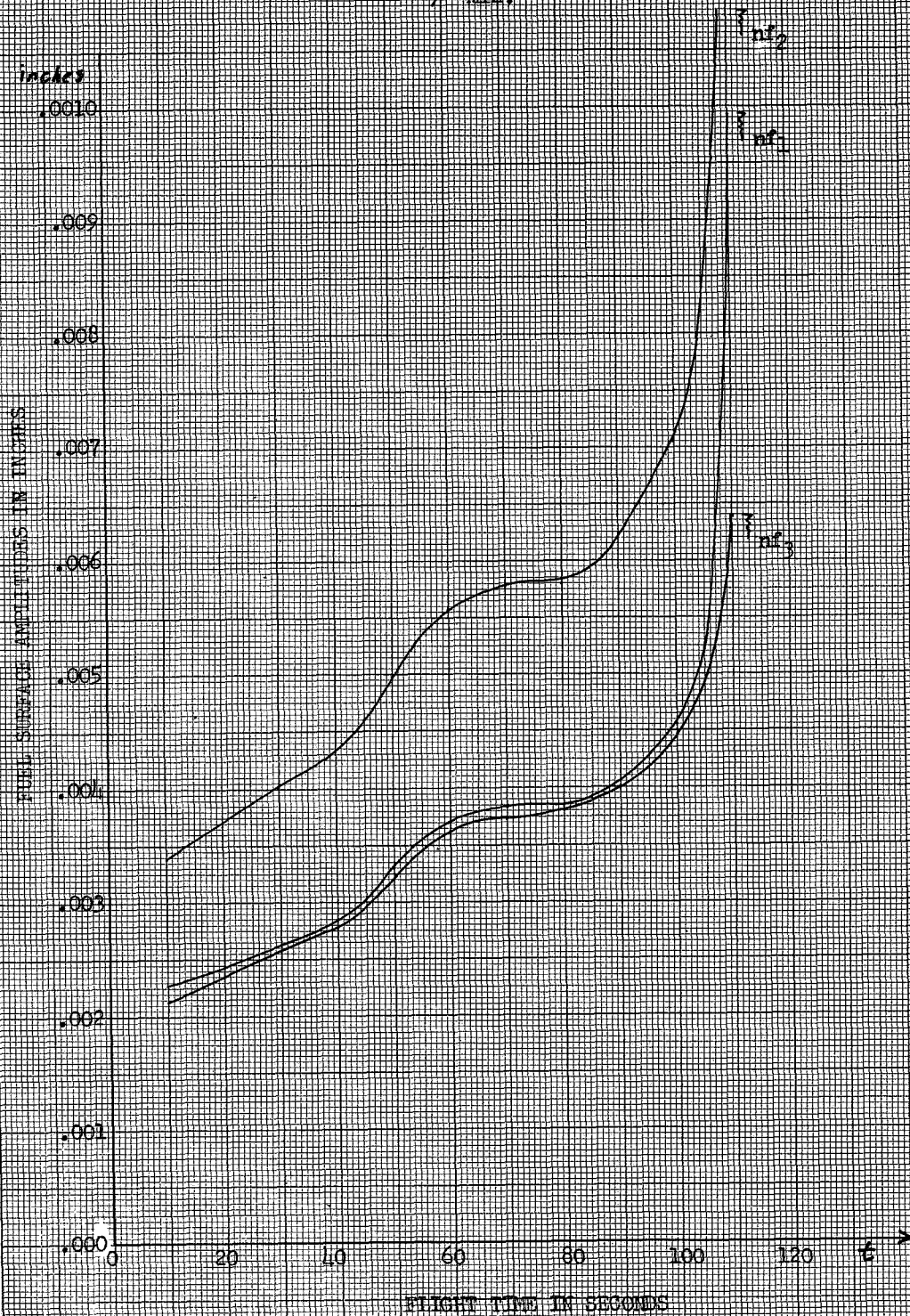
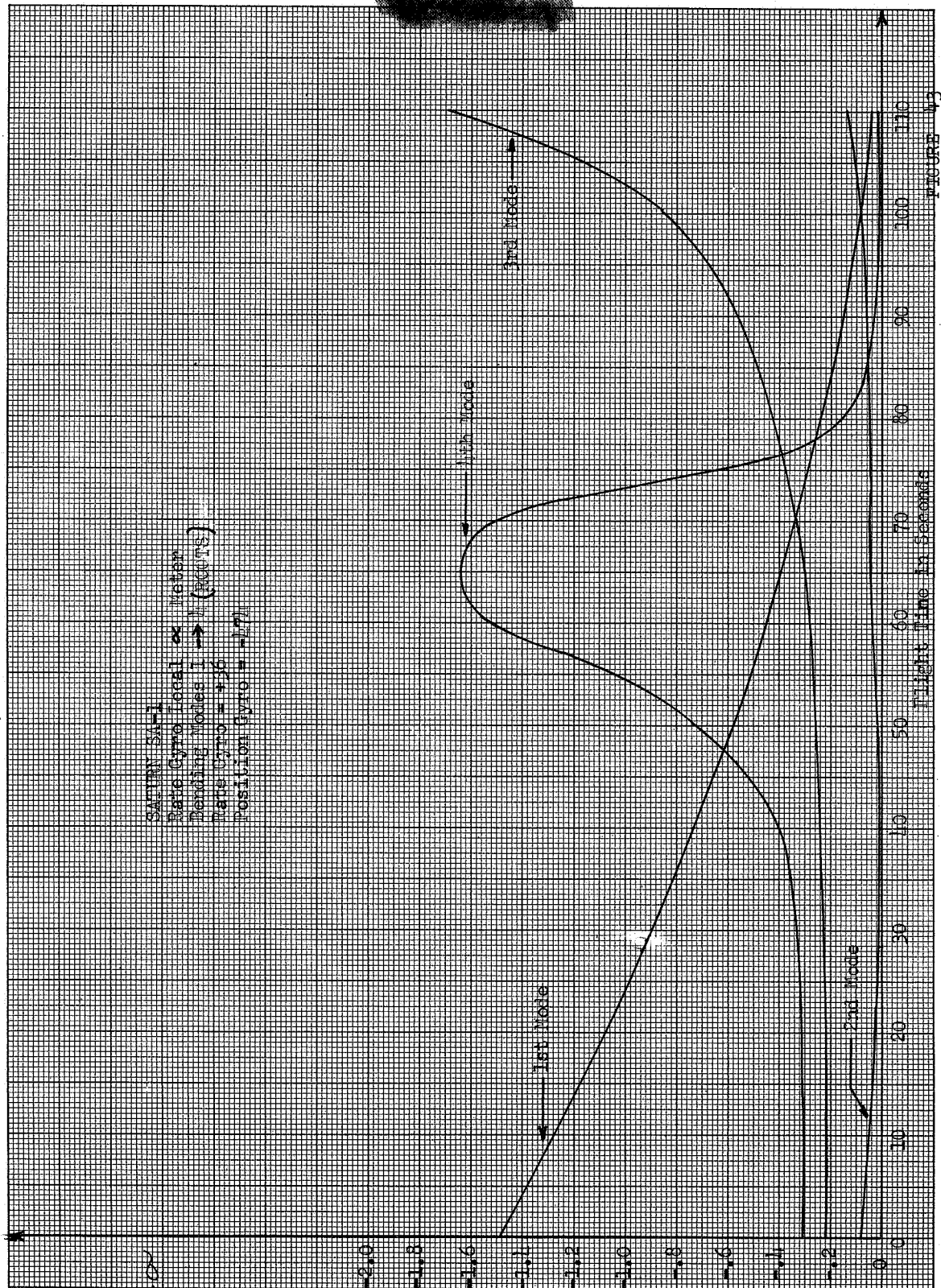
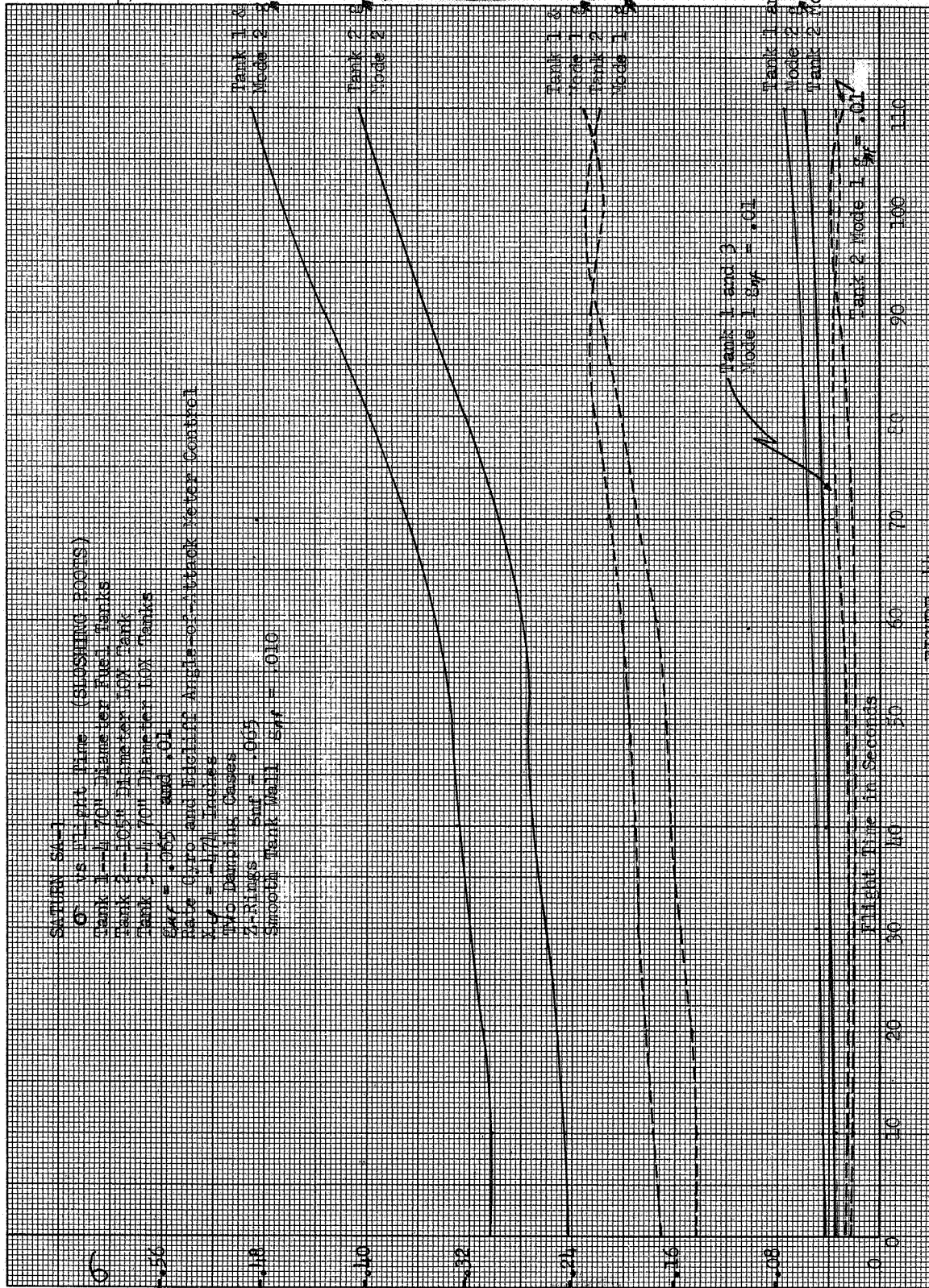
 β min.

FIGURE 42





Saturn S-41
Rate Gyro Local Meter

6" vs Flight Time
70" and 105" Diameter Tanks
Sloshing Bores

$X_{g2} = -474$

Settings for Dumping $\zeta_{g2} = .065$

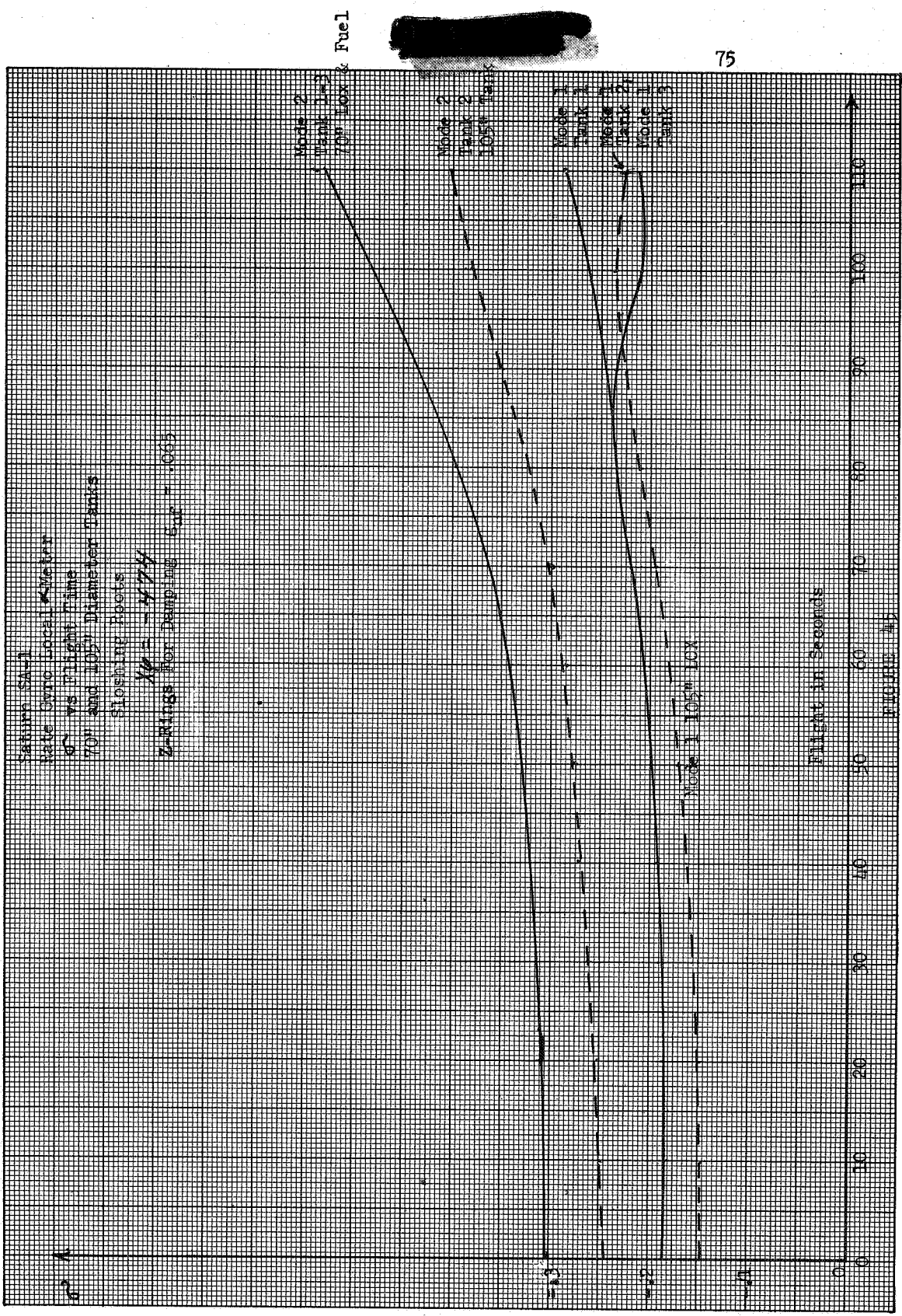


FIGURE 45

SARUM SA-1
 C vs Flight Time Cushing Roots
 TANK 1-4 70" Diameter FUEL Tanks
 $\epsilon = .005$
 Lead Network Local Meter
 $X_4 = 7.36$

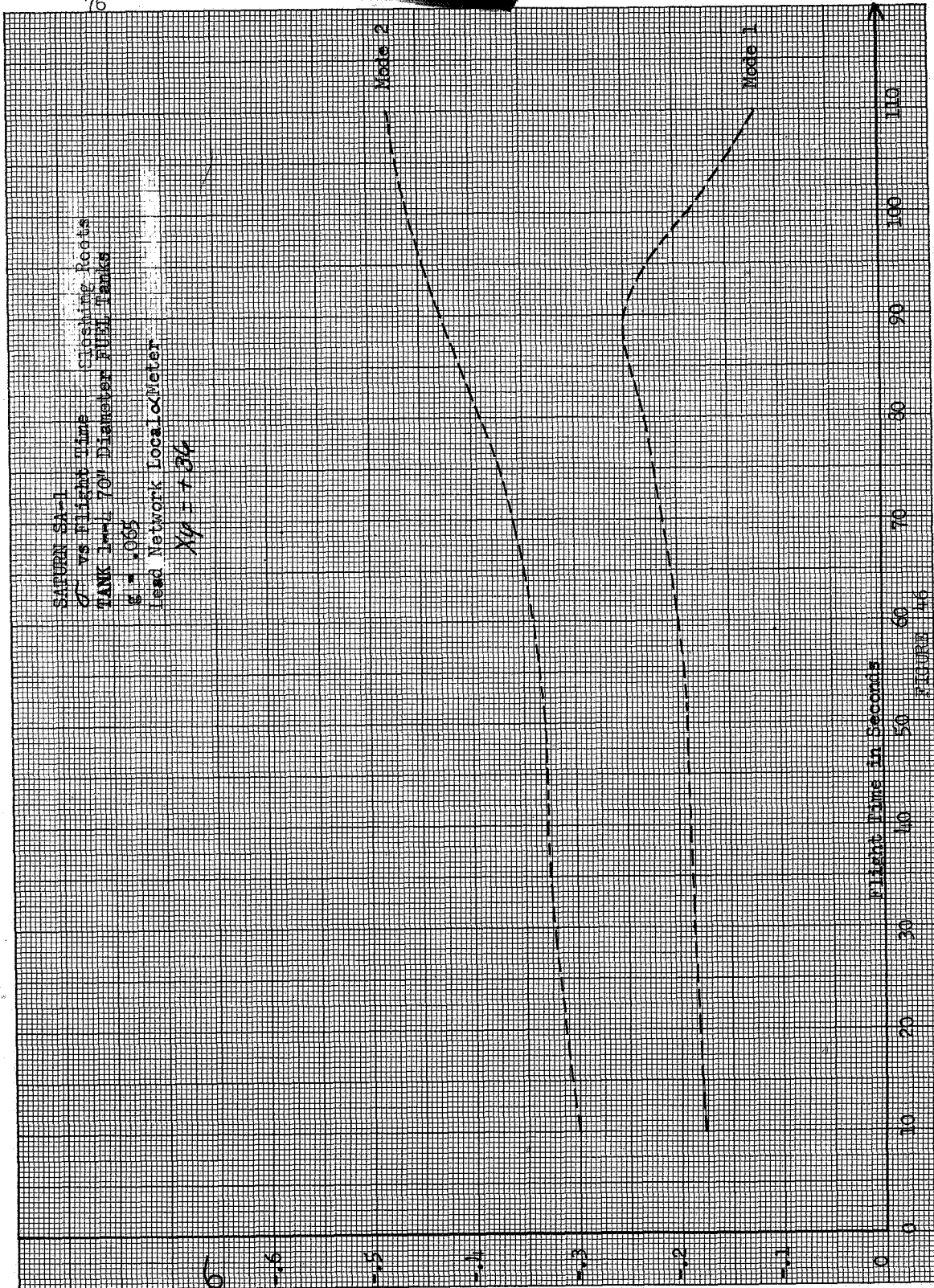
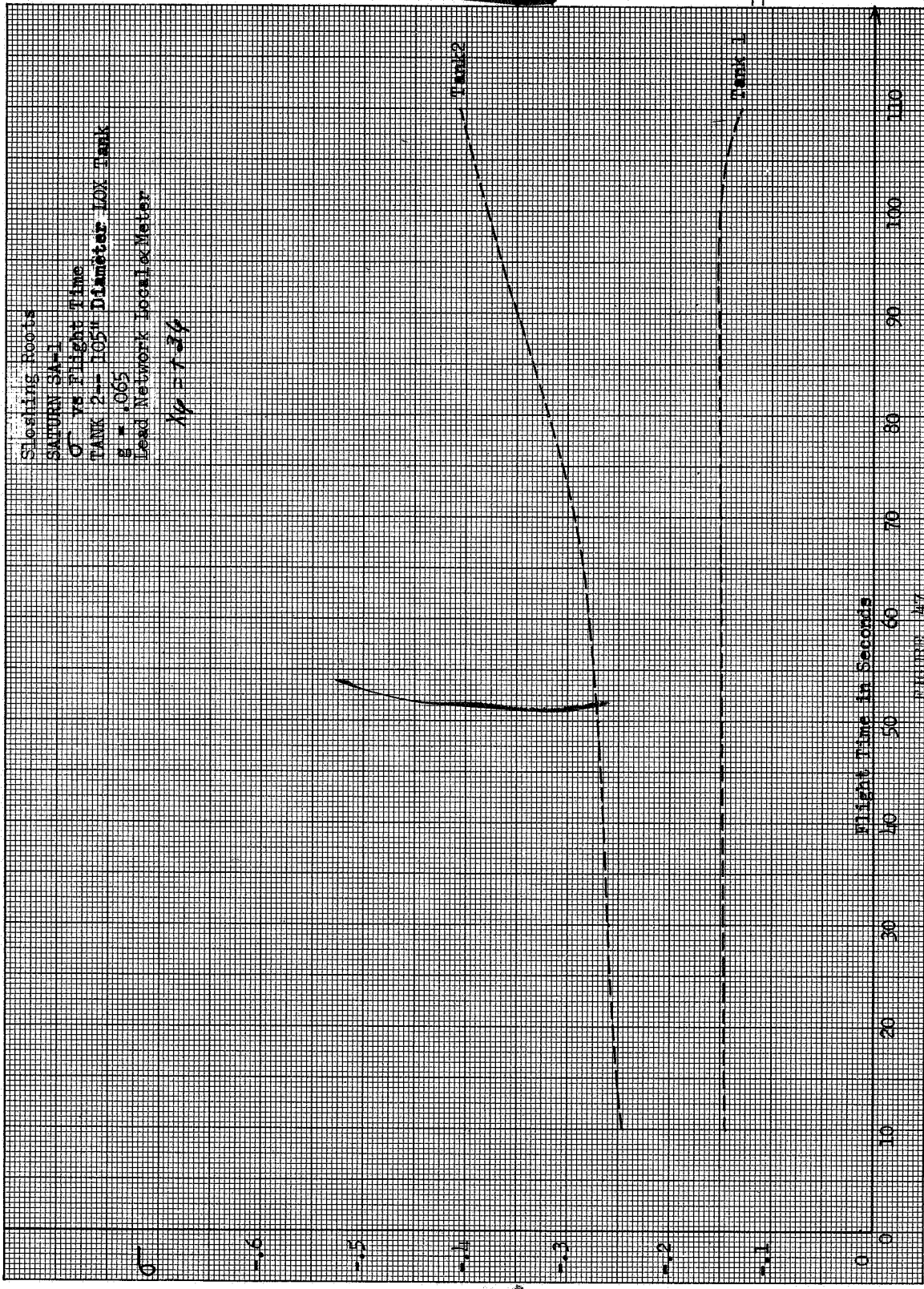


FIGURE 46



Sloshing Roots

SATURN SA-1

C vs Flight Time

TANK 3--4 70" Diameter LOX Tanks

$\delta = .065$

Lead Network Localizer Water

$Xp = +36$

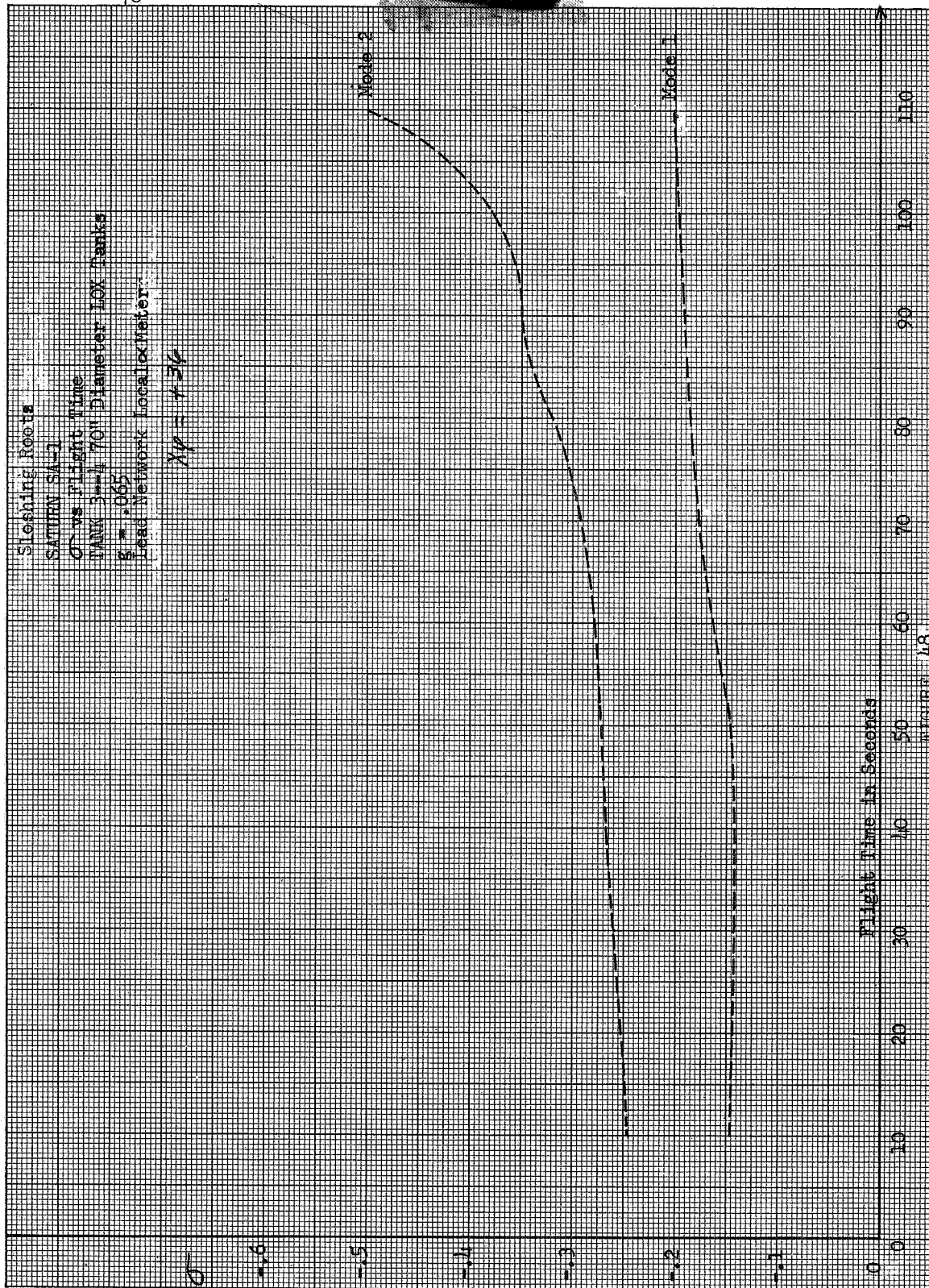
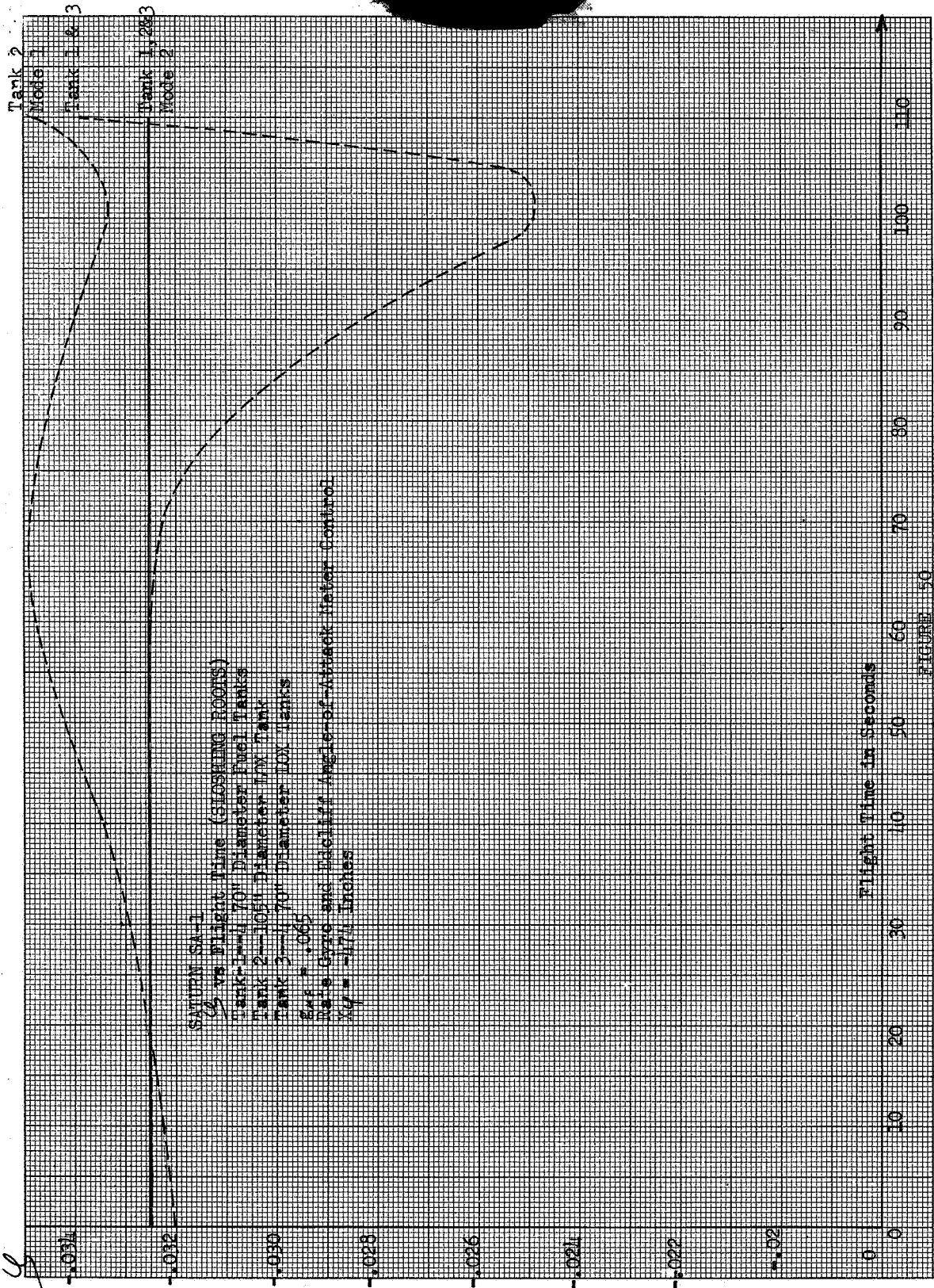
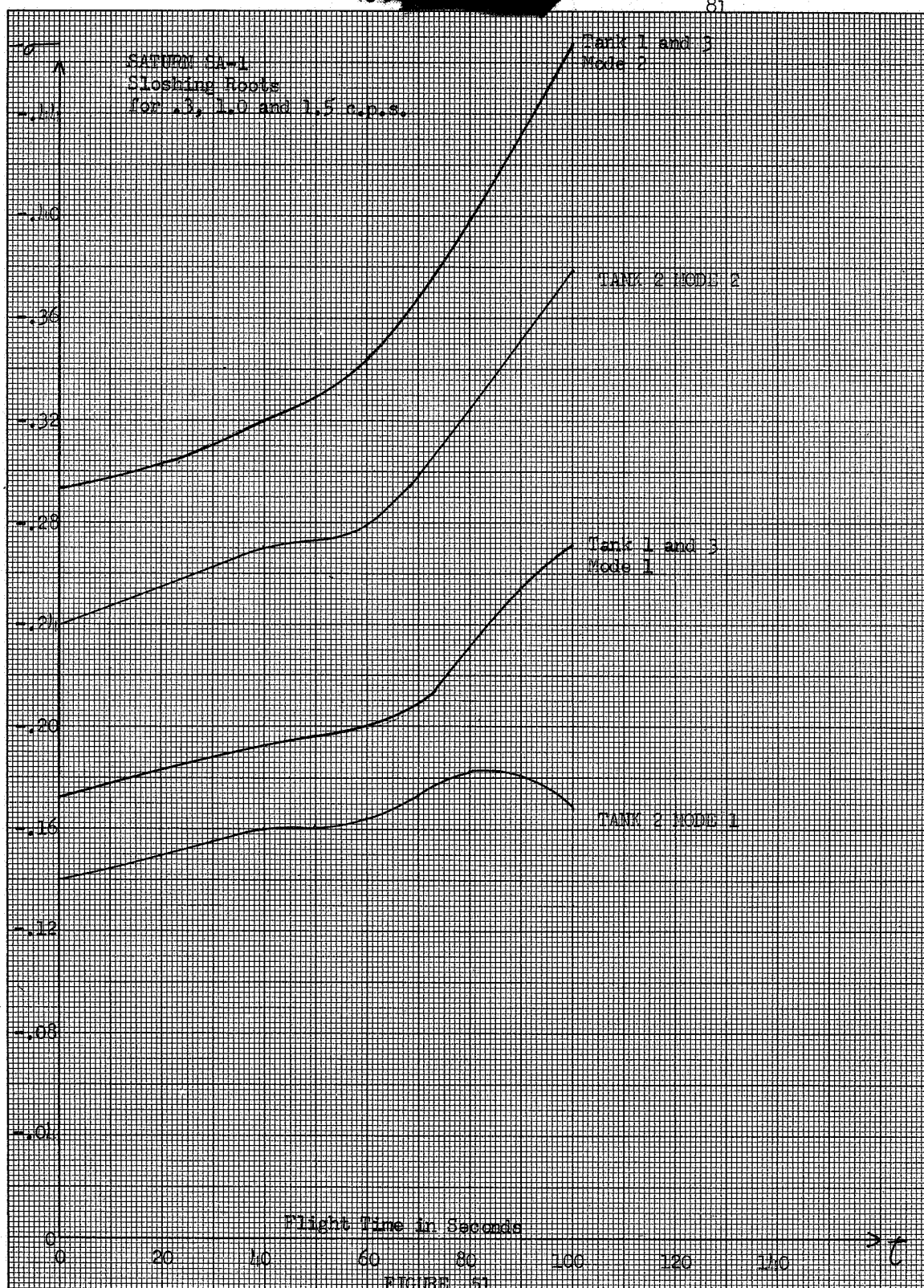


FIGURE 48







RALE CYC AND LOCAL α - METER
1st MODE SLOSHING ROOTS
ABSOLUTE VALUE OF VARIABLES

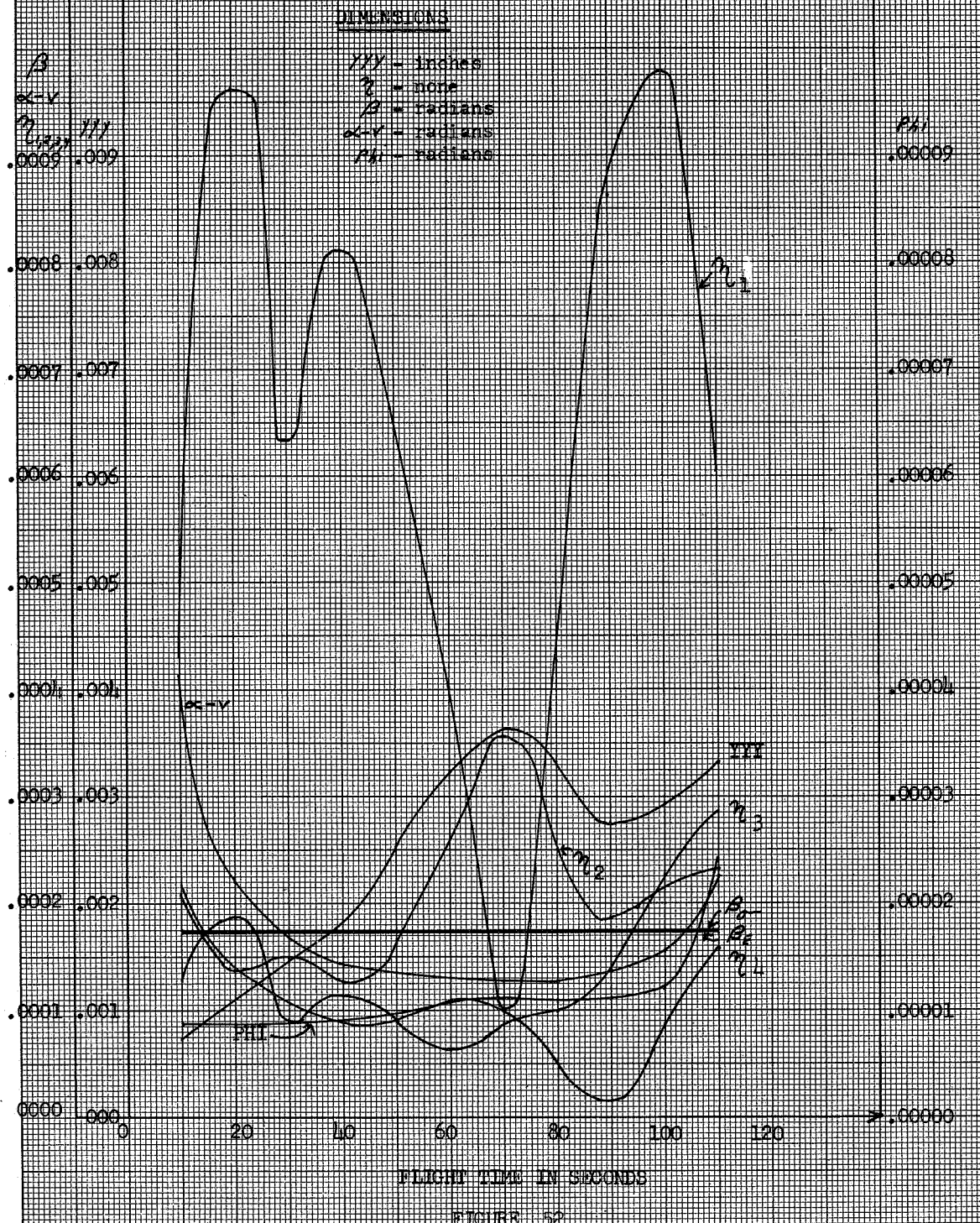
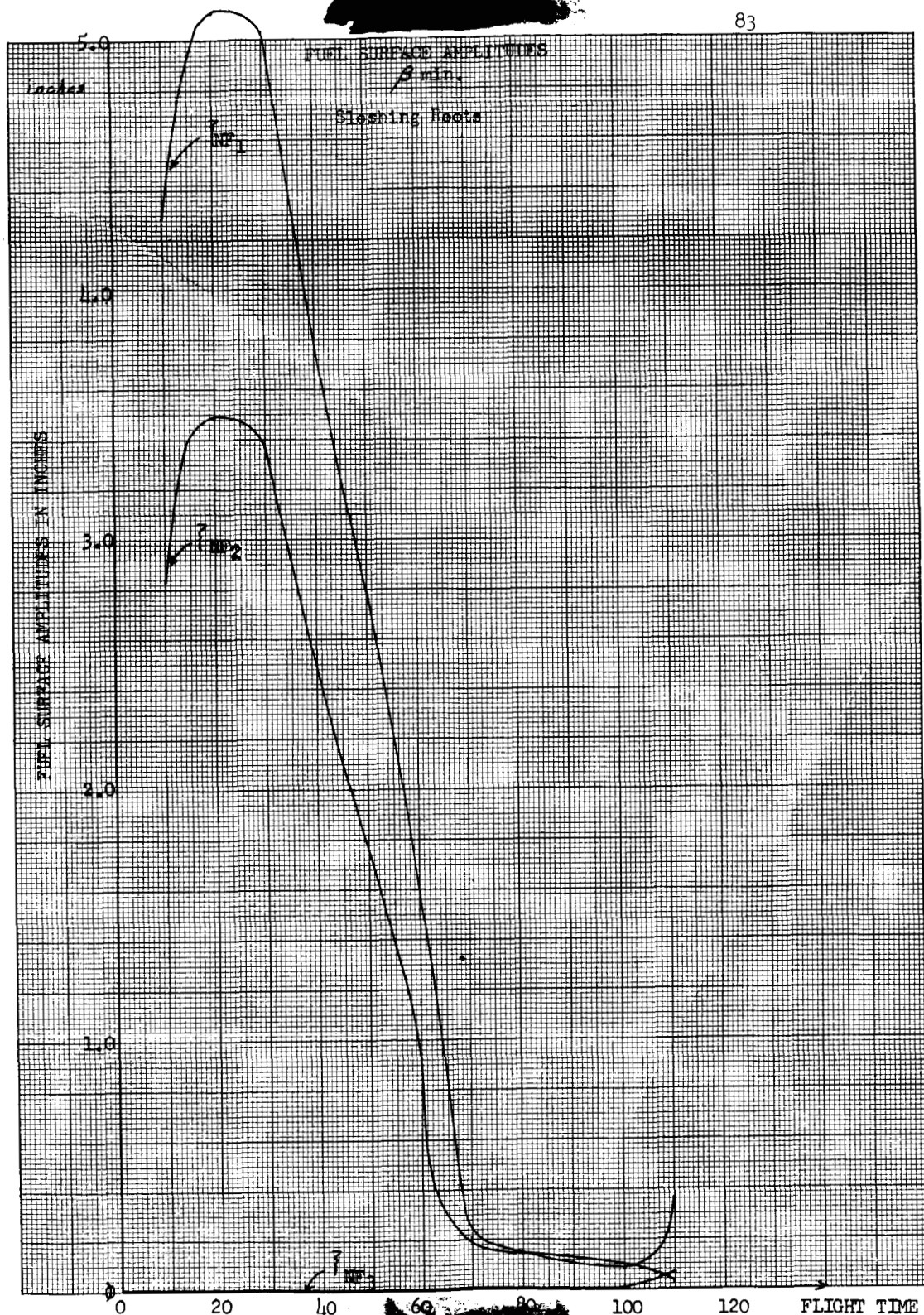


FIGURE 52



03712201030

8

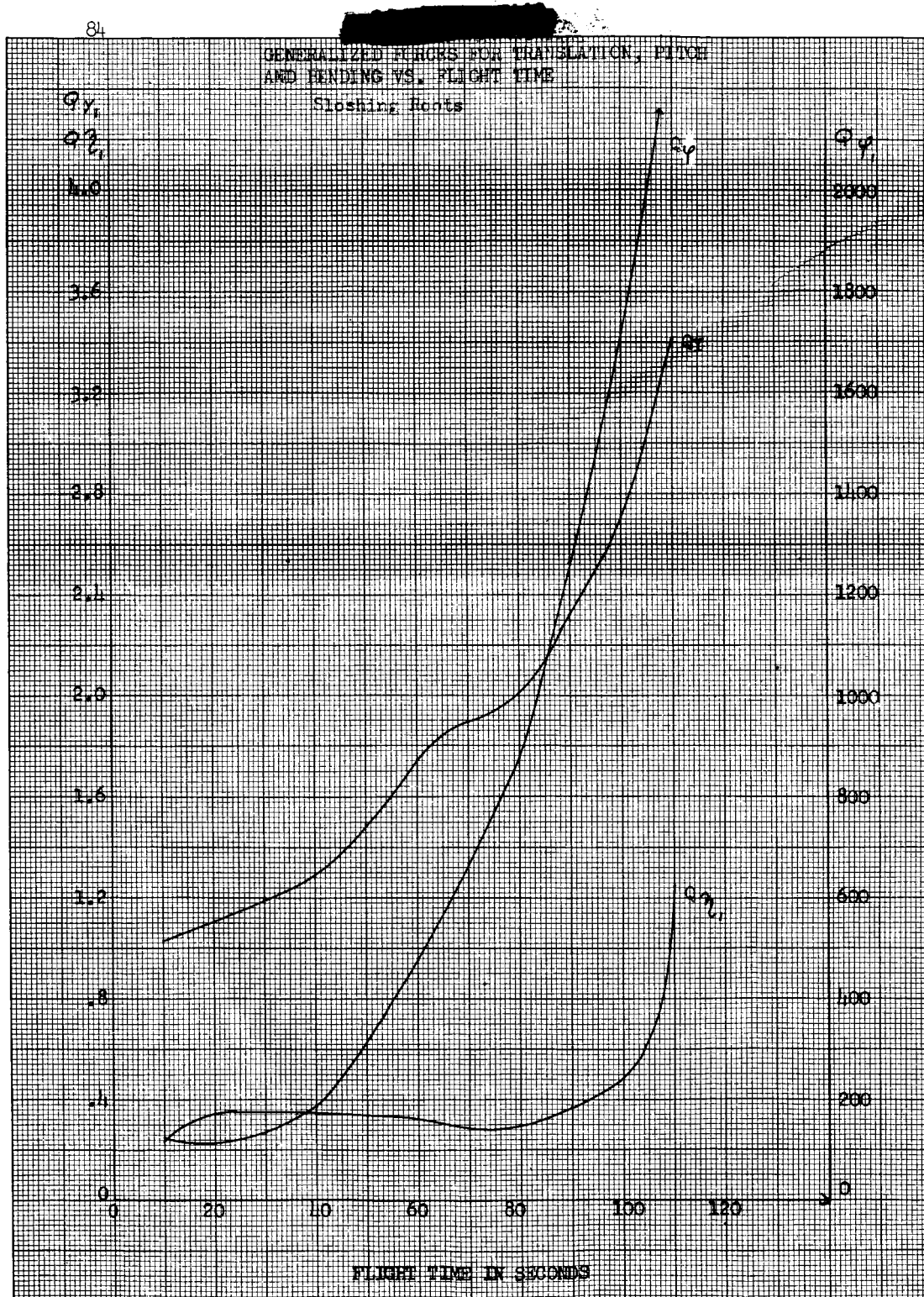


FIGURE 54

8

DECLASSIFIED

85

